



Short-Period Building Collapse Performance and Recommendations for Improving Seismic Design

Volume 1 – Overarching Findings, Conclusions, and
Recommendations

FEMA P-2139-1 / November 2020



FEMA



Short-Period Building Collapse Performance and Recommendations for Improving Seismic Design

Volume 1 – Overarching Findings, Conclusions, and Recommendations

Prepared by

APPLIED TECHNOLOGY COUNCIL
201 Redwood Shores Parkway, Suite 240
Redwood City, California 94065
www.ATCouncil.org

Prepared for

FEDERAL EMERGENCY MANAGEMENT AGENCY
Mai (Mike) Tong, Project Officer
Robert D. Hanson, Technical Advisor
Washington, D.C.

APPLIED TECHNOLOGY COUNCIL
Jon A. Heintz, Project Executive
Justin Moresco, Project Manager
Scott D. Schiff, Associate Project Manager

PROJECT TECHNICAL COMMITTEE
Charles A. Kircher (Project Tech. Director)
Jeffrey W. Berman
Kelly Cobeen
J. Daniel Dolan
Andre Filiatrault
James R. Harris
Gregory Kingsley
Dawn Lehman
Weichiang Pang
P. Benson Shing

PROJECT REVIEW PANEL
Anthony Court*
William T. Holmes
Larry Kruth
Onder Kustu
Phil Line
James O. Malley
Steve Pryor
Jason Thompson

COMMONALITIES WORKING GROUP
Andrew Sen

MASONRY WORKING GROUP
Jianyu Cheng
Jeff Corson
Andreas A. Koutras
Linda Peters

SOIL-STRUCTURE INTERACTION
WORKING GROUP
Lisa Star
Jonathan P. Stewart

STEEL WORKING GROUP
Alex Stone
Sarah Wichman

WOOD WORKING GROUP
D. Jared DeBock
Maria Koliou
Ershad Ziaei

*ATC Board Representative



FEMA



Notice

Any opinions, findings, conclusions, or recommendations expressed in this publication do not necessarily reflect the views of the Applied Technology Council (ATC), the Department of Homeland Security (DHS), or the Federal Emergency Management Agency (FEMA). Additionally, neither ATC, DHS, FEMA, nor any of their employees, makes any warranty, expressed or implied, nor assumes any legal liability or responsibility for the accuracy, completeness, or usefulness of any information, product, or process included in this publication. Users of information from this publication assume all liability arising from such use.

Cover photographs – Steel special concentrically braced frame system (credit: C-M. Uang, UCSD); wood light-frame system (credit: Degenkolb Engineers); and special reinforced masonry shear wall system (credit: T. Escobar, Masonry Institute of America).

Foreword

Most buildings in the United States are less than five stories tall. These low-rise buildings typically possess fundamental periods less than one-half second and thus are referred to as short-period buildings. Many commonly used analytical models have predicted that short-period buildings designed to current building codes are likely to suffer severe damage or collapse during design-level earthquakes. However, post-earthquake field investigations have not confirmed these predictions. Since this uncertainty is found across all types of building structures and construction materials permitted by current building codes and standards, it decreases confidence in the earthquake resilience of such code-compliant buildings. This technical resource series provides the findings and conclusions related to this issue and recommendations for improving seismic design of short-period buildings.

The National Earthquake Hazards Reduction Program (NEHRP) at the Federal Emergency Management Agency (FEMA) has a responsibility to help translate and implement new knowledge and research results to increase earthquake resilience nationwide. This FEMA-supported multi-year project series has successfully applied new analytical modeling techniques to investigate the long-standing problem of short-period building seismic collapse performance. This report is the first volume of the series, and it summarizes the commonalities among short-period buildings and their seismic performances in various past earthquakes. Through a study based on a generic analytical model, the report has confirmed a flaw in the traditional earthquake engineering approach and proposed a new concept and methodology, which offers a general solution to the uncertainty issue. Based on the select material studies in the series and the new concept, the report provides recommendations for improving codes and standards and future seismic design of short-period buildings.

FEMA is grateful to the Applied Technology Council (ATC) for managing this sophisticated multi-year project series to a successful completion, to the Project Technical Committee and the Project Review Panel for their dedicated effort leading to invaluable technical findings and recommendations. FEMA is also thankful to the project workshop participants for their scrutiny and valuable comments. Resolving the uncertainty in short-period building seismic collapse performance will strengthen confidence in seismic building codes. This project series will also contribute to improving seismic design and predicting collapse potential of short-period buildings in high-seismic communities in the nation.

Federal Emergency Management Agency

Preface

Recent analytical studies investigating a wide range of modern seismic-force-resisting systems have predicted collapse rates for short-period buildings that are significantly larger than those observed in earthquakes during the past 50 years. This gap between analytically predicted and historically observed collapse rates is known as the *short-period building seismic performance paradox*. Analytically predicted collapse rates for short-period buildings are also generally larger than maximum collapse rates used in national model codes and standards to establish seismic design requirements. If these analytical predictions are accurate, it means that the goal of acceptable collapse performance for all seismic-force-resisting systems at all building periods is not being achieved.

In 2013, the Applied Technology Council (ATC) was awarded the first in a series of task orders under contracts HSFE60-12-D-0242 and HSFE60-17-D-0002 with the Federal Emergency Management Agency (FEMA) to investigate “Solutions to the Issue of Short Period Building Performance,” designated the ATC-116 Project series. The purpose of this series of projects was to investigate the response behavior and collapse performance of different structural systems and to identify causes and develop solutions for the short-period building seismic performance paradox. Studies investigated three structural systems: wood light-frame, special reinforced masonry shear wall, and steel special concentrically braced frame (SCBF) systems.

This report—which summarizes results, conclusions, and recommendations from the three system-specific studies and presents a common understanding of the seismic response and collapse performance of short-period buildings—is one of four principal products of the ATC-116 series of projects:

- FEMA 2139-1, *Short-Period Building Collapse Performance and Recommendations for Improving Seismic Design, Volume 1 – Overarching Findings, Conclusions, and Recommendations*
- FEMA 2139-2, *Short-Period Building Collapse Performance and Recommendations for Improving Seismic Design, Volume 2 – Study of One-to-Four Story Wood Light-Frame Buildings*

- FEMA 2139-3, *Short-Period Building Collapse Performance and Recommendations for Improving Seismic Design, Volume 3 – Study of One-to-Four Story Special Reinforced Masonry Shear Wall Buildings*
- FEMA 2139-4, *Short-Period Building Collapse Performance and Recommendations for Improving Seismic Design, Volume 4 – Study of One-to-Four Story Steel Special Concentrically Braced Frame Buildings*

These reports are the result of a collaborative effort of more than 30 individuals tasked with the design of archetypes, development of numerical models, and interpretation of results across all three structural systems, in addition to the many others who participated in review workshops where draft versions of the reports were presented and discussed. ATC is indebted to the leadership of Charlie Kircher, Project Technical Director, and to the other members of the ATC-116 project team for their efforts in developing these reports. The Project Technical Committee, consisting of Jeff Berman, Kelly Cobeen, Dan Dolan, Andre Filiatrault, Jim Harris, Greg Kingsley, Dawn Lehman, Weichi Pang, and Benson Shing, managed and performed the technical development effort.

Andy Sen assisted in the collapse performance study using single-degree-of-freedom models. The Project Review Panel, consisting of Tony Court, Bill Holmes, Larry Kruth, Onder Kustu, Phil Line, Jim Malley, Steve Pryor, and Jason Thompson, provided technical review and advice at key stages of the work.

ATC also gratefully acknowledges Mike Tong (FEMA Project Officer) and Bob Hanson (FEMA Technical Advisor) for their input and guidance in the preparation of this report, Scott Schiff who assisted in ATC project management, and Carrie J. Perna who provided ATC report production services. The names and affiliations of all who contributed to this report, including those who participated in the review workshop focused on commonalities, are provided in the list of Project Participants at the end of this report.

Justin Moresco
ATC Director of Projects

Jon A. Heintz
ATC Executive Director

Table of Contents

Foreword.....	iii
Preface.....	v
List of Figures.....	ix
List of Tables	xiii
1. Introduction.....	1-1
1.1 Background and Purpose.....	1-2
1.2 Approach and Scope.....	1-5
1.3 Organization and Content.....	1-7
2. Short-Period Building Background.....	2-1
2.1 Selection of Short-Period Building Systems for Detailed Studies	2-1
2.2 Short-Period Building Seismic Performance Paradox.....	2-7
2.3 Prior Analytical Studies of Bilinear SDOF Models	2-8
3. Observed Collapse Performance and Benchmarks.....	3-1
3.1 Overview	3-1
3.2 U.S. Earthquakes (1964–2014) and Building-Related Fatalities and Economic Losses	3-2
3.3 Collapse Performance of Short-Period Buildings in Past Earthquakes	3-4
3.3.1 Wood Light-Frame Buildings	3-6
3.3.2 Reinforced Masonry Buildings	3-9
3.3.3 Steel SCBF Buildings.....	3-11
3.4 Benchmark Collapse Metrics of Short-Period Buildings Based on Wood Light-Frame Building Performance	3-15
3.5 Summary of Key Observations of Short-Period Building Performance	3-20
4. Archetypes, Parametric Studies, and Findings	4-1
4.1 Overview of Parametric Studies of Short-Period Buildings.....	4-1
4.2 Summary of Archetype Designs and Configurations	4-5
4.2.1 Design of Wood Light-Frame Archetypes	4-5
4.2.2 Design of Reinforced Masonry Archetypes	4-7
4.2.3 Design of Steel SCBF Archetypes	4-8
4.3 Summary of Numerical Modeling.....	4-9
4.3.1 Numerical Modeling of Wood Light-Frame Archetypes.....	4-9
4.3.2 Numerical Modeling of Reinforced Masonry Archetypes.....	4-11
4.3.3 Numerical Modeling of Steel SCBF Archetypes	4-14

4.4	Summary of Numerical Results: High-Seismic Baseline Archetypes	4-16
4.5	Key Findings Applicable to All Three Short-Period Systems	4-22
4.5.1	Key Findings of Baseline High-Seismic Studies	4-22
4.5.2	Key Findings of Collapse Displacement Capacity Studies	4-23
4.5.3	Key Findings of Baseline Very High-Seismic Studies	4-24
4.5.4	Relationship between Strength and Collapse Displacement Capacity	4-25
4.5.5	Key Findings of SSI and Foundation Flexibility Studies	4-26
5.	Generic Collapse Performance.....	5-1
5.1	SDOF Study Purpose and Methods	5-1
5.1.1	Introduction	5-1
5.1.2	SDOF Models	5-2
5.1.3	Incremental Dynamic Analysis.....	5-4
5.1.4	Collapse Evaluation Criteria.....	5-5
5.2	SDOF Study Results	5-8
5.2.1	Peak Inelastic Displacement.....	5-8
5.2.2	Collapse Fragility Curves	5-9
5.2.3	Median Collapse Trends.....	5-13
5.2.3	<i>ACMR</i> and <i>ACMR/ACMR_{10%}</i>	5-15
5.3	Comparison of <i>ACMR</i> Results with those of Prior SDOF Studies	5-17
5.4	Notional Collapse Surfaces.....	5-18
5.4.1	Approach	5-19
5.4.2	Collapse Surface Metrics.....	5-19
5.4.3	SDOF Model Analysis and Collapse Results	5-22
5.4.4	Development of Notional Collapse Surfaces.....	5-26
6.	Paradox Solved	6-1
6.1	Resolution of the Short-Period Building Seismic Performance Paradox.....	6-1
6.1.1	Collapse Trends with Period Reversed.....	6-1
6.1.2	MCE_R Collapse Performance.....	6-3
6.2	Applicability to Other SFRSs of Short-Period Buildings	6-5
6.2.1	Conceptual Relationship.....	6-5
6.2.2	SFRSs of ASCE/SEI 7-16	6-7
6.3	Extrapolation to Other SFRSs of Short-Period Buildings	6-9
7.	Recommendations.....	7-1
7.1	Introduction.....	7-1
7.2	Recommendations for Improved Seismic Design Codes and Standards	7-1
7.3	Recommendations for Advanced Seismic Design and Analysis	7-7
7.4	Recommendations for Enhanced Modeling, Testing, and Data Collection	7-9
	References	A-1
	Project Participants.....	B-1

List of Figures

Figure 1-1	Trends in the probability of collapse of selected systems as a function of design period	1-3
Figure 2-1	Pie chart illustrating the distribution of the example inventory of FEMA MBTs of Table 2-2	2-5
Figure 2-2	Equal energy criterion of an elasto-plastic SDOF model	2-8
Figure 2-3	FEMA P-695 collapse results for bilinear SDOF systems modeled with 10 percent post-yield strain hardening without P-delta effects and collapse displacement capacity 10 times yield displacement	2-11
Figure 3-1	Percentage of wood and non-wood buildings assigned a red tag as a function of 0.3-second response spectral acceleration for five MMI regions (V–IX) based on post-earthquake safety inspections following the 1994 Northridge earthquake	3-6
Figure 3-2	Red Tag percentages as a function of 0.3-second spectral acceleration for post-1960 wood light-frame buildings for the 1994 Northridge earthquake, along with a best-fit lognormal collapse fragility curve and a theoretical collapse curve of newer W1 buildings	3-17
Figure 4-1	Isometric view of the two-story, high-seismic wood light-frame MFD archetype	4-6
Figure 4-2	Isometric view of the two-story, high-seismic reinforced masonry commercial archetype	4-7
Figure 4-3	Isometric view of the two-story, high-seismic steel SCBF commercial archetype	4-8
Figure 4-4	Schematic illustration of a three-dimensional one-story wood light-frame archetype model	4-10
Figure 4-5	Finite-element model for a two-story reinforced masonry archetype	4-12
Figure 4-6	Frame model for a two-story reinforced masonry archetype	4-13

Figure 4-7	Annotated steel SCBF model with callouts for component models	4-15
Figure 4-8	Schematic of spread footing with soil springs and dampers	4-16
Figure 4-9	MCE _R collapse probabilities of high-seismic baseline archetype models and those of comparable archetype models of prior FEMA P-695 studies plotted as a function of archetype design period (T), and benchmark (BM) values of MCE _R collapse probabilities and the MCE _R collapse-safety objective of ASCE/SEI 7	4-20
Figure 4-10	MCE _R collapse probabilities of high-seismic baseline archetype models and those of comparable archetype models of prior FEMA P-695 studies plotted as a function of pushover strength normalized by weight (V_{max}/W), and benchmark (BM) values of MCE _R collapse probabilities and the MCE _R collapse-safety objective of ASCE/SEI 7.....	4-21
Figure 4-11	MCE _R collapse probabilities of (a) high-seismic baseline archetype models and (b) those of comparable archetype models of prior FEMA P-695 studies plotted as a function of archetype design period (T), and benchmark (BM) values of MCE _R collapse probabilities and the MCE _R collapse-safety objective of ASCE/SEI 7	4-22
Figure 5-1	Example hysteretic behavior of SDOF models with periods, $T = 0.25$ seconds and $T = 0.50$ seconds and maximum strength, $V_{max} = 0.4W$	5-3
Figure 5-2	Example IDA results for the SDOF model with period, $T = 0.25$ seconds and maximum strength, $V_{max} = 0.4W$ showing median spectral accelerations at a story-drift ratio of 1.6 percent (corresponding to $\mu = 8$) and at a story-drift ratio of 7.5 percent (see Table 5-1)	5-4
Figure 5-3	Example collapse fragility curves of the SDOF model with maximum strength, $V_{max} = 0.4W$ and period, $T = 0.25$ seconds and corresponding collapse fractions.....	5-8
Figure 5-4	Peak elastic drift ratio versus median peak inelastic drift ratio for four SDOF model maximum strengths, where circles indicate design level response ($2/3 \times$ MCE _R)	5-9
Figure 5-5	Collapse fragility curves for SDOF models with maximum strength, $V_{max} = 0.2W$	5-10
Figure 5-6	Collapse fragility curves for SDOF models with maximum strength, $V_{max} = 0.4W$	5-11

Figure 5-7	Collapse fragility curves for SDOF models with maximum strength, $V_{max} = 0.6W$ 5-12
Figure 5-8	Collapse fragility curves for SDOF models with maximum strength, $V_{max} = 0.8W$ 5-13
Figure 5-9	Trends in the ratios of drift-based \hat{S}_{CT} to ductility-based \hat{S}_{CT} as function of model period for SDOF model maximum strengths, $V_{max} = 0.2W, 0.4W, 0.6W,$ and $0.8W$ assuming first-story failure for evaluation of drift-based \hat{S}_{CT} 5-14
Figure 5-10	Trends in the ratios of drift-based \hat{S}_{CT} to ductility-based \hat{S}_{CT} as function of model period for SDOF model maximum strengths, $V_{max} = 0.2W, 0.4W, 0.6W,$ and $0.8W$ assuming multi-story failure for evaluation of drift-based \hat{S}_{CT} 5-14
Figure 5-11	Plots of $ACMR$ and the ratio of $ACMR/ACMR10\%$ as a function of the model period of SDOF models evaluated using drift-based and ductility-based collapse displacement limits. Drift-based values of $ACMR$ are shown for SDOF models evaluated assuming (1) first-story failure and (2) multi-story failure. Also shown is a plot of $ACMR/ACMR10\%$ as a function of model period of SDOF models of comparable maximum strengths taken from Figure 3-1 of NIST GCR 12-917-20 5-15
Figure 5-12	Plots of $ACMR$ target data as a function of the model period of SDOF models evaluated using drift-based collapse displacement limits ($DR = 0.075$) assuming either (1) first-story failure or (2) multi-story failure and the corresponding predicted values of $ACMR$ excluding values for $T \leq 0.2$ seconds 5-28
Figure 5-13	Plots of notional collapse surfaces for SDOF models with periods, $T = 0.15$ seconds, $T = 0.25$ seconds, $T = 0.35$ seconds, and $T = 0.45$ seconds assuming first-story failure 5-29
Figure 5-14	Plots of notional collapse surfaces for SDOF models with periods, $T = 0.15$ seconds, $T = 0.25$ seconds, $T = 0.35$ seconds, and $T = 0.45$ seconds assuming multi-story failure 5-30
Figure 5-15	Values of $ACMR$ derived from Equation 5-4 using the first-story failure coefficients of Table 5-6 versus the values of $ACMR$ determined directly from FEMA P-695 collapse evaluations using detailed numerical models for wood light-frame commercial (COM), multi-family dwelling (MFD), and two-story single-family dwelling (SFD) building archetypes 5-33

Figure 6-1 Values of *ACMR* derived from Equation 5-4 using the first-story failure coefficients of Table 5-6 versus the values of *ACMR* determined directly from FEMA P-695 collapse evaluations using detailed numerical models for wood light-frame COM, MFD, and SFD archetypes; reinforced masonry COM archetypes; and steel SCBF COM archetypes..... 6-6

List of Tables

Table 2-1	Seismic-Force-Resisting Systems Permitted in High-Seismic Regions and Their Respective <i>R</i> Factors from Table 12.2-1, ASCE/SEI 7-16 and the Corresponding FEMA Model Building Type (MBT) from FEMA P-155.....	2-3
Table 2-2	Estimates of the Percentage of Residential (RES), Commercial (COM), and Other Occupancies (by Square Footage) of All Low-Rise Buildings in 19 Counties of Northern California.....	2-4
Table 3-1	Dates and Magnitudes of Selected Large-Magnitude (>M5.5) U.S. Earthquakes, 1964 through 2014, and Associated Fatalities and Building-Related Economic Losses	3-2
Table 3-2	Dates, Magnitudes, and Sources of Damage Data Used to Investigate the Collapse Performance of Short-Period Wood Light-Frame, Reinforced Masonry, and Steel SCBF Buildings in U.S., Japanese (JP), and New Zealand (NZ) Earthquakes.....	3-4
Table 3-3	Description of Damage to Steel Braced Frames in Past Earthquakes.....	3-12
Table 3-4	Summary of Observed Structural Damage to Steel Braced Frame Buildings in the 1994 Northridge Earthquake	3-14
Table 3-5	Red Tag Data by Census Tract for Post-1960 Wood Light-Frame Buildings for the 1994 Northridge Earthquake	3-16
Table 3-6	Tagging Data for Post-1960 Wood Light-Frame Buildings for the 1994 Northridge Earthquake.....	3-19
Table 4-1	Parametric Studies Used to Investigate the Collapse Performance of Short-Period Buildings.....	4-3
Table 4-2	Summary of Key Model Properties and Collapse Results of High-Seismic Baseline Archetype Models and Comparable Archetypes of Prior FEMA P-695 Studies of Short-Period Buildings Designed for High-Seismic Loads.....	4-17

Table 5-1	Summary of Ductility-Based and Drift-Based Collapse Displacements Used to Evaluate SDOF Study Models.....	5-6
Table 5-2	Summary of Adjusted Collapse Margin Ratios (<i>ACMRs</i>) of SDOF Models Evaluated for the Ductility-Based ($\mu = 8$) and Drift-Based (drift ratio, $DR = 0.075$) Collapse Displacements of Table 5-1.....	5-16
Table 5-3	Summary of Drift-Based Collapse Displacements as a Function of the Drift Ratio, <i>DR</i> , Used to Evaluate SDOF Models for Development of Notional Collapse Surfaces	5-23
Table 5-4	Summary of SDOF Model Properties, MCE_R Ground Motions, Strength Parameter (Ω/R), and 180 Values of <i>ACMR</i> of SDOF Models Assuming First-Story Failure	5-23
Table 5-5	Summary of SDOF Model Properties, MCE_R Ground Motions, Strength Parameter (Ω/R), and 180 Values of <i>ACMR</i> of SDOF Models Assuming Multi-Story Failure	5-25
Table 5-6	Summary of Coefficients Describing Notional <i>ACMR</i> Collapse Surfaces and Related Results of Multi-Linear Regression Analyses of SDOF Model Data	5-27
Table 5-7	Example Values of the MCE_R Collapse Probability for Values of <i>ACMR</i> Ranging from 1.0 to 4.0 and Values of the Total System Uncertainty Factor, β_{TOT} , Ranging from 0.5 to 0.7	5-31
Table 6-1	SFRSs Permitted in High-Seismic Regions by ASCE/SEI 7-16 and the Corresponding Studied SFRS Deemed Equivalent in Terms of Collapse Performance and the Corresponding FEMA Model Building Type (MBT) from FEMA P-155	6-8

This report summarizes the approaches, analyses, findings, conclusions, and recommendations for a series of studies on the gap between analytically predicted and historically observed earthquake-induced collapse rates for short-period buildings. It also presents a common understanding of the response behavior and collapse performance of short-period buildings subjected to strong earthquake ground motions. The Applied Technology Council (ATC) was commissioned by the Federal Emergency Management Agency (FEMA) to conduct these studies as part of the ATC-116 Project series, “Solutions to the Issue of Short Period Building Performance.”

Short-period buildings, such as low-rise residential and commercial buildings, comprise a major portion of the building stock in U.S. communities with high-seismic hazard. The gap between analytically predicted and historically observed collapse rates for short-period buildings exists across many seismic-force-resisting systems and construction materials. As a result, it is believed that the seismic collapse performance for short-period buildings is not accurately predicted by current analytical models. Based on a review of previous studies and available research and data, three seismic-force-resisting systems were selected for detailed investigation in the ATC-116 Project series: wood light-frame walls with wood structural panel sheathing (herein referred to as “wood light-frame”), special reinforced masonry shear wall (herein referred to as “reinforced masonry”), and steel special concentrically braced frame (SCBF) systems.

The FEMA P-2139 series of reports include the following:

- FEMA P-2139-1, *Short-Period Building Collapse Performance and Recommendations for Improving Seismic Design, Volume 1 – Overarching Findings, Conclusions, and Recommendations*
- FEMA P-2139-2, *Short-Period Building Collapse Performance and Recommendations for Improving Seismic Design, Volume 2 – Study of One-to-Four Story Wood Light-Frame Buildings*
- FEMA P-2139-3, *Short-Period Building Collapse Performance and Recommendations for Improving Seismic Design, Volume 3 – Study of One-to-Four Story Special Reinforced Masonry Shear Wall Buildings*

- FEMA P-2139-4, *Short-Period Building Collapse Performance and Recommendations for Improving Seismic Design, Volume 4 – Study of One-to-Four Story Steel Special Concentrically Braced Frame Buildings*

1.1 Background and Purpose

At the time the ATC-116 Project series began, commercial and multi-family residential buildings were designed in accordance with ASCE/SEI 7-10, *Minimum Design Loads for Buildings and Other Structures* (ASCE, 2010), which was adopted by reference in the 2015 edition of the *International Building Code* (IBC) (ICC, 2015a). Design seismic loads in ASCE/SEI 7-10 are based on the risk-targeted maximum considered earthquake (MCE_R) ground motions, which were introduced in FEMA P-750, *NEHRP Recommended Seismic Provisions for New Buildings and Other Structures* (FEMA, 2009a). Buildings designed and constructed in accordance with national model codes and seismic design standards (e.g., ASCE/SEI 7-10) are expected to meet general seismic performance targets, which are described in terms of not exceeding a specified probability of collapse given MCE_R ground motions. For reference, a collapse probability of no more than 10 percent, given MCE_R ground motions, is the anticipated “reliability” in ASCE/SEI 7-10 (Table C1.3.1b) for Risk Category II buildings, which constitute the vast majority of all buildings. Further, the use of MCE_R ground motions in building design is intended to provide a reasonable assurance of seismic performance for all buildings—regardless of building period, seismic-force-resisting system, or other characteristic—designed in accordance with the governing building code.

Studies conducted prior to the ATC-116 Project series have used the methodology described in FEMA P-695, *Quantification of Building Seismic Performance Factors* (FEMA, 2009b), to evaluate the collapse performance of common code-permitted seismic-force-resisting systems. For example, one widely cited collapse performance study is described in NIST GCR 12-917-20, *Tentative Framework for Development of Advanced Seismic Design Criteria for New Buildings* (NIST, 2012). This and other similar studies have shown that many seismic-force-resisting systems achieve the collapse performance target (i.e., less than a 10 percent probability of collapse given MCE_R ground motions). However, these studies have also found that shorter-period buildings have calculated probabilities of collapse that are larger than those of longer-period buildings and generally exceed the 10 percent target for acceptable collapse performance.

This can be observed in Figure 1-1, taken from NIST GCR 12-917-20. The figure plots the calculated collapse probabilities for groups of structural

systems, as identified in Table 12.2-1 of ASCE/SEI 7-10, over a range of periods. Bearing wall systems (diamonds) include special reinforced masonry shear walls (A.7), ordinary reinforced masonry shear walls (A.9) and light-frame (wood) walls with wood structural panel sheathing (A.15). Building frame systems (squares) include steel special concentrically braced frames (B.2), special reinforced concrete shear walls (B.4), ordinary reinforced concrete shear walls (B.5), and steel buckling-restrained braced frames (B.25). Moment frame systems (triangles) include steel special moment frames (C.1), special reinforced concrete moment frames (C.5), and ordinary reinforced concrete moment frames (C.7)

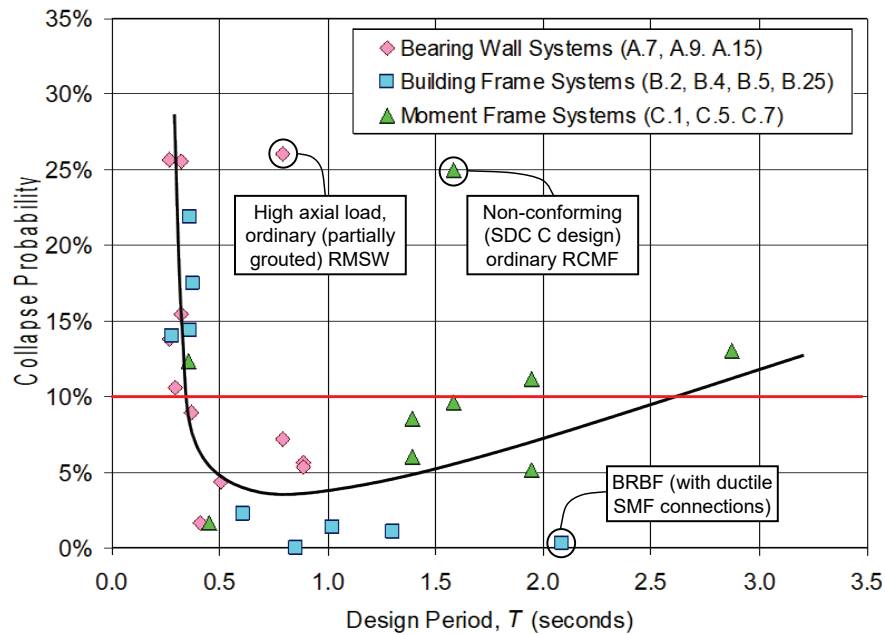


Figure 1-1 Trends in the probability of collapse of selected systems as a function of design period (adapted from NIST, 2012).

In the figure, FEMA P-695 collapse performance studies on a variety of structural systems over a range of periods suggest that, for systems with design periods less than about 0.5 seconds, the probability of collapse given MCE_R ground motions increases significantly as the design period decreases. If these analytical predictions are accurate, then the goal of acceptable collapse performance for all seismic-force-resisting systems at all building periods is not being achieved, and short-period buildings are exceeding the 10 percent collapse performance target of ASCE/SEI 7.

The importance of building period on the calculation of peak response of inelastic systems dates back to studies of response and design spectra in the 1960s and 1970s by Veletsos, Newmark, and others (e.g., Veletsos and Newmark, 1960). These studies found that the ratio of inelastic displacement to elastic displacement of simple single-degree-of-freedom (SDOF)

numerical models was period dependent and increased as the periods of the numerical models decreased, implying worse collapse performance for short-period buildings.

Findings from other numerical studies of earthquake response and collapse performance are consistent and suggest that seismic design coefficients (e.g., R) could be period dependent or more stringent for shorter-period buildings (e.g., Miranda and Bertero, 1994). Although ASCE/SEI 7 does not include period-dependent seismic modification factors, the underlying concepts can be found in other seismic codes. For example, Section 5.2.3 of Eurocode 8 (CEN, 2004) increases inelastic seismic demands as a function of period for detailing of reinforced-concrete elements in areas of plastic hinging when the building period is relatively short (i.e., T less than T_s , where T_s is the code-defined transition period between spectral response domains of constant acceleration and constant velocity). Explicit incorporation of period-dependent properties can also be found in the “coefficient method” of ASCE/SEI 41-17, *Seismic Evaluation and Retrofit of Existing Buildings* (ASCE, 2017).

Trends in observed earthquake damage of short-period buildings, however, do not support the high collapse probabilities shown in Figure 1-1. Analysis of available historical data on short-period building performance is described in Chapter 3. For example, based on data compiled by the California Office of Emergency Services (OES, 1995) from the 1994 Northridge earthquake, the fraction of all inspected wood-frame buildings that were posted with an ATC-20 Restricted Use (yellow) placard or an Unsafe (red) placard (ATC, 1989; 2005) suggests that collapse risk for this class of short-period buildings is not elevated, which is contrary to the results of analytical studies used to predict collapse probabilities. Because observed damage in short-period buildings is less than would be implied by the body of analytical results available in the literature, the opinion of many structural engineers suggests that numerical models overestimate the actual collapse risk of short-period buildings.

The apparent discrepancy between analytical prediction of collapse performance and the opinions and observations of structural engineers has been designated the *short-period building seismic performance paradox*. With the standardized collapse evaluation methodology of FEMA P-695, additional testing of structural elements and assemblies, and the evolution of high-speed computer processing, we now have the capability to effectively investigate and resolve this paradox.

Given this context, the purpose of the ATC-116 Project series was to investigate the response behavior and collapse performance of different structural systems. The results of this work are intended to:

- Identify the causes of the short-period building seismic performance paradox, quantify factors contributing to short-period building performance, and develop solution concepts.
- Improve and validate numerical modeling methods for short-period buildings to more accurately capture response behavior and collapse performance characteristics.
- Improve code seismic design methods and engineering practices for short-period buildings so that seismic performance targets are achieved across all seismic-force-resisting systems and all design periods.
- Inform future research so that better data and improved numerical modeling can be used in the development of more efficient and effective structural systems, seismic assessment methodologies, and engineering design procedures.

1.2 Approach and Scope

A phased approach for investigation was developed and presented in the ATC-116 report, *Roadmap for Solutions to the Issue of Short Period Building Performance* (ATC, 2015). Many factors are thought to contribute to the apparent discrepancy between analyzed and observed seismic performance of short-period buildings. Reasons for the paradox could include an underestimation of the peak strength and post-peak capacity of short-period buildings, an overestimation of the demands on short-period buildings, or a combination of both. Possible causes include building configuration issues (e.g., incorporation of all structural and nonstructural components, including interior and exterior wall finishes, that contribute to building strength and stiffness), hysteretic response backbone curve issues (e.g., realistic characterization of peak strength and collapse displacement capacity), and other factors (e.g., soil-structure interaction and foundation flexibility) that affect building response behavior and collapse performance.

The overall approach was to: (1) establish benchmarks for the historically observed performance of short-period buildings; (2) conduct parametric analytical studies on archetypical short-period buildings using advanced numerical models and the latest available research and test data; and (3) identify modeling parameters or building characteristics that provide the best match between the simulated and benchmark performance.

Although there are a number of parameters by which seismic performance can be measured, these studies were primarily interested in collapse performance as measured by the conditional probability of collapse given a ground motion intensity (e.g., MCE_R ground motions), based on observations from historical earthquake data, as described in Chapter 3, or collapse statistics obtained from incremental dynamic analysis (IDA), as described in Chapter 4.

For the purpose of these studies, short-period buildings were defined as those with first-mode periods less than about 0.5 seconds, which typically corresponds to buildings that are one-to-four stories in height. Studies investigated different systems, configurations, and materials commonly used in the United States for design and construction of new short-period buildings in regions of moderate, high, and very high seismicity.

A suite of archetypes, with variations in occupancy, height, and seismic design level, was selected for each of the seismic-force-resisting systems investigated: wood light-frame, reinforced masonry, and steel SCBF. These systems, in aggregate, are used in most low-rise buildings, as described in Chapter 2. Archetypes were intended to represent code-compliant modern construction for occupancies classified under Risk Category II. Three occupancies were selected for study: (1) single-family dwellings (SFD); (2) multi-family dwellings (MFD); and (3) commercial (COM) buildings.

Archetype design methods and details represented typical modern practice exercised in areas of significant seismicity based on the usual and customary standard of care. Archetype configurations for each occupancy were selected to be realistic and representative of actual buildings in terms of size and proportion. They were designed to meet code-minimum base shear strength requirements, but were not biased with overstrength through deliberate conservatism in the design or understrength caused by the use of wall configurations or member sizes that would be considered unrealistic based on gravity load or architectural considerations. More details about the selected archetypes and their seismic design criteria are provided in Chapter 4.

The archetype designs provided the basis for three-dimensional numerical models that were used for IDA. These models, which are described in more detail in Chapter 4, incorporated advanced nonlinear techniques for analytically predicting the performance of structures. Using FEMA P-695 procedures, the IDA results provided collapse performance metrics in terms of the conditional probability of collapse given MCE_R ground motion.

To investigate the apparent discrepancy between analyzed and observed seismic performance of short-period buildings, a series of parametric studies

was performed. For example, the study of wood light-frame systems investigated the effects of nonstructural sheathing on interior and exterior structural walls and interior partitions, and the studies of all three systems investigated the effects of soil-structure interaction and foundation flexibility. The specific parametric studies that were investigated varied by seismic-force-resisting system and are described in more detail in Chapter 4. “Baseline” models considered the results of other parametric studies and incorporated a best estimate for each parameter to provide an overall best estimate of the simulated response of each short-period system. The collapse results from the baseline models, along with the benchmark targets, are provided in Chapter 4 and compared with results from prior FEMA P-695 studies.

In addition to the detailed system-specific studies, this investigation into short-period buildings included a collapse performance study using bilinear SDOF models. Collapse performance was evaluated for the same set of SDOF models for two different collapse displacement limits: (1) collapse displacement capacity based on an assumed displacement ductility of the SDOF model; and (2) collapse displacement capacity based on an assumed drift capacity of the SDOF model. The former criterion is consistent with prior FEMA P-695 studies, whereas the latter criterion is consistent with the detailed system-specific studies. Chapter 5 describes the SDOF study and presents the results of the different collapse displacement limits on collapse performance. The SDOF study helps to explain the short-period building seismic performance paradox. Further, the results are used to illustrate a notional relationship, represented by “collapse surfaces,” between short-period building collapse performance and key building response properties, such as strength and displacement capacity. As described in Chapter 6, collapse surfaces could provide a means for extending the results of the detailed system-specific studies to other seismic-force-resisting systems that were not explicitly investigated.

1.3 Organization and Content

This report summarizes the studies of the response behavior and collapse performance of short-period wood light-frame, reinforced masonry, and steel SCBF buildings. More details about each study are included in the three other reports comprising the FEMA P-2139 series of reports. This report presents a common understanding of the response behavior and collapse performance of short-period buildings and describes the resolution of the short-period building seismic performance paradox by drawing from the results and conclusions of the three system-specific studies. Additional information, which is not discussed in the other reports, is presented about the historical context of the short-period building seismic performance paradox and about the collapse

performance study using SDOF models. An explanation of the resolution of the short-period building seismic performance paradox is provided in Chapter 6, along with a discussion about the applicability of the findings to other seismic-force-resisting systems. The report ends with recommendations for improved seismic design, engineering practice, and research.

Chapter 2 presents a rationale for the selection of the three seismic-force-resisting systems investigated through detailed studies and presents background information about prior numerical studies that led to the development of the short-period building seismic performance paradox.

Chapter 3 summarizes fatalities and economic losses in major U.S. earthquakes, observed collapse performance of short-period buildings in U.S., Japanese, and New Zealand earthquakes, and the development of benchmark collapse metrics that are used in Chapter 4 to verify the reliability of improved numerical models of short-period buildings.

Chapter 4 discusses the designs and configurations of the archetypes used in the system-specific studies, presents the parametric studies, summarizes the results from the system-specific studies, compares the results with the target benchmarks and results from prior FEMA P-695 studies, and describes the key findings that are applicable to all three seismic-force-resisting systems.

Chapter 5 presents the methods and results of the collapse performance study using SDOF models, compares the results to those of prior SDOF studies, and uses the results from the SDOF models to illustrate a notional relationship between short-period building collapse performance and key building response properties.

Chapter 6 describes the resolution of the short-period building seismic performance paradox by drawing from data on the observed performance of short-period buildings in past earthquakes and the results of the system-specific studies and the collapse performance study using SDOF models. The chapter includes a discussion about the applicability of the findings of the system-specific studies to other seismic-force-resisting systems permitted by ASCE/SEI 7 and ends with a conceptual extrapolation of the system-specific studies and the collapse trends from the SDOF models to the prediction of short-period building collapse as a function of key building response properties.

Chapter 7 presents key recommendations that are common to all three of the systems investigated through detailed studies.

References and a list of project participants are provided at the end of this report.

Short-Period Building Background

This chapter provides a rationale for the three seismic-force-resisting systems (SFRS) selected for detailed study, describes the short-period building seismic performance paradox, and presents background information about prior analytical studies of bilinear single-degree-of-freedom models that contributed to the paradox.

2.1 Selection of Short-Period Building Systems for Detailed Studies

Currently, commercial and multi-family residential buildings are designed in accordance with ASCE/SEI 7-16, *Minimum Design Loads and Associated Criteria for Buildings and Other Structures* (ASCE, 2016), which is adopted by reference in the 2018 edition of the *International Building Code* (IBC) (ICC, 2018a). Residential one-family and two-family dwellings can be constructed in accordance with the 2018 edition of the IBC or the *International Residential Code* (IRC) (ICC, 2018b). However, when this investigation into short-period buildings began in 2013, commercial and multi-family residential buildings were designed in accordance with ASCE/SEI 7-10, which was adopted by reference in the 2015 edition of the IBC, and residential one-family and two-family dwellings could be constructed in accordance with the 2015 edition of the IBC or IRC (ICC, 2015b). These national model codes and seismic design standards were used for the design of the short-period archetypes of wood light-frame, reinforced masonry, and steel SCBF buildings in three detailed system-specific studies. However, there would be no significant differences in the designs and hence seismic performance of these short-period building archetypes had they been designed to current (2018) codes and standards.

For the purpose of these studies, short-period buildings were defined as those with first-mode periods less than 0.5 seconds, corresponding approximately to the theoretical spectral domain of “constant acceleration,” where values of design response spectral acceleration are the same at all short periods. As such, a 0.1-second building is designed for the same earthquake forces as those required for design of a 0.5-second building with the same SFRS.

Wood light-frame buildings have traditionally been used for low-rise commercial buildings and multi-family and single-family dwellings. Recent construction trends, however, have shown increased construction of taller wood light-frame buildings (e.g., four story and five story), many of which are constructed on top of a podium base having a structural system of structural steel or concrete (cast-in-place or precast) construction. With the possible exception of buildings five stories or taller, all wood light-frame buildings would typically be considered short-period buildings.

ASCE/SEI 7-16 recognizes two classes of buildings using either masonry or reinforced concrete shear walls: (1) Bearing Wall Systems; where the shear walls resist the gravity loads in addition to the seismic loads; and (2) Building Frame Systems, where an independent system carries the gravity loads and the masonry or reinforced concrete shear walls resist the seismic loads. The estimated first-mode period of masonry or reinforced concrete shear wall buildings is a function of the length of shear walls within the building. Consequently, for a given building, the use of greater total length of shear walls will result in a shorter first-mode period. Given both specified and practical height limitations, all masonry and reinforced concrete shear wall buildings with rigid floor and roof diaphragms are likely short-period buildings, with the possible exception of this class of buildings exceeding about 75 feet in height.

ASCE/SEI 7-16 also recognizes steel frame building with either concentric, eccentric, or buckling-restrained bracing schemes within the Building Frame Systems classification. The eccentric and buckling-restrained bracing systems are considered more ductile and more flexible than a concentric bracing system. Typically, concentrically braced buildings less than 75 feet in height are considered short-period buildings, whereas eccentrically or buckling-restrained braced buildings not much more than 40 feet in height are considered short-period buildings.

Table 12.2-1 of ASCE/SEI 7-16 specifies design parameters and limitations for a total of 85 SFRSs, of which 18 are Bearing Wall systems, 26 are Building Frame systems, and 12 are Moment-Resisting Frame systems. Any of these systems could be used as the SFRS of a short-period building, although not all would be permitted in regions of high or very high seismicity (i.e., not permitted as a Seismic Design Category, SDC, D or E SFRS). Table 2-1 lists the seven Bearing Wall systems, the 15 Building Frame systems, and the 7 Moment-Resisting Frame systems permitted in regions of high seismicity, along with their respective values of the response modification factor (R) and the corresponding FEMA Model Building Type (MBT), as described in FEMA P-155, *Rapid Visual Screening of Buildings for Potential Seismic Hazards: Supporting Documentation* (FEMA, 2015).

Table 2-1 Seismic-Force-Resisting Systems Permitted in High-Seismic Regions and Their Respective *R* Factors from Table 12.2-1, ASCE/SEI 7-16 and the Corresponding FEMA Model Building Type (MBT) from FEMA P-155

No.	Description	<i>R</i> Factor	FEMA MBT
Bearing Wall Systems			
A.1	Special reinforced concrete shear walls	5	C2
A.5	Intermediate precast shear walls	4	PC1, PC2
A.7	Special reinforced masonry shear walls	5	RM1, RM2
A.15	Light-frame (wood) walls with rated wood structural panels	6 1/2	W1, W1A, W2
A.16	Light-frame (CFS) walls with rated wood structural panels	6 1/2	W1, W1A, W2
A.17	Light-frame walls with shear panels of all other materials	2	W1, W1A, W2
A.18	Light-frame (CFS) walls with flat strap bracing	4	S3
Building Frame System			
B.1	Steel eccentrically braced frames	8	S2
B.2	Steel special concentrically braced frames	6	S2
B.3	Steel ordinary concentrically braced frames	3 1/4	S2
B.4	Special reinforced concrete shear walls	6	C2
B.8	Intermediate precast shear walls	5	PC1, PC2
B.10	Steel/concrete composite eccentrically braced frames	8	S2, C2
B.11	Steel/concrete composite special concentrically braced frames	5	S2, C2
B.13	Steel/concrete composite plate shear walls	3	-
B.14	Steel/concrete composite special shear walls	6 1/2	-
B.16	Special reinforced masonry shear walls	5 1/2	RM1, RM2
B.22	Light-frame wood with rated-wood sheathed shear walls	7	W1, W1A, W2
B.23	Light-frame (CFS) with rated-wood or steel sheet shear walls	7	W1, W1A, W2
B.24	Light-frame walls with other sheathing materials	2 1/2	W1, W1A, W2
B.25	Steel buckling-restrained braced frames	8	S2
B.26	Steel special plate shear walls	7	-
Moment-Resisting Frame Systems			
C.1	Steel special moment frames	8	S1
C.2	Steel special truss moment frames	7	S1
C.3	Steel intermediate moment frame	4 1/2	S1
C.5	Special reinforced concrete moment frames	8	C1
C.8	Steel/concrete composite special moment frames	8	S1, C1
C.9	Steel/concrete composite intermediate moment frames	5	S1, C1
C.10	Steel/concrete composite partially restrained moment frames	6	-
C.12	Cold-formed steel – special bolted moment frame	3 1/2	S3

The three SFRSs selected for study (A.7, A.15, and B.2) are bolded in Table 2-1. Systems not permitted as an SDC D or SDC E SFRS are omitted from Table 2-1, since the focus of this investigation was on the performance of

short-period buildings in regions of significant seismicity. The MBT is used with regional inventory data to establish which SFRSs are more common than others for construction of modern residential, commercial, or other low-rise building occupancies (Table 2-2). SFRSs without an MBT in Table 2-1 indicate systems rarely used for construction of short-period buildings.

Of the three systems selected for study, the wood light-frame SFRS is by far the most common used for construction of short-period buildings. For example, Table 2-2 provides an estimate of the percentage of low-rise residential (RES), commercial (COM) and other occupancies extracted from a HAZUS inventory of about two million buildings in 19 counties of Northern California (Kircher et al., 2006a). Other occupancies include industrial, agricultural, educational, government, and religious buildings. The inventory of Table 2-2 lists all FEMA MBTs but excludes the square footage of older (pre-1940) buildings, manufactured housing (MH), and the three (C3, S5, and URM) MBTs that are no longer permitted by modern seismic codes. Non-zero percentages for unreinforced masonry (URM) buildings indicate inventory that has been seismically retrofitted. The percentages shown in Table 2-2 represent roughly 80 percent of all low-rise buildings in the 19-county region of Northern California.

Table 2-2 Estimates of the Percentage of Residential (RES), Commercial (COM), and Other Occupancies (by Square Footage) of All Low-Rise Buildings in 19 Counties of Northern California

ID	FEMA MBT Description	RES	COM	Other	All
W1	One & two family detached wood frame dwelling <5000 square feet	65.1%	0.00%	0.30%	65.4%
W1A	Wood frame residential >5000 square feet	7.23%	0.00%	0.00%	7.23%
W2	Wood frame commercial and industrial	0.00%	4.06%	0.56%	4.63%
S1	Steel moment frame	0.08%	1.05%	0.70%	1.83%
S2	Steel braced frame	0.09%	0.44%	0.77%	1.30%
S3	Light pre-manufactured steel	0.10%	0.38%	0.39%	0.87%
S4	Steel frame with concrete shear walls	0.32%	0.43%	0.16%	0.91%
S5	Steel frame with infill masonry walls	0.0%	0.0%	0.0%	0.0%
C1	Concrete moment frame	0.03%	0.32%	0.03%	0.37%
C2	Concrete shear wall	0.76%	2.30%	0.89%	3.94%
C3	Concrete frame with infill masonry walls	0.00%	0.00%	0.02%	0.02%
PC1	Tilt-up concrete shear walls	0.00%	1.98%	0.98%	2.96%
PC2	Precast concrete frame or walled building	0.03%	0.31%	0.16%	0.50%
RM1	Reinforced masonry bearing walls with flexible diaphragm	1.50%	3.61%	1.09%	6.20%
RM2	Reinforced masonry bearing walls with stiff diaphragm	0.02%	0.49%	0.13%	0.64%
URM	Unreinforced masonry bearing walls	0.03%	0.07%	0.01%	0.10%
MH	Manufactured Housing	0.00%	0.00%	0.00%	0.00%
	All Low-Rise FEMA MBTs	77.7%	15.9%	6.4%	100%

Figure 2-1 is a pie chart illustrating the distribution of the example inventory of FEMA MBTs of Table 2-2, indicating the relative use of wood light-frame (W1, W1A and W2), reinforced masonry (RM) and steel braced frame (S2) MBTs, the three SFRSs studied by this project series.

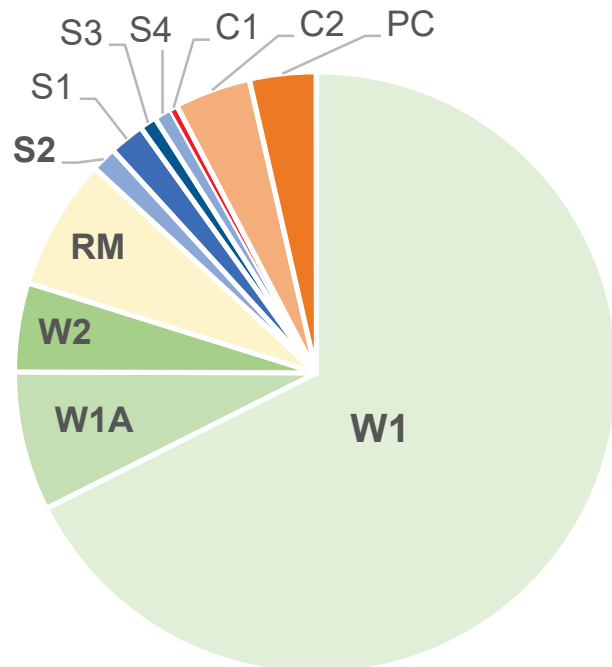


Figure 2-1 Pie chart illustrating the distribution of the example inventory of FEMA MBTs of Table 2-2.

Manufactured housing represents a significant percentage of MBT square footage excluded from Table 2-2 (and Figure 2-1). Manufactured housing (e.g., mobile homes) is excluded from Table 2-2 since manufactured housing is not subject to the building code requirements of either the IBC or the IRC and is not an SFRS included in Table 12.2-1 of ASCE/SEI 7-16.

Manufactured housing is inherently rugged and factory-built in accordance with federal standards but typically installed without adequate seismic bracing below the chassis and, as a result, has performed poorly in past earthquakes, such as by shifting and falling off of support piers.

In terms of square footage, the low-rise building inventory of Table 2-2 supports the selection of the wood light-frame system (A.15 in Table 2-1), which represents about 77.3 percent of all modern low-rise buildings with SFRSs included in ASCE/SEI 7-16, and special reinforced masonry shear walls (A.7 in Table 2-1), which represents the next most commonly used SFRS, about 6.8 percent of all modern low-rise buildings with SFRSs included in ASCE/SEI 7-16. The third system investigated by this project, steel SCBFs (B.2 in Table 2-1), represents only about 1.3 percent of all modern low-rise buildings but proved to be informative, in particular with

respect to rocking response (of braced frames on strip foundations), which is likely applicable to other low-rise SFRSs that can rock rather than yield. The three systems selected for study represent more than 85 percent of the square footage of all buildings in Table 2-2. By count, rather than square footage, the three systems selected for study represent more than 90 percent of all modern low-rise buildings with SFRSs included in ASCE/SEI 7-16 since the most common low-rise MBT (W1) is typically much smaller than other low-rise MBTs. Although these building inventory statistics are based on a sample of modern construction in Northern California, they are generally representative of modern construction in other high-seismic regions of the United States.

Other commonly used systems that were not explicitly evaluated include: (1) special reinforced concrete shear walls (B.4 in Table 2-1), which represent about 3.9 percent of all modern low-rise buildings (C2 in Table 2-2); (2) intermediate pre-cast shear walls (A.5 in Table 2-1), which represent about 3.5 percent of all modern low-rise buildings (PC1 and PC2 in Table 2-2); and (3) steel special moment frames (C.1 in Table 2-1), which represent about 1.8 percent of all modern low-rise buildings (S1 in Table 2-2). Due to the similarity of the materials and construction, the findings of the study of the special reinforced masonry shear walls are informative with respect to special reinforced concrete shear walls.

Intermediate pre-cast concrete shear walls, typically used for tilt-up buildings, performed poorly in the 1994 Northridge earthquake. Precast concrete panels collapsed out-of-plane due to failure of the diaphragm, the diaphragm-to-wall connections, or both. Tilt-up building collapse was due to a mode of failure not related to the in-plane design capacity of the pre-cast concrete shear walls. Following the 1994 Northridge earthquake, significant changes were made to the seismic-design requirements of diaphragms and diaphragm-to-wall connections intended to preclude out-of-plane failures of shear walls, but there has not yet been a significant earthquake “test” of these newer tilt-up buildings. Similar arguments can be made for not selecting the steel special moment frame for study. Significant and extensive damage to the beam-to-column connections of welded-steel moment frame buildings was observed in the 1994 Northridge earthquake, which led to major research (i.e., the SAC Steel Project) and a comprehensive set of changes to the design requirements for steel special moment frame buildings, but there has not yet been a significant earthquake “test” of these newer steel special moment frame buildings.

2.2 Short-Period Building Seismic Performance Paradox

Prior FEMA P-695 collapse evaluations have been performed for a large number of archetype models of common SFRSs designed in accordance with the IBC and ASCE/SEI 7, all of which exhibit similar behavior for archetypes with short periods. As shown in Figure 1-1, for archetypes of SFRSs with a design period less than about 0.5 seconds, prior FEMA P-695 studies suggest that the probability of collapse given MCE_R ground motions increases significantly as the design period decreases.

Collapse results shown in Figure 1-1 are taken from NIST GCR 12-917-20, which summarizes results from two original sources: (1) the example applications of special and ordinary reinforced concrete moment frame and wood light-frame building systems of Chapter 9 of FEMA P-695; and (2) the trial applications of seven additional SFRSs of NIST GCR 10-917-8, *Evaluation of the FEMA P-695 Methodology for Quantification of Building Seismic Performance Factors* (NIST, 2010). The purpose of the FEMA P-695 methodology is to provide a rational basis for determining values of global seismic performance factors, including the response modification factor (R), the system overstrength factor (Ω_0), and the deflection amplification factor (C_d) of a new (proposed) SFRS.

The example and trial applications of the FEMA P-695 methodology evaluated existing SFRSs as if they were proposed as new SFRSs. As such, the designs of the archetypes of the various systems were based on “code-minimum” requirements (e.g., minimum shear wall length, minimum amount of bracing) and did not include structural elements or nonstructural components (e.g., interior and exterior wall finishes) not part of the SFRS, which, if included, would add strength and stiffness to the archetypes. This investigation into short-period buildings has found that the numerical methods used to model nonlinear response behavior of archetypes of prior studies generally underestimated the peak strength and collapse displacement capacity of actual buildings. For these reasons, the results of example and trial applications of the FEMA P-695 methodology shown in Figure 1-1 tend to overstate the collapse risk of actual short-period buildings. Detailed comparisons of analytical results from this investigation to those from prior FEMA P-695 collapse studies are presented in Chapter 4, and a complete explanation of the resolution of the short-period building seismic performance paradox is provided in Chapter 6. The next section provides more background information about the origins of the short-period building seismic performance paradox and highlights a fundamental problem with a key assumption underlying the prior studies that led to the paradox.

2.3 Prior Analytical Studies of Bilinear SDOF Models

The trend of increased collapse probability for short-period buildings shown in Figure 1-1 is consistent with studies of bilinear (e.g., elasto-plastic) single-degree-of-freedom (SDOF) models dating to the original work in the 1960s and 1970s by Veletsos, Newmark, and others (Veletsos and Newmark, 1960; Veletsos et al., 1965). These studies developed theoretical concepts relating inelastic response spectra to elastic response spectra as a function of ductility, μ , defined as the ratio of maximum inelastic displacement, δ_I , of the SDOF model to the yield displacement, δ_Y , of the SDOF model (i.e., $\mu = \delta_I/\delta_Y$). In the domain of constant acceleration (i.e., when the period, T , of the SDOF model is about 0.125 seconds to 0.5 seconds), the studies found that the maximum inelastic displacement (δ_I) of the yielded SDOF model was greater than the elastic displacement, δ_E , of the model if it were to remain linearly elastic, as shown in Equation 2-1. Equation 2-2 shows the relationship between the yield strength (F_I) and the maximum elastic force, F_E , that would have been developed by the SDOF model if it were to remain linearly elastic.

$$\frac{\delta_I}{\delta_E} = \frac{\mu}{\sqrt{2\mu - 1}} \quad (0.125 \text{ s} \leq T \leq 0.50 \text{ s}) \quad (2-1)$$

$$\frac{F_I}{F_E} = \frac{1}{\sqrt{2\mu - 1}} \quad (0.125 \text{ s} \leq T \leq 0.50 \text{ s}) \quad (2-2)$$

The relationship of inelastic-to-elastic response is based on the equal energy criterion, as illustrated in Figure 2-2. Although useful to illustrate concepts, the bilinear, elasto-perfectly plastic curve shown in Figure 2-2 is not how real structures yield. The curvilinear response of real structures is quite different, as characterized by the advanced numerical models of short-period buildings presented in Chapter 4.

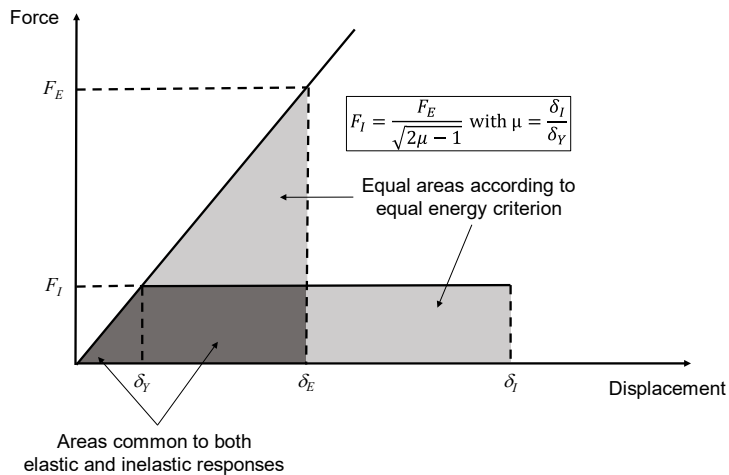


Figure 2-2 Equal energy criterion of an elasto-plastic SDOF model.

In the domain of constant velocity (i.e., when the period, T , of the SDOF model is about 1 second or greater), the maximum inelastic displacement, δ_I , of the yielded SDOF model is equal to the elastic displacement, δ_E , of the SDOF model if it were to remain linearly elastic, and as a consequence, the yield strength (F_I) is related to the maximum elastic force, F_E , that would have been developed if the model were to remain linearly elastic.

$$\frac{\delta_I}{\delta_E} = 1.0 \quad (T \geq 1.0 \text{ s}) \quad (2-3)$$

$$\frac{F_I}{F_E} = \frac{1}{\mu} \quad (T \geq 1.0 \text{ s}) \quad (2-4)$$

The ratio δ_I/δ_E increases from 1.0 at 1.0 second to $\mu / \sqrt{2\mu - 1}$ at 0.5 seconds, and the ratio F_I/F_E decreases from $1/\mu$ at 1.0 second to $1/\sqrt{2\mu - 1}$ at 0.5 seconds. Chapter 2 of *Earthquake Spectra and Design* (Newmark and Hall, 1982) provides a more complete description of the methods for developing inelastic spectra from elastic spectra. Equation 2-3 has become commonly known as the “equal displacement rule,” wherein lateral displacements for an inelastic system, δ_I , are approximately equal to the elastic displacements, δ_E , of an elastic system of the same initial stiffness. The original work of Veletsos, Newmark, and others is remarkable because it was based largely on a hypothesis verified for a limited number of strong earthquake ground motion records available at that time (circa 1960). The number of strong-motion earthquake records increased significantly after the 1971 San Fernando earthquake, and much larger sets of strong earthquake ground motion records became available from the U.S. Geological Survey (USGS) and the California Division of Mines and Geology, now known as the California Geological Survey (CGS).

A host of other researchers (Qi and Moehle, 1991; Krawinkler and Nasser, 1992; Miranda and Bertero, 1994; Miranda, 2000; Ruiz-Garcia and Miranda, 2003 and 2004; Chopra and Chintanapakdee, 2004) and related research studies, such as those documented in FEMA 440, *Improvement of Nonlinear Static Analysis Procedures* (FEMA, 2005), and FEMA 440A, *Effects of Strength and Stiffness Degradation on Seismic Response* (FEMA, 2009c), have found similar relationships that were based on systematic response history analysis of bilinear SDOF models using more robust sets of available earthquake ground motions. These studies were driven largely by two related areas of research interest: (1) performance-based design; and (2) displacement-based design, both of which require realistic estimates of peak inelastic response. These studies either influenced or helped to refine the original performance-based design methods of FEMA 273, *NEHRP Guidelines for the Seismic Rehabilitation of Buildings*

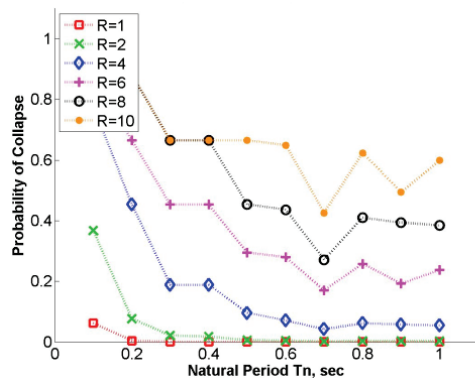
(FEMA, 1997), which guided the development of FEMA 356, *Prestandard and Commentary for the Seismic Rehabilitation of Buildings* (FEMA 2000), which can now be found in ASCE/SEI 41-17, *Seismic Evaluation and Retrofit of Existing Buildings* (ASCE, 2017).

Three important refinements to the theoretical concepts of the original studies evolved. First, using actual earthquake records, the ratio of inelastic-to-elastic response at short periods was found to vary continuously with period (i.e., the ratio of peak inelastic-to-elastic displacement was not the same for all response periods from 0.125 seconds to 0.50 seconds), increasing most significantly at very short periods. Second, inelastic response at short periods was related to the ratio of elastic strength demand to yield strength (e.g., the $\mu_{strength}$ parameter of ASCE/SEI 41-17), rather than to the displacement ductility demand parameter (μ). Conceptually, the $\mu_{strength}$ parameter of ASCE/SEI 41-17 is the ratio of F_I/F_E (Figure 2-2). Third, inelastic response at short periods was made a function of site conditions (i.e., a function of the site class), recognizing the importance of the frequency content of earthquake ground motions to the period range of the acceleration domain.

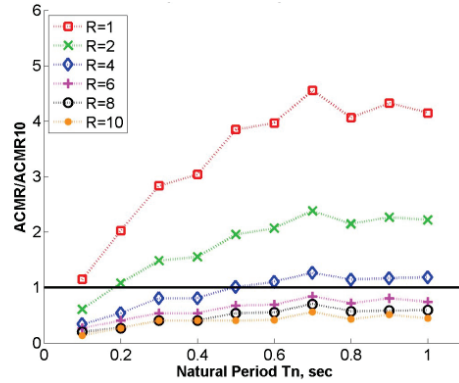
As described in FEMA 440, the coefficient C_I of the nonlinear static procedure of ASCE/SEI 41-17 embodies these three improvements in the estimation of the amount by which the peak inelastic displacement exceeds the elastic displacement at yield of short-period systems. Although very different in format, the C_I coefficient of ASCE/SEI 41-17 is rooted in the original ductility-based concepts of Veletsos and Newmark and subsequent studies, such as those conducted as part of FEMA 440.

NIST GCR 12-917-20 includes a study of short-period bilinear SDOF models using the earthquake records and collapse evaluation methods of FEMA P-695. The results of this SDOF study reaffirm the findings of prior studies of SDOF models (e.g., at short periods, inelastic displacement exceeds elastic displacement).

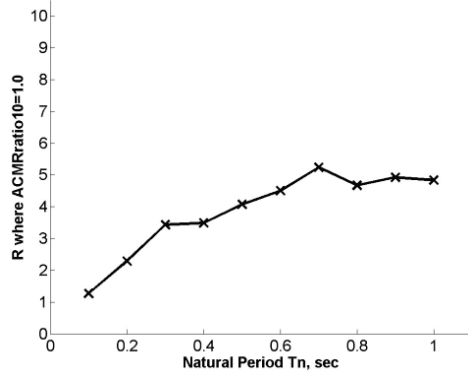
Figure 2-3, taken from the NIST GCR 12-917-20 report, illustrates period-dependent trends in the results of the analyses of SDOF models with different yield strengths (i.e., based on values of the R factor ranging from 1 to 10). The bilinear SDOF models included a modest 10 percent post-yield strain hardening, ignored P-delta effects, and assumed collapse at a ductility demand of $\mu=10$. In these figures, the R factor is the ratio of MCE_R response spectral acceleration to the normalized yield strength of the SDOF model (V_y/W), corresponding implicitly to an overstrength of 1.5 (i.e., the ratio of MCE_R to design-level ground motions) and, as such, should be factored by 1.33 to 2.0 for comparison with the R factors of Bearing Wall, Building Frame or Moment-Resisting Frame systems of Table 12.2-1 of ASCE/SEI 7-16.



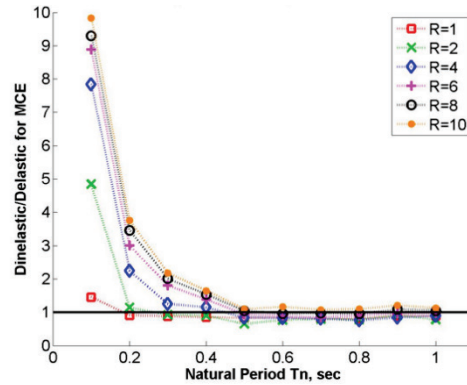
(a) Probability of collapse



(b) ACMR ratios for 10% probability of collapse



(c) R values for 10% probability of collapse



(d) Inelastic-to-elastic drift ratios

Figure 2-3 FEMA P-695 collapse results for bilinear SDOF systems modeled with 10 percent post-yield strain hardening without P-delta effects and collapse displacement capacity 10 times yield displacement (adapted from NIST, 2012).

Figure 2-3a shows that, in all cases, the shorter the first-mode period of the SDOF model, the larger the probability of collapse given MCE_R ground motions. Figure 2-3d similarly shows that, in all cases, the shorter the first-mode period of the SDOF model, the larger the ratio of inelastic-to-elastic response. Figure 2-3b identifies SDOF models with insufficient design strength to meet the 10 percent probability of collapse objective of ASCE/SEI 7-16 (i.e., probability of collapse is not more than 10 percent given MCE_R ground motions for Risk Category II structures), as the ratio of the adjusted collapse margin ratio ($ACMR$) to the value of the adjusted collapse margin ratio corresponding to a 10 percent probability of collapse ($ACMR_{10\%}$). Values of the $ACMR/ACMR_{10\%}$ ratio less than 1.0 identify those SDOF models that do not meet the 10 percent probability of collapse objective of ASCE/SEI 7-16. Figure 2-3c shows the minimum values of R required to meet the 10 percent probability of collapse objective (i.e., assuming the system has an overstrength of 1.5). Values of R required to meet the 10 percent probability of collapse objective are similar at SDOF model periods greater than about 0.5 seconds but decrease as a function of period for periods less than about 0.5 seconds.

The findings of the SDOF study of the NIST GCR 12-917-20 report are consistent with those of other prior analytical studies of bilinear SDOF models that have suggested values of the response modification factor (R) should be period dependent and smaller for short-period buildings (e.g., Miranda and Bertero, 1994). Despite analytical evidence to the contrary, structural engineers in the United States have been reluctant to adopt seismic-code requirements for new buildings that would be more restrictive for short-period buildings, in part because these buildings have not shown a propensity for collapse in recent earthquakes (as described in Chapter 3) and because the findings of these analytical studies were contrary to their intuition (even if the reasons were not clear). The remainder of this section identifies a fundamental shortcoming in these analytical studies that lends credence to the intuition of structural engineers.

The trends of Figure 2-3 showing worse collapse performance as the period decreases are directly related to the underlying assumption that collapse occurs at a predefined displacement ductility demand (e.g., $\mu = 10$), regardless of the value of the period of the bilinear SDOF model. Similar assumptions of period-independent ductility-based collapse limit states are inherent to the studies of other prior analytical studies of bilinear SDOF models that have recommended that the R factor used for seismic design should be period dependent and be more stringent for short-period buildings. The assumption of failure at a ductility of $\mu = 10$ is reasonable (perhaps even generous) for a bilinear SDOF model with a period of 0.5 seconds, since this corresponds to a maximum inelastic displacement, δ_I , at collapse of about 10 inches:

$$\delta_I = \mu \delta_Y = \mu F_Y / K_e = \mu F_Y (g/W) (T/2\pi)^2 = \mu (g/4\pi^2) (F_Y/W) T^2 \quad (2-5)$$

$$\delta_I = 10(9.8)(0.4)0.5^2 = 9.8 \text{ inches}$$

where K_e is the initial elastic stiffness and the yield strength, F_Y , in this example is 40 percent of the weight, W , of the SDOF model.

In contrast, the assumption of failure at a ductility of $\mu = 10$ is not reasonable for a bilinear SDOF model with a period of 0.1 seconds, since this corresponds to a maximum inelastic displacement, δ_I , at collapse of only about 0.4 inches (i.e., $\delta_I = 10(9.8)(0.4)0.1^2 = 0.39$ inches) for a bilinear SDOF model with the same yield strength as a percentage of weight. Real buildings do not collapse at such small earthquake displacements. But this implication was inherent to prior studies of bilinear SDOF models, which have contributed to a theoretical misconception regarding the expected poor earthquake performance of short-period buildings.

A more realistic collapse metric for evaluation of short-period bilinear SDOF models would be a drift-based collapse displacement limit (e.g., median collapse displacement based on story-drift ratio, where the story-drift ratio is defined as the displacement at a story divided by its height), rather than a ductility-based collapse displacement limit (e.g., median collapse displacement based on story ductility, where story ductility is defined as the maximum inelastic displacement divided by the yield displacement of a story). Chapter 5 describes a study using simple SDOF models undertaken to investigate generic collapse performance and, in part, to answer the question:

How would re-evaluation of nonlinear SDOF models using a drift-based collapse displacement limit (rather than a ductility-based collapse displacement limit) change the findings of prior studies of nonlinear SDOF models of short-period buildings and hence the long-standing perception that the shorter the period, the worse the collapse performance?

Chapter 3

Observed Collapse Performance and Benchmarks

This chapter summarizes fatalities and economic losses in major U.S. earthquakes, observed collapse performance of short-period buildings in U.S., Japanese, and New Zealand earthquakes, and the development of benchmark collapse metrics that are used in Chapter 4 to verify the reliability of improved numerical models of short-period buildings.

3.1 Overview

An essential element of this investigation was the collection of data on short-period building response and collapse performance in past earthquakes and, where available, data from shake-table tests for each of the three SFRSs evaluated. For the wood light-frame system, response data were also collected for comparison of actual building periods with analytical model periods and design periods. These data were used to establish “benchmark” behavior of short-period buildings for verification that the improved numerical models reliably predict building response and collapse performance. These data also provide evidence of the relatively good performance of short-period buildings in past earthquakes. Although the focus of this investigation is on modern U.S. construction, short-period building data from non-U.S. earthquakes were considered to the extent that such data were available and considered representative of the systems of interest.

Although shake-table tests of full-scale short-period buildings to collapse are limited, the few tests that have been conducted provide valuable information on nonlinear response behavior, damage patterns, and collapse failure modes of test buildings. In particular, observations of damage patterns and collapse failure modes of test buildings in high-amplitude shake-table tests establish qualitative targets for the behavior and performance expected of numerical models of comparable construction and configuration. For example, peak dynamic response story-drift ratios of at least 10 percent at the first story of a two-story residential wood light-frame building were reached before collapse (Isoda et al., 2008), and a shake-table test of a single-story reinforced-masonry coupled T-wall structure demonstrated that the structure was able to

reach a story-drift ratio of 13 percent without collapse (Cheng et al., 2020). Chapter 2 of FEMA P-2139-2 provides additional information on shake-table testing of wood light-frame test structures, and Chapter 2 of FEMA P-2139-3 provides additional information on shake-table testing of reinforced masonry test structures.

This chapter summarizes the observed performance of short-period buildings in past earthquakes, as documented in greater detail in Chapter 2 of the reports for the system-specific studies.

3.2 U.S. Earthquakes (1964–2014) and Building-Related Fatalities and Economic Losses

Table 3-1 presents the dates and earthquake magnitudes, as well as the number of fatalities and building-related economic losses, of the four most significant large-magnitude (>M5.5) U.S. earthquakes that occurred in the 50-year period 1964–2014. (Table 3-1 is based on data presented in Chapter 2 of FEMA P-2139-2.) The collective effects of 23 other large-magnitude events during that period are also shown. Building economic losses are shown for the date of the earthquake (e.g., as reported in the literature) and as an estimate of these losses in 2014 dollars (i.e., estimated economic losses if the earthquake had occurred in 2014).

The four most significant events are the 1964 Anchorage earthquake, the 1971 San Fernando earthquake, the 1989 Loma Prieta earthquake, and the 1994 Northridge earthquake, which account for 95 of the 109 building-related U.S. earthquake fatalities and 90 percent of building-related dollar losses from 1964 to 2014. Most of the 128 fatalities in the 1964 Anchorage earthquake were due to tsunami flooding of coastal areas.

Table 3-1 Dates and Magnitudes of Selected Large-Magnitude (>M5.5) U.S. Earthquakes, 1964 through 2014, and Associated Fatalities and Building-Related Economic Losses

Earthquake			Fatalities		Building Loss (billions)	
Name	Date	Magnitude	Total	Building Related	Date of Earthquake	Est. 2014 Dollars
1964 Anchorage, Alaska	3/28/1964	M9.2	128	10	\$0.3	\$5.0
1971 San Fernando, California	2/9/1971	M6.6	65	53	\$1.5	\$20.0
1989 Loma Prieta, California	10/17/1989	M6.9	63	12	\$6.5	\$17.5
1994 Northridge, California	1/17/1994	M6.7	57	20	\$25.0	\$55.0
Other Earthquakes (23)			33	14	\$3.7	\$7.4
Total All Earthquakes			346	109	\$37.0	\$104.9

In general, deaths due to ground motions or ground failure are primarily due to injuries sustained as a result of building collapse, but also include deaths due to bridge collapse (e.g., 42 deaths due to the collapse of the Cypress viaduct in the 1989 Loma Prieta earthquake) and medical-related deaths, such as heart failure brought on by the earthquake. The relatively small number of building-related earthquake fatalities in recent U.S. earthquakes reflects both good fortune (i.e., typically earthquakes have occurred at off-hours or away from areas of dense population), as well as the generally good earthquake resistance of U.S. (mostly California) buildings. Larger magnitude events closer to the center of dense urban areas, particularly if outside of California, would be expected to cause a much greater loss of life due to collapse of vulnerable buildings, such as those that have significant structural irregularities.

Most of the building-related fatalities of Table 3-1 were primarily due to collapse of vulnerable buildings, including unreinforced masonry (URM) buildings, non-ductile reinforced concrete buildings, and soft/weak story wood light-frame buildings. Collapse of these three types of buildings, which are typically low rise (short period), caused more than 70 of the 109 building-related earthquake deaths listed in Table 3-1. These types of buildings accounted for 47 of the 58 fatalities in the 1971 San Fernando earthquake, which occurred at the Veterans Administration (VA) complex due to collapse of non-ductile concrete frames, 8 of the 12 fatalities in the 1989 Loma Prieta earthquake due to out-of-plane collapse of URM walls, and 16 of the 20 fatalities in the 1994 Northridge earthquake, which occurred at the Northridge Meadows apartment complex due to soft (weak) first-story collapse of this multi-story wood light-frame building. These vulnerable building types are either no longer permitted in regions of moderate-to-high seismicity (e.g., URM buildings) or more stringent code provisions are now required for seismic design.

The number of fatalities is not equal to the number of short-period buildings that collapsed in an earthquake. In some cases, the number of fatalities is greater, since many occurred in the same building (e.g., 16 fatalities in the Northridge Meadows apartment complex). In most cases, however, collapse of a short-period building (e.g., wood light-frame single-family dwelling) does not cause any fatalities, and the number of collapsed buildings is, on average, much greater than the number of fatalities. Even so, the takeaway from Table 3-1 is that the very low number of building-related fatalities (109) in the 50-year period implies that a relatively small number of buildings collapsed. By comparison, approximately 5,000 of the 6,343

fatalities in the M6.8 1995 Kobe, Japan earthquake were caused by the 81,203 buildings that collapsed in that earthquake (AIJ, 1995a).

3.3 Collapse Performance of Short-Period Buildings in Past Earthquakes

Building damage data for post-earthquake surveys and associated studies of these data were collected and reviewed to investigate the collapse performance of short-period buildings in past earthquakes. In general, these investigations were qualitative in nature due to the lack of reliable data necessary to quantify the rate of building collapse as a function of ground motion intensity. An exception is the 1994 Northridge earthquake, for which there is sufficient data for wood light-frame buildings to establish collapse rates as a function of response spectral acceleration.

Six past earthquakes in the U.S., Japan, and New Zealand and sources of damage data used to investigate the collapse performance of short-period wood light-frame, reinforced masonry, and steel SCBF buildings are listed in Table 3-2.

Table 3-2 Dates, Magnitudes, and Sources of Damage Data Used to Investigate the Collapse Performance of Short-Period Wood Light-Frame, Reinforced Masonry, and Steel SCBF Buildings in U.S., Japanese (JP), and New Zealand (NZ) Earthquakes

Earthquake			Sources of Damage Data		
Name	Date	Magnitude	Wood Light-Frame	Reinforced Masonry	Steel SCBF
1971 San Fernando	02/09/1971	M6.6			(6)
1978 Miyagi-ken-okl (JP)	06/12/1978	M7.4			(7)
1987 Whittier	10/01/1987	M5.9		(3)	
1994 Northridge	01/17/1994	M6.7	(1)	(4)	(8)
1995 Kobe (JP)	01/17/1995	M6.8	(2)		(9)
2011 Christchurch (NZ)	02/22/2011	M6.2		(5)	

(1) OES, 1995; HUD, 1994; ATC, 2000; Schierle, 2003.

(2) AIJ, 1995a; Yamaguchi and Yamazaki, 2000; Yamazaki and Murao, 2000.

(3) Hart et al., 1988.

(4) OES, 1995; TMS, 1994.

(5) Dizhur et al., 2011.

(6) Simpson, 2017; NOAA, 1973.

(7) Simpson, 2017; Tanaka et al., 1980.

(8) OES, 1995; Krawinkler, 1996; Tremblay et al., 1995.

(9) AIJ, 1995a; AIJ, 1995b; Tremblay et al., 1996.

Many post-earthquake safety assessments use the guidelines provided in ATC-20, *Procedures for Postearthquake Safety Evaluation of Buildings* (ATC, 1989; 2005). The ATC-20 safety assessment procedure is a rapid evaluation tool that focuses on the integrity of the structural system.

Inspectors are instructed to affix a placard (colored tag) on an inspected structure, according to the following guidelines:

- **Inspected Placard (green tag).** No apparent hazard found, although repairs may be required. Original lateral load capacity not significantly decreased. No restriction on use or occupancy.
- **Restricted Use Placard (yellow tag).** Dangerous condition believed to be present. Entry by owner permitted only for emergency purposes and only at own risk. No usage on a continuous basis. Entry by public not permitted. Possible major aftershock hazard.
- **Unsafe Placard (red tag).** Extreme hazard, may collapse. Imminent danger of collapse from aftershock. Unsafe for occupancy or entry, except by authorities.

The 1994 Northridge earthquake is by far the most important source of building damage data for investigating the collapse performance of modern short-period U.S. buildings. The number of short-period buildings that collapsed in this earthquake is not well documented, and red tag data are used as a surrogate for collapse. Red tag data from post-earthquake safety inspections of about 114,000 buildings in Los Angeles County were compiled by the California Governor's Office of Emergency Services (OES, 1995) and provide a more reliable measure of building damage. Red tag data are a conservative (upper bound) estimate of collapsed buildings since, by definition, they include all severely damaged buildings considered a threat to life safety, even if not collapsed (e.g., buildings that are leaning). Although it is likely that some un-inspected buildings would have been assigned a red tag if they had been inspected, it is unlikely that such buildings collapsed.

Red tag building percentages are shown in Figure 3-1 for wood buildings and for other (non-wood) buildings for each of five MMI regions (V–IX). Here, the red tag percentage is the ratio of the number of buildings assigned a red tag (Table 4-3, OES, 1995) to the number of buildings in the MMI region of interest (Table 6, Kircher et al., 2006b). Red tag percentages are plotted as a function of the average value of 0.3-second response spectral acceleration of the MMI region of interest (Table 6, Kircher et al., 2006b). Non-wood buildings of the OES database include three primary construction classes: (1) steel frame; (2) concrete frame; and (3) brick, block, or poured-in-place concrete. Non-wood construction classes are grouped together since the red

tag percentages could not be reliably estimated for individual construction classes (other than wood).

As shown in Figure 3-1, red tag percentages are quite low, less than 1.0 percent, even for the MMI IX region (e.g., average 0.3-second response spectral acceleration of 1.35g). The number of buildings assigned a red tag are also shown in the figure for MMI regions VII and VIII. For example, 230 of all 1,614 wood buildings assigned a red tag and 25 of all 313 non-wood buildings assigned a red tag are in the MMI IX region. Qualitatively, non-wood buildings have similar trends and values of red tag percentages as wood buildings (e.g., about 1.0 percent for the MMI IX region).



Figure 3-1 Percentage of wood and non-wood buildings assigned a red tag as a function of 0.3-second response spectral acceleration for five MMI regions (V–IX) based on post-earthquake safety inspections following the 1994 Northridge earthquake.

3.3.1 Wood Light-Frame Buildings

1994 Northridge Earthquake. In general, modern wood light-frame buildings performed well in the 1994 Northridge earthquake with relatively few collapsed buildings, as demonstrated by the very small red tag rates shown in Figure 3-1. A more refined statistical evaluation of the collapse performance was made using census-tract-based data and post-1960 wood building inventory, as described in Section 3.4, which found similar trends and very low red tag rates.

Low red tag rates are supported by other sources documenting the generally good observed performance of modern short-period wood light-frame

buildings in the 1994 Northridge earthquake. These sources include field surveys conducted by the ATC-38 Project (ATC, 2000), by the CUREE-Caltech Woodframe Project (Schierle, 2003) and by the National Association of Home Builders (NAHB) for the U.S. Department of Housing and Urban Development (HUD, 1994).

The NAHB/HUD study surveyed and assessed damage to a random sample of residential buildings located in the San Fernando Valley and nearby hills, generally within a 10-mile radius of the epicenter. Two groups of building types were surveyed: single-family detached (SFD) homes and single-family attached and multi-family low-rise (SFA/MFLR) properties of one and two stories. Construction characteristics and damage to 341 SFD homes and 30 SFA/MFLR buildings were recorded. Although ground motions were not determined at each sample building site, the sample area represents the region of strongest ground motions in the 1994 Northridge earthquake.

The NAHB/HUD survey found for SFD homes: (1) they suffered minimal structural damage; (2) structural damage was most common in the foundation systems (e.g., in areas that endured localized ground effects or problems associated with hillside sites); and (3) interior and exterior finishes fared much worse than foundations and framing, with nearly 50 percent of the homes experiencing at least some damage (e.g., typically limited to the lowest level of the buildings).

The NAHB/HUD survey found that damage to SFA construction performed similarly to that reported for the SFD homes. However, structural damage to MFLR construction was notably more dramatic and costly to lives, especially for certain construction types located in the San Fernando Valley. The more remarkable structural failures were associated with the older MFLR buildings situated on soft-story garage foundations.

1995 Kobe Earthquake. Another important source of wood building damage data is the 1995 Kobe earthquake, for which ground motions were, on average, much stronger than those of the 1994 Northridge earthquake. Construction of older Japanese wood-frame buildings is very different from U.S. wood light-frame buildings, and the relatively poor performance of older Japanese wood-frame buildings in the 1995 Kobe earthquake is not representative of U.S. wood light-frame buildings. Construction of newer (post-1981) Japanese wood-frame buildings is much more similar to that of U.S. wood-light frame buildings, and observed damage to newer Japanese wood-frame buildings in the 1995 Kobe earthquake is used for comparison with observed damage to modern U.S. wood-light frame buildings in the 1994 Northridge earthquake, recognizing: (1) significant difference in the

level of ground motions of these two earthquakes; and (2) fundamental differences in building configuration and construction (e.g., the typical Japanese wood-frame residence is two stories in height, whereas the typical U.S. wood residence is one story in height).

Building damage data for the 1995 Kobe earthquake are reported in Yamaguchi and Yamazaki (2000) for Nishinomiya City and in Yamazaki and Murao (2000) for Nada Ward of Kobe City for various building types, including wood-frame, reinforced concrete, and steel buildings. In the case of wood-frame buildings, “heavy” damage data are given for each of five construction periods, pre-1952, 1952–1961, 1962–1971, 1972–1981, and 1982–1994. Heavy damage is not defined precisely in the referenced studies but includes both collapsed buildings and buildings with severe structural damage, roughly equivalent to the life-safety criterion used to define a red tag building in the 1994 Northridge earthquake. A summary of observed damage is provided below.

In Nishinomiya City, 22,500 of 67,592 (33 percent) of all wood-frame buildings were heavily damaged. In the Nada Ward of Kobe City, 11,907 of 22,710 (52 percent) of all wood-frame buildings were heavily damaged. Median ground motions causing heavy damage in Nishinomiya were more than 1.5g at short-period (0.3-second) response spectral acceleration, and median ground motions causing heavy damage in Nada Ward were about 2.0g at short-period (0.3-second) response spectral acceleration. More than 2,000 people died in Nada Ward of Kobe and Nishinomiya City primarily due to collapse of wood-frame buildings, the vast majority of which were of older (pre-1981) construction.

In contrast to the very poor performance of all Japanese wood-frame buildings in the 1995 Kobe earthquake, newer (1982–1994) Japanese wood-frame buildings performed relatively well considering the strength of the ground motions. In Nishinomiya City, 850 of 12,072 (7.0 percent) of all newer wood-frame buildings were heavily damaged, where median short-period (0.3-second) spectral accelerations were a little more than 1.5g. In the Nada Ward of Kobe City, 384 of 2,449 (15.7 percent) of all wood-frame buildings were heavily damaged, where median short-period (0.3-second) spectral accelerations were about 2.0g. Heavy damage statistics for newer Japanese wood-frame buildings from the 1995 Kobe earthquake provide an upper bound on the performance of multi-story U.S. wood light-frame buildings, because ground motions exceeded those of the 1994 Northridge earthquake (i.e., 0.3-second response spectral accelerations greater than 1.5g).

3.3.2 Reinforced Masonry Buildings

The literature on the performance of short-period reinforced masonry buildings in earthquakes is limited and not sufficient to develop a quantitative measure of collapse failure rates. This is due, in part, to the relatively small population of all short-period buildings that are constructed of reinforced masonry and to the relatively good performance of modern reinforced masonry buildings in past earthquakes. Still, only a small number of modern reinforced masonry buildings have been “tested” by very strong (e.g., MCE_R or greater) ground motions.

The development of shear cracks in reinforced masonry walls due to strong earthquake ground shaking has been widely observed, and in some cases, walls have “failed.” But there are no reported collapses of modern reinforced masonry buildings in the U.S. due to in-plane failure of shear walls, and there are no reported instances of out-of-plane failure of reinforced masonry walls without diaphragm connection failure. This contrasts with the common observation of the failure of unreinforced masonry building walls, which tend to collapse out of plane after sustaining in-plane damage. Summaries of reinforced masonry damage patterns and statistics from the 1987 Whittier earthquake, the 1994 Northridge earthquake, and the 2011 Christchurch earthquake are presented below.

1987 Whittier Earthquake. After the 1987 Whittier earthquake, a comprehensive survey of 50 reinforced masonry buildings and 38 URM buildings was made in downtown Whittier (Table 2, Hart et al., 1988), which was the area of strongest ground-motion intensity (MMI VIII). Damage data were never published, but anecdotal information suggests that few, if any, of the 50 reinforced masonry buildings had significant structural damage.

A strong-motion instrument located in the basement of a 10-story building in downtown Whittier (Bright Avenue) close to the masonry building survey area recorded a peak ground acceleration of 0.63g (Figure 4, Brady et al., 1988) and a peak response spectral acceleration of about 1.8g at short periods (Figure 10, Wald, et al., 1988), which are approximately the same as the MCE_R ground motions required by ASCE/SEI 7-16 for this site. However, the 1987 Whittier earthquake was only a magnitude M5.9 event, the duration of strong shaking was short (i.e., only about 10–15 seconds), and the frequency content of ground motions at 1 second-and-longer periods was very low (e.g., response spectral acceleration of the Bright Avenue records was less than 0.2g at periods of 1 second). The low level of ground motions at 1 second-and-longer periods implies a peak displacement response of short-period buildings of not more than about 2 inches, which could not have caused building collapse even if the

spectral accelerations at short periods were strong enough to have caused damage (i.e., cracking of reinforced masonry walls).

1994 Northridge Earthquake. After the 1994 Northridge earthquake, a reconnaissance team of The Masonry Society (TMS) surveyed approximately 140 masonry buildings in the greater Los Angeles area (TMS, 1994). The TMS reconnaissance report found that in the greater Los Angeles area, and particularly in the epicentral region, very little distress was shown in modern reinforced masonry buildings. In contrast, un-retrofitted URM buildings generally had more extensive wall damage. In general, masonry structures built since the 1950s that were engineered, grouted, reinforced, and inspected in accordance with then-current building codes experienced little damage in the earthquake.

The 140 reinforced masonry buildings surveyed after the 1994 Northridge earthquake represent only a fraction of all reinforced masonry buildings in the area of strongest ground motions, although the total number of reinforced masonry buildings is not known. For reference, post-earthquake safety evaluations of 114,039 potentially damaged buildings included 10,393 commercial and industrial buildings, of which 637 (6.1 percent) were deemed unsafe and assigned a red tag (Table 4-2, OES, 1995). Those safety inspections included 3,068 “Class C” structures having exterior walls of brick, concrete block, or poured-in-place concrete (e.g., tilt-up buildings), of which 277 (9.0 percent) were assigned a red tag (Table 4-3, OES, 1995), where “Class C” structures include unreinforced masonry buildings that are much more vulnerable to earthquake damage than reinforced masonry buildings. Only a fraction of all buildings was safety inspected, and red tag percentages based on the number of inspected buildings, rather than the total number of buildings in the affected area, are not particularly meaningful. A more meaningful estimate of red tag percentages is shown in Figure 3-1 for non-wood buildings, which should be considered an upper bound on red tag rates for reinforced masonry buildings since non-wood buildings with a red tag include unreinforced masonry and tilt-up buildings, which were much more vulnerable to damage in the 1994 Northridge earthquake.

2011 Christchurch Earthquake. After the February 22, 2011, Christchurch, New Zealand earthquake, an international team of researchers was deployed to document the observed earthquake damage to masonry buildings and to churches (Dizhur, 2011). The study focused on investigating commonly encountered failure patterns and collapse mechanisms. External evaluations of 342 reinforced masonry buildings with solid wall construction located within the central business district of Christchurch found the majority of these buildings (83 percent) had little or no damage, 15 percent had moderate

damage, and only 5 percent had severe damage. Diagonal in-plane shear cracking was the most common failure mode (64 percent), including both step-pattern cracking along the head and bed mortar joints and diagonal cracking through masonry blocks. Vertical cracking of the block was also commonly observed (20 percent), followed less frequently by horizontal cracking along bed joints and spalling of the block.

In contrast to the relatively good performance of reinforced masonry buildings, almost 200 unreinforced masonry buildings were demolished in the first five months following the earthquake (approximately 85 percent of all buildings demolished during this time), and of those that remained, few were in a usable condition (Dizhur, 2011).

3.3.3 Steel SCBF Buildings

The literature on the performance of modern short-period steel SCBF buildings in earthquakes is limited and not sufficient to develop a quantitative measure of collapse failure rates. This is due, in part, to the relatively small population of all short-period buildings that are constructed with steel SCBF systems and to the relatively good performance of modern steel SCBF buildings in past earthquakes. A notable exception is the large number of steel braced frame buildings with severe or collapse damage in the 1995 Kobe earthquake, although arguably most of these buildings are not representative of modern steel SCBF buildings. Nonetheless, observed damage and collapse of these buildings provides valuable information, since the 1995 Kobe earthquake exposed these buildings to very strong (i.e., MCE_R or greater) ground motions.

Table 3-3 is taken from Simpson et al. (2017). Information on the types of damage observed to steel braced frames is summarized for four earthquakes: (1) the 1971 San Fernando earthquake; (2) the 1978 Miyagi-ken-oki, Japan earthquake; (3) the 1994 Northridge earthquake; and (4) the 1995 Kobe, Japan earthquake. These four earthquakes were selected for this summary since damage data for these events was available in the literature. Notably missing from this set of earthquakes is the 1989 Loma Prieta earthquake, for which there is only anecdotal accounts of damage to steel braced frames (e.g., brace buckling) in a few buildings.

The steel braced frame buildings damaged in the older (pre-1981) 1971 San Fernando and 1978 Miyagi-ken-oki earthquakes are not representative of modern steel braced frame buildings. Braced frame buildings of older vintages are expected to sustain more damage and collapse than newer (post-1981) construction. Summaries of steel braced frame damage and collapse statistics (where available) from the four earthquakes follow.

Table 3-3 Description of Damage to Steel Braced Frames in Past Earthquakes

Year	Location	Magnitude	Description of Damage
1971	San Fernando, California	M6.6	Buckling and fracture of bar and double-angle braces
1978	Miyagi-ken-oki, Japan	M7.4	Buckling and fracture of bar and double-angle braces. Premature connection failures
1994	Northridge, California	M6.7	Local buckling and fracture of bracing members Premature connection failure Deformation of beam Uplift of column base Weak-story behavior
1995	Kobe, Japan	M7.2	Local buckling and fracture of small- and large-section braces Premature connection failure Distortion of beam near connections Significant yielding of beams

1971 San Fernando Earthquake. Although moderate in energy release (M6.6), the San Fernando earthquake caused significant damage and led to detailed post-earthquake case studies of damaged buildings (Volume I of NOAA, 1973). These case studies included 38 “earthquake-resistant” buildings: (1) 17 low-rise industrial and commercial buildings; (2) 9 hospital and medical facilities; and (3) 12 high-rise buildings and 6 “non-earthquake-resistant” buildings (e.g., unreinforced masonry and non-ductile reinforced concrete). Buildings were selected for study because they had sustained significant damage and, in some cases, had collapsed (e.g., Olive View Hospital).

Only one of the buildings studied, the two-story Foothill Medical Center, was a steel building with braced frames (single-story, double-angle X brace). Principal structural damage to this building was at the base of a column, severely bent due to brace eccentricity. Although some braces failed leading to glass and partition damage, the building did not collapse and was repaired. Although most damage after the San Fernando earthquake was reported in reinforced concrete structures, there were a few observed cases of brace buckling and rupture (Simpson et al., 2017). One case was of flat bar braces in a temporary wall in a mixed-use construction building. The other case was of buckling of steel double-angle X-bracing damage in a three-story metal-skin building.

1978 Miyagi-ken-oki Earthquake. The Miyagi-ken-oki earthquake occurred offshore of Sendai City, Japan, and generated peak ground accelerations of 1/5g, 1/4g, and 1/3g in areas surrounding the city (EERI, 1978). The majority of the steel buildings were relatively new braced frames typically consisting of bar or double-angle braces with bolted gusset-plate

connections. The gusset connections were usually welded to the beams and columns. Braced frames were commonly found in long-span structures, such as factories, warehouses, or gymnasiums (Simpson et al., 2017).

Following the earthquake, a team of Japanese researchers performed field investigations of damaged buildings in a 4 km-by-4 km (2.5 mile-by-2.5 mile) area east of old Sendai City that had a relatively large number of commercial and industrial steel buildings: (1) 861 one-story steel buildings; (2) 412 steel buildings of two stories or taller; and (3) 150 light-gauge steel buildings (Table 1, Tanaka et al., 1980). With the exception of long-span buildings (e.g., industrial structures and sports arenas), one-story steel buildings had limited structural damage, and the field investigations focused on steel buildings two stories and taller. Surveyed steel buildings included both moment frames and braced frames, although only a few moment frames had structural damage. Of the 454 steel buildings two stories or taller that were investigated, only 6 buildings (1.3 percent) were collapsed and only 13 buildings (2.8 percent) had significant structural damage with residual displacements of at least 1/30 relative story drift angle (Table 3, Tanaka et al., 1980). Fracture of jointed brace connections was observed in the 6 buildings that collapsed (Table 4, Tanaka et al., 1980), with collapse damage attributed to “fatal” defects (Kato et al., 1980). In response to the Miyagi-ken-oki earthquake, the Ministry of Construction in Japan recommended that earthquake design lateral forces be increased by a factor of 1.5 for steel braced frames and that connection forces be 1.2 times larger than the yield strength of the braces designed for those lateral forces.

1994 Northridge Earthquake. Damage observed after the 1994 Northridge earthquake highlighted a variety of unexpected damage states in steel structural systems (Simpson et al., 2017), but none resulted in building collapse (Krawinkler, 1996). Observed structural damage to 10 steel concentrically braced frame (CBF) buildings, some with a moment resisting frame (MRF) in one direction, is summarized in Table 3-4 (Table 1, Tremblay et al., 1995).

The 10 steel buildings listed in Table 3-4 represent a small fraction of all of steel CBF buildings in the area of strongest ground motions, although the total number of steel CBF buildings is not known. For reference, post-earthquake safety evaluations of 114,039 potentially damaged buildings included 10,393 commercial and industrial buildings, of which 637 (6.1 percent) were deemed unsafe and assigned a red tag (Table 4-2, OES, 1995). Those safety inspections included 189 “steel frame” buildings, of which 10 (5.3 percent) were assigned a red tag (Table 4-3, OES, 1995), where “steel frame” does not distinguish between braced frame and moment frame construction.

Table 3-4 Summary of Observed Structural Damage to Steel Braced Frame Buildings in the 1994 Northridge Earthquake

Structure	Type	Structural Damage
Kaiser Permanente Hospital penthouse	CBF	Buckling of bracing members; excessive sway
Two-story First Interstate Bank Building in Northridge	CBF	Buckling of brace connecting plates; possible yielding of anchor bolts
Four-story Student Union Building, California State University at Northridge	CBF	No structural damage observed
Roof structure for the bleachers of the football field	Other	Failure of anchor bolts (uplift)
Four-story Oviatt Library, California State University at Northridge	CBF	Failure of brace connecting plates; cracking of baseplates; yielding of anchor bolts
Three-story building under construction in Van Nuys	CBF, MRF	Buckling of bracing members
Four-story No. 2 Brew-house, Anheuser-Busch Co. Inc.	CBF	Buckling of bracing members
Department of Water and Power San Fernando Generating Station	CBF	No structural damage observed
Four-story commercial office structure	CBF	Buckling and failure of brace-welded connections; failure of beam-column moment connections
Two-story fashion plaza	CBF, MRF	Cracking in floor slab; buckling of bracing members

Only a fraction of all buildings was safety inspected, and red tag percentages based on the number of inspected buildings, rather than the total number of buildings in the affected area, are not particularly meaningful. More meaningful estimates of red tag percentages are shown in Figure 3-1 for non-wood buildings. These percentages should be considered an upper bound on red tag rates for steel SCBF buildings since non-wood buildings with a red tag include unreinforced masonry and tilt-up buildings, which were much more vulnerable to damage, and none of the 25 non-wood buildings assigned a red tag in the MMI IX region were steel frame construction.

1995 Kobe Earthquake. The preliminary earthquake reconnaissance report of the Architectural Institute of Japan (AIJ, 1995a) provides summaries of damage by building location and structure type. A total of 1,776 steel buildings were investigated, of which 457 (26 percent) collapsed or suffered severe damage (Table 1.3.2, AIJ, 1995a). The relatively high percentage of steel building collapses (26 percent) is consistent with collapse percentage for all buildings (21 percent) located within 5 km (3.1 miles) of fault rupture. The 1,776 steel buildings surveyed included steel buildings of all vintages and construction type.

A more focused and in-depth reconnaissance of observed damage to 988 “modern” steel buildings was performed by The Steel Committee of Kinki

Branch of the AIJ (AIJ, 1995b). Older steel buildings with light-gauge columns were omitted from the survey. The steel buildings surveyed included three structural types: (1) moment frames (370 buildings); (2) braced frames in one direction and moment frames in the other (123 buildings); and (3) braced frames in both directions (26 buildings), with 469 buildings of unknown structure type. Of the 988 steel buildings surveyed, 90 buildings (9.1 percent) were rated as collapsed, and of the 149 buildings with braced frames in one or both directions, 10 buildings (6.7 percent) were rated as collapsed.

Damage was associated with the bracing type (where bracing type was known), distinguishing between rods, angles, and flat bars (“smaller” braces) and round tubes, wide flanges, square tubes, and channels (“larger” braces). Of the 165 steel buildings with “smaller” braces, 14 (8.5 percent) were rated as collapsed, and of the 60 steel buildings with “larger” braces, none (0 percent) were rated as collapsed (Table 6, Tremblay et al., 1996). Of the 227 steel buildings of unknown bracing type, 15 (6.6 percent) were rated as collapsed. The “larger” brace types (e.g., tubes) are representative of steel SCBFs used in the United States; the “smaller” brace types (e.g., rods and flat bars) are not (i.e., tension-only bracing is not permitted in regions of high seismicity by U.S. building codes). Although there are no reported collapses of steel buildings with “larger” brace types, some of the 15 steel buildings of unknown bracing type that were rated as collapsed could have had such bracing.

3.4 Benchmark Collapse Metrics of Short-Period Buildings Based on Wood Light-Frame Building Performance

This section describes “benchmark” collapse metrics used in Chapter 4 to verify that improved numerical models reliably predict building response and collapse performance. These metrics also provide direct evidence of the relatively good performance of short-period buildings in past earthquakes.

Benchmark collapse metrics are based on the performance of wood light-frame buildings in the 1994 Northridge earthquake, for which there are sufficient data to quantify collapse rates as a function of ground-motion intensity. The number of collapsed buildings is not well known and is approximated by the number of buildings assigned a red tag by post-earthquake safety evaluations obtained from a database of inspected buildings compiled by the California Governor’s Office of Emergency Services (OES, 1995). As discussed in Section 3.3, red tag data provide a conservative (upper-bound) estimate of collapsed buildings since, by definition, they include all severely damaged buildings considered a threat to life safety, even if not collapsed (e.g., buildings that are leaning excessively).

Red tag rates were developed from 219,301 post-1960 wood light-frame buildings from 186 census tracts of strongest ground shaking in Los Angeles County, of which 24,710 buildings were inspected and 435 buildings were assigned a red tag. For each census tract of interest, values of 1994 Northridge earthquake 0.3-second spectral accelerations were obtained from Somerville’s (geomean) map (SAC, 1995) and factored by 1.2 to represent shaking in the maximum horizontal direction of response consistent with ASCE/SEI 7-16 and FEMA P-695. The number of all wood light-frame buildings in each of the 186 census tracts was estimated from the building inventory of HAZUS99 with improvements based on the building inventory developed as part of the Southern California ShakeOut Scenario (Porter et al., 2011). HAZUS99 refers to a prior release of HAZUS (FEMA, 2003) with 1990 census tract and building inventory data deemed more suitable for evaluating 1994 Northridge earthquake damage. The total number of buildings, number of buildings with red tags, red tag percentages, and mean values of 0.3-second spectral acceleration are summarized in Table 3-5 for each of 22 census-tract groups of roughly equal building count (i.e., about 10,000 buildings each) and increasing ground-motion intensity.

Very small red tag percentages (rates) are shown by the data in Table 3-5, even for census-tract groups with significant values of 0.3-second spectral acceleration. There are no red tag rates greater than 1 percent for any census-tract group, although 0.3-second spectral acceleration reaches or exceeds 1.5g for census-tract groups in the areas of strongest shaking. For reference, a short-period MCE_R response spectral acceleration of 1.5g is typical of ASCE/SEI 7-16 requirements for sites in areas of strongest shaking in the 1994 Northridge earthquake. There are a few individual census tracts with red tag rates more than 1 percent, but none is greater than 2.6 percent, as shown in Figure 3-2.

Table 3-5 Red Tag Data by Census Tract for Post-1960 Wood Light-Frame Buildings for the 1994 Northridge Earthquake

Group No.	Building Count	Number of Red Tags	Red Tag Percentage (%)	Mean 0.3-second Spectral Acceleration (g)
1	10,467	0	0.00	0.31
2	9,689	0	0.00	0.36
3	10,918	0	0.00	0.38
4	9,739	0	0.00	0.42
5	10,084	0	0.00	0.50
6	8,959	2	0.02	0.59
7	7,834	8	0.10	0.63

Table 3-5 Red Tag Data by Census Tract for Post-1960 Wood Light-Frame Buildings for the 1994 Northridge Earthquake (continued)

Group No.	Building Count	Number of Red Tags	Red Tag Percentage (%)	Mean 0.3-second Spectral Acceleration (g)
8	11,160	5	0.04	0.70
9	9,763	7	0.07	0.76
10	9,116	19	0.21	0.85
11	10,290	15	0.15	0.90
12	9,901	10	0.10	0.94
13	10,135	17	0.17	0.97
14	9,927	19	0.19	1.03
15	10,092	14	0.14	1.10
16	10,534	7	0.07	1.18
17	10,365	36	0.35	1.24
18	10,444	58	0.56	1.30
19	10,266	73	0.71	1.36
20	10,078	55	0.55	1.41
21	10,028	64	0.64	1.53
22	9,512	26	0.27	1.67
All	219,301	435	-	-

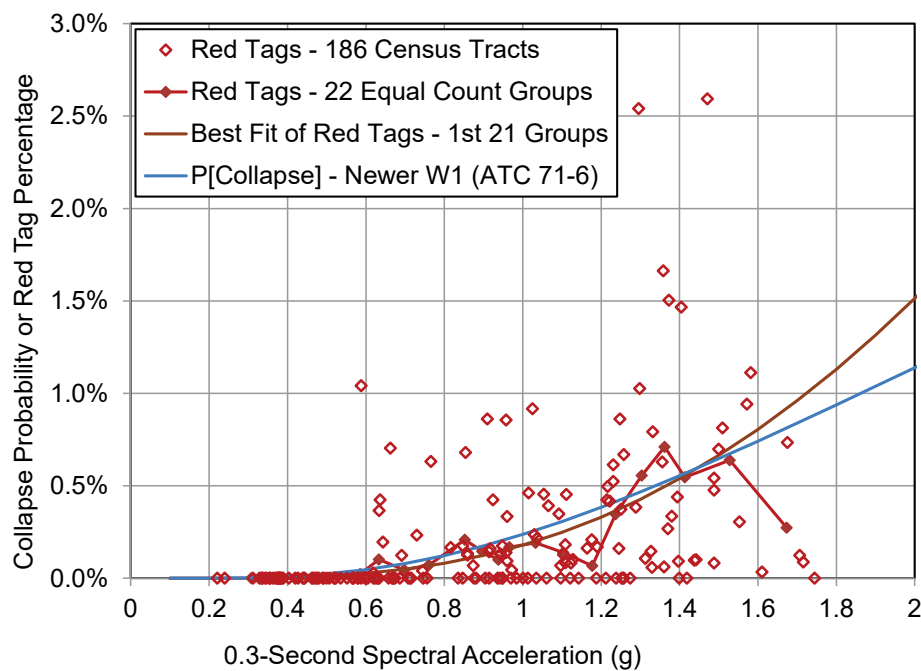


Figure 3-2 Red Tag percentages as a function of 0.3-second spectral acceleration for post-1960 wood light-frame buildings for the 1994 Northridge earthquake, along with a best-fit lognormal collapse fragility curve and a theoretical collapse curve of newer W1 buildings.

Red Tag percentages for each of the 184 individual census tracts, as well as the 22 groups of aggregated data, plotted as function of 0.3-second spectral acceleration are shown in Figure 3-2. The general trend of increasing red tag rate with ground-motion intensity is shown in the aggregated data, with a best-fit lognormal fragility curve fit to the first 21 data points of the 22 building group data using the Maximum Likelihood Estimation calculation tool of Baker (2015). For comparison, a theoretical collapse curve of newer W1 buildings developed by the ATC 71-6 project and reported in FEMA P-155 is shown in Figure 3-2. Additional background on the best-fit lognormal fragility curve of red tag data and the theoretical collapse curve of newer W1 buildings can be found in Chapter 2 of FEMA P-2139-2.

The building inventory and red tag data summarized in Table 3-5 effectively lump one-story wood light-frame buildings with two-or-more-story wood light-frame buildings, which are only a small fraction of all wood light-frame buildings. Observations of earthquake damage and collapse and shake-table tests of full-scale test structures suggest that multi-story wood light-frame buildings have a greater likelihood of collapse than one-story wood light-frame buildings, all else equal. This observation was investigated by parsing the 24,710 post-1960 wood light-frame buildings with tagging data into three groups: (1) buildings of one story in height; (2) buildings greater than one story in height; and (3) buildings of unknown height (i.e., OES database does not always provide building height data). Green tag, yellow tag, and red tag percentages were then developed separately for one-story buildings and for buildings greater than one story in height.

Tagging data and the calculation of tagging percentages are summarized in Table 3-6. In these calculations, tagging percentages are based on the number of buildings of a given tag (e.g., red tags) divided by the number of buildings inspected, rather than dividing by the total inventory of all post-1960 wood light-frame buildings. Hence, tagging rates shown in Table 3-6 are much greater than those of Table 3-5, which are based on the full inventory of post-1960 wood light-frame buildings.

The tagging ratios shown in Table 3-6 suggest two important trends in wood light-frame building damage. First, wood light-frame building of two-or-more stories in height are roughly 2.5 times more likely to collapse or have severe structural damage (requiring a red tag) than one-story wood light-frame buildings, all else equal. Second, the importance of height diminishes with the degree of damage. For example, there is essentially no height bias for buildings with minimal, nonstructural-only damage as characterized by a green tag (i.e., the percentage of one-story buildings assigned a green tag is almost equal to the percentage of buildings two stories or more assigned a green tag).

Table 3-6 Tagging Data for Post-1960 Wood Light-Frame Buildings for the 1994 Northridge Earthquake

Building	Number of Post-1960 Wood Light-Frame Buildings by Safety Inspections				
	All Tags	Red Tags	Yellow Tags	Green Tags	Unknown
All	24,710	435	2,342	21,533	400
Unknown	9,382	71	389	8,616	306
Known	15,328	364	1,953	12,917	94
One Story	8,402	116	812	7,423	51
Two Stories or More	6,926	248	1,141	5,494	43
Percentage of Post-1960 Wood Light-Frame Buildings of Known Height by Safety Inspections					
One Story	99.4	1.38	9.7	88	0.6
Two Stories or More	99.4	3.6	16.5	79	0.6
Comparison of Post-1960 Wood Light-Frame Buildings by Safety Inspections					
Ratio of Two Story-or-More to One-Story Buildings	1.0	2.6	1.7	0.9	1.0

The calculation of the tagging ratios in Table 3-6 assumes that there is no bias in the data due to potential differences in the spatial mix of building heights with respect to ground-motion intensity. This assumption is reasonable given that these data are based on a large number of inspected buildings (i.e., approximately 25,000 buildings) spatially distributed over many census tracts of cities and suburban areas affected by the 1994 Northridge earthquake.

Based on the quantitative statistical evaluation of wood light-frame building performance in the 1994 Northridge earthquake and the qualitative observation that reinforced masonry and steel SCBF buildings have performed as well as wood light-frame buildings in past earthquakes, benchmark MCE_R collapse probabilities were established as follows:

- **One-Story Buildings.** 1 percent (0 percent to 2 percent) probability of collapse given MCE_R ground motions of $S_{MS} = 1.5g$; and
- **Two-or-More-Story Buildings.** 2.5 percent (0 percent to 5 percent) probability of collapse given MCE_R ground motions of $S_{MS} = 1.5g$.

Benchmark MCE_R collapse probabilities represent short-period building collapse that includes both partial collapse and full collapse of the building structure, consistent with the ASCE/SEI 7-16 and FEMA P-695 definitions of collapse. As previously discussed, benchmark MCE_R collapse

probabilities based on red tag data provide a conservative (upper-bound) estimate of collapsed buildings since, by definition, they include all severely damaged buildings considered a threat to life safety, even if not collapsed. The higher benchmark MCE_R collapse probabilities for buildings two-or-more stories in height is based on an observed first-story failure mechanism (e.g., of wood light-frame buildings) and may not be applicable to other collapse failure modes (e.g., foundation rocking of steel SCBF buildings), which have not been observed.

3.5 Summary of Key Observations of Short-Period Building Performance

The key findings of the observations of the collapse performance of short-period buildings in past earthquakes and full-scale shake-table tests are summarized below.

Collapse Performance. In general, modern short-period buildings have performed well in past earthquakes and collapse is relatively uncommon (i.e., typically much less than a 10 percent collapse rate given MCE_R ground motions with a 0.3-second response spectral acceleration of 1.5g).

Collapse Failure Mode. Collapse of short-period buildings in an earthquake is typically a result of large displacements at the first story (e.g., Northridge Meadows apartment complex in the 1994 Northridge earthquake). Shake-table tests of full-scale wood light-frame and reinforced masonry test structures have confirmed this mode of failure (e.g., Isoda et al., 2008; Cheng, 2020).

Large Lateral Displacement at Incipient Collapse. Observations of short-period buildings severely damaged by an earthquake or strongly shaken by shake-table testing indicate large lateral displacement at the point of incipient collapse (e.g., mean story-drift ratio of 10 percent or greater).

Chapter 4

Archetypes, Parametric Studies, and Findings

This chapter provides an overview of the parametric studies conducted to investigate the collapse performance of short-period buildings. Three seismic-force-resisting systems were investigated: (1) wood light-frame; (2) reinforced masonry; and (3) steel SCBF systems. This chapter describes the configurations, designs, and modeling of the archetypes used for these studies, presents results from these studies and compares them with results from prior FEMA P-695 studies, and summarizes key findings of the studies applicable to all three systems

4.1 Overview of Parametric Studies of Short-Period Buildings

Parametric studies were used to investigate the influence of building occupancy, configuration, seismic design level, and modeling assumptions on the collapse performance of short-period buildings. Advanced nonlinear numerical models were developed from designs of short-period building archetypes and analyzed using incremental dynamic analysis (IDA) in accordance with the collapse evaluation procedures of FEMA P-695. A summary of the short-period building archetype configurations, designs, and modeling methods are provided in Section 4.2 and Section 4.3. More detailed descriptions are provided in FEMA P-2139-2, FEMA P-2139-3, and FEMA P-2139-4.

A suite of archetypes was selected for each of the seismic-force-resisting systems investigated. The archetype design methods and details represented typical modern practice—and not simply code-minimum designs—exercised in areas of significant seismicity using the normal standard of care. The occupancies selected included single-family dwellings (SFD) and multi-family dwellings (MFD) for the wood light-frame system only and commercial (COM) buildings for all three systems. Short-period buildings were defined as those with fundamental periods less than about 0.5 seconds. The archetypes include one-story, two-story, and four-story buildings, which have fundamental periods below (or just slightly above) the 0.5-second threshold.

The short-period building archetypes were designed to capture a range of seismic ground-motion levels. “High-seismic” archetypes were designed for a value of short-period MCE_R spectral response acceleration adjusted for site class effects (S_{MS}) of 1.5g. “Very high-seismic” archetypes were designed for a value of short-period MCE_R spectral response acceleration adjusted for site class effects (S_{MS}) of 2.25g (i.e., 1.5 times that for high-seismic archetypes). The very high-seismic value of S_{MS} is not required by FEMA P-695 (e.g., for evaluation of a new SFRS proposed for ASCE/SEI 7) but was used to investigate the collapse performance of short-period buildings for MCE_R ground motions that are unlikely but could occur in areas of very high seismicity (e.g., at sites located relatively close to fault rupture).

A series of parametric studies investigated the effects of variations in archetype configuration and modeling parameters on the collapse potential of each of the three systems. The best estimate of each modeling parameter was incorporated into each “baseline” model, and response behavior and collapse performance were evaluated. Models of baseline archetypes designed for high-seismic ground motions ($S_{MS} = 1.5g$) were the most useful for investigating the short-period paradox since: (1) short-period archetypes of prior analytical studies were typically designed for high-seismic criteria; and (2) there were sufficient observations of collapse performance in past earthquakes to establish benchmark collapse rates for this level of ground motion.

Key configuration and modeling parameters of variant numerical models were investigated for each of the three SFRSs. Some modeling parameters were common across the three systems (e.g., soil-structure interaction and foundation flexibility), but others were system specific (e.g., variation of brace configuration of a steel SCBF). Table 4-1 lists the parametric studies for each SFRS, along with the occupancies and number of stories considered. A brief description of each parametric study is provided after Table 4-1.

Baseline Configuration Parametric Studies: investigated the variation in the response behavior and collapse performance of archetypes of short-period buildings with numerical models that represented best-estimate response behavior and collapse performance of the SFRS of interest. Baseline archetypes incorporated all elements of real buildings that might affect behavior (e.g., nonstructural wall finishes for wood light-frame building archetypes). These studies considered differences in archetype configurations due to occupancy, building height, and seismic design level. Baseline archetypes were designed and evaluated for both high-seismic ($S_{MS} = 1.5g$) and very high-seismic ($S_{MS} = 2.25g$) criteria. Only baseline archetypes were designed and evaluated for very high-seismic loads; building archetypes of all other parametric studies were designed and evaluated for high-seismic criteria.

Table 4-1 Parametric Studies Used to Investigate the Collapse Performance of Short-Period Buildings

Parametric Study	Seismic-Force-Resisting System				
	Wood Light-Frame			Reinforced Masonry	Steel SCBF
	COM	MFD	SFD	COM	COM
Baseline: High Seismic	1, 2, and 4 stories	1, 2, and 4 stories	1, 2, and 4 stories	1, 2, and 4 stories	1, 2, and 4 stories
Baseline: Very High Seismic	1, 2, and 4 stories	1, 2, and 4 stories	1 and 2 stories	1, 2, and 4 stories	1, 2, and 4 stories
Collapse Displacement Capacity	1 and 2 stories	1 and 2 stories	1 and 2 stories	1, 2, and 4 stories	-
SSI and Foundation Flexibility	1, 2, and 4 stories	1, 2, and 4 stories	-	2 stories	2 and 4 stories
Nonstructural Wall Finishes	2 stories	2 stories	1 and 2 stories	-	-
Backbone Curve Shape	4 stories	-	-	-	-
Brace Configuration	-	-	-	-	2 and 4 stories
No Redundancy	-	-	-	-	2 stories
No Reserve Moment Frame	-	-	-	-	2 stories

Displacement Capacity Parametric Studies: investigated the effects of collapse displacement capacity on response behavior and collapse performance. Shake-table and pull tests of full-scale test structures have shown story-drift ratios of 10 percent or greater without loss of stability (Isoda, 2008; Cheng et al., 2020), which are significantly greater than collapse displacement capacity of the nonlinear models of prior FEMA P-695 studies. Variations in the collapse displacement capacity of numerical models of archetypes were represented by different modeling assumptions of post-capping residual strength. For wood light-frame archetype models, displacement capacity was investigated by varying the strength of the residual strength plateau. For the reinforced masonry archetype models, the displacement capacity was investigated by varying the slope of the post-peak base shear-vs.-story drift curves from the baseline models. Response and collapse results of variant archetype models were compared with those of the corresponding baseline configuration archetype models.

Soil-Structure Interaction (SSI) and Foundation Flexibility Parametric Studies: investigated SSI inertial and kinematic effects and foundation flexibility for two soil conditions (stiff and soft sites) on response behavior and collapse performance. SSI inertial effects were modeled with a distributed set of discrete nonlinear soil springs and dashpots below flexible foundation elements. SSI kinematic effects were evaluated by modifying the frequency content of ground motion records (filtered records) used for response history analysis. Response and collapse results of variant archetype

models with nonlinear soil springs, dashpots, and flexible foundation elements analyzed using filtered records were compared with those of the corresponding baseline configuration archetype models on fixed bases (i.e., rigid foundations) analyzed using unfiltered records. SSI modeling was limited to nonlinear soil springs (SSI inertial effects) below flexible foundation elements for wood light-frame archetypes.

Nonstructural Interior and Exterior Wall Finishes Parametric Study: investigated the effects of nonstructural interior and exterior wall finishes (e.g., gypsum wallboard, stucco, and horizontal wood siding) on the response behavior and collapse performance of short-period wood light-frame buildings by removing interior and exterior wall finishes from baseline configuration archetype models. Response and collapse results of variant archetype models were compared with those of the corresponding baseline configuration archetype models.

Backbone Curve Shape Parametric Study: investigated the effects of the backbone curve shape used to define the peak and post-capping strength and stiffness of shear wall components to determine the sensitivity of the probability of collapse to the backbone curve shape of the numerical models of wood light-frame building archetypes. This study focused on wood structural panel systems and used the design values published in the *Special Design Provisions for Wind and Seismic* (AWC, 2008) as anchors to peak strengths. Response and collapse results of variant archetype models were compared with those of the corresponding baseline configuration archetype models.

Brace Configuration Parametric Study: investigated the effects of different types of brace configurations on the response behavior and collapse performance of steel SCBF buildings. Steel SCBF buildings can be designed with different brace configurations, including diagonal bracing, chevron bracing, and double-story X-bracing. Response and collapse results of variant archetype models designed with chevron bracing were compared with the results of the corresponding baseline configuration archetype models with double-story X-bracing (two-story and four-story archetypes).

No Redundancy Parametric Study: investigated the effects of redundancy on response behavior and collapse performance of steel SCBF buildings. Section 12.3.4 of ASCE/SEI 7 requires a redundancy factor (ρ) to be assigned in each of the two orthogonal directions of the SFRS based on the configuration of the system and system-specific redundancy criteria. The redundancy factor increases horizontal seismic loads required for design of members of structures not meeting the redundancy criteria. Response and collapse results of variant

archetype models designed to be code compliant assuming the redundancy criteria were not met (i.e., $\rho = 1.3$) were compared with the results of the corresponding baseline configuration archetype models designed to be code compliant where the redundancy criteria were met (i.e., $\rho = 1.0$).

No Reserve Moment Frame Capacity Parametric Study: investigated the effects of the reserve moment frame action within the braced frames on response behavior and collapse performance of steel SCBF buildings. After brace fracture occurs on a given story, lateral resistance is still provided by reserve moment-frame action within the braced frames resulting from the presence of the gusset plate connections at beam-to-column connections and the column braces. Response and collapse results of variant archetype models that removed the reserve moment frame action within the braced frames were compared with the results of the corresponding baseline configuration archetype models that preserved the reserve moment frame-action within the braced frames.

4.2 Summary of Archetype Designs and Configurations

This section summarizes the designs and configurations of the wood light-frame, reinforced masonry, and steel SCBF archetypes.

4.2.1 Design of Wood Light-Frame Archetypes

Three common occupancies of wood light-frame buildings were investigated: single-family dwellings (SFD), multi-family dwellings (MFD), and commercial (COM) buildings. All archetypes relied upon structural wood panels nailed to walls framed with wood studs and plates as the yielding elements of the SRFS. All archetypes were Risk Category II structures. The SFD archetypes had plan dimensions of 32 feet by 48 feet, and the MFD and COM archetypes had plan dimensions of 48 feet by 96 feet. One- and two-story versions of the SFD were designed and analyzed, whereas one-, two-, and four-story versions of the other occupancies were designed and analyzed. Designs were prepared for moderate-, high-, and very high-seismic ground-motion levels.

The structural configurations were idealistically simplified but still appropriate to capture the significant aspects of nonlinear seismic response. Figure 4-1 shows an isometric view of the two-story, high-seismic MFD archetype.

Floor and roof framing in the COM archetypes were parallel-chord wood trusses. The floors in the MFD archetypes were the same, but the roofs were framed with pitched wood trusses. The second floor of the two-story SFD archetypes were framed with wood I joists, and the roof of both SFD

archetype designs were pitched trusses. All floors and roofs were sheathed with oriented strand board (OSB) panels. The spacing of interior shear walls was close enough for all designs, except the one-story COM archetypes, that minimum nailing sufficed for the diaphragms. In all cases, the yielding in the SFRS was predicted to be confined to the walls, not the diaphragms.

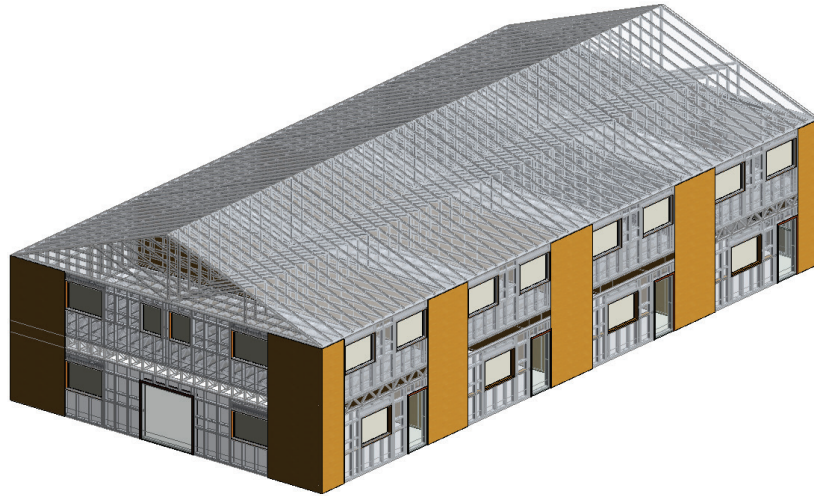


Figure 4-1 Isometric view of the two-story, high-seismic wood light-frame MFD archetype.

The designs were intended to conform to the 2015 IBC and to follow common practice in high-seismic hazard areas of the western United States. The one exception is that variants of the SFD archetypes were designed according to the conventional construction rules of the IRC. The plan layout of the two-story MFD archetypes was configured as single-family attached houses (e.g., “row houses” or “townhouses”). The one- and four-story MFD archetypes were configured as apartments with central corridors. The one-story COM archetypes were configured with open plans, such as is found in a retail shops or restaurants. The multi-story COM archetypes were configured as small office buildings with interior partitions. Floor openings for stairs were not included, but all designs included openings for doors in interior and exterior walls and for exterior windows.

Shear wall lengths were in 4-foot modules for the SFD and MFD archetypes and 8-foot modules for the COM archetypes, largely to facilitate development of the nonlinear models for collapse analysis. The foundations were all designed as shallow spread footings cast integrally with slabs-on-grade. The only significant departure of common design practice was that the sheathings and coverings applied to the walls and partitions were quantified for use in the collapse analysis. These quantities were based upon informal surveys of common buildings, and they were not considered in the designs of the seismic-force-resisting systems, only in the nonlinear response analyses.

4.2.2 Design of Reinforced Masonry Archetypes

All archetypes were intended to represent code-compliant modern construction for common commercial office (COM) occupancies that routinely adopt a reinforced masonry structural system. The SFRS for all archetypes was load bearing, fully grouted, reinforced hollow-unit concrete masonry with cantilever shear walls, a system which is common in the western United States. Originally, archetypes were selected to represent three occupancies in Risk Category II: commercial buildings, multi-family residential buildings, and retail or industrial “big box” occupancies; ultimately, only the commercial occupancies were analyzed. An isometric view of the two-story, high-seismic reinforced masonry commercial archetype is shown in Figure 4-2.

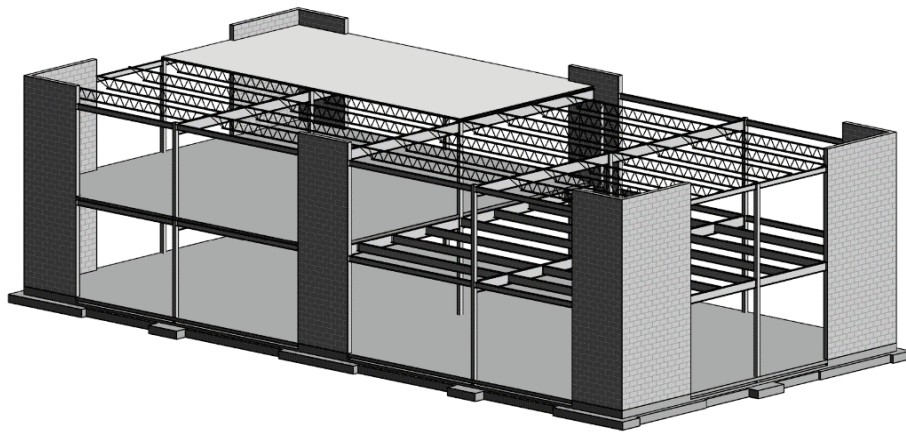


Figure 4-2 Isometric view of the two-story, high-seismic reinforced masonry commercial archetype.

The same 48 foot-by-96 foot plan dimensions used for wood light-frame COM archetypes was also used for the reinforced masonry COM archetypes. One-, two-, and four-story archetypes were designed, organized on a regular 24 foot-by-24 foot grid, with shear walls organized symmetrically around the exterior of the plan. In each archetype, the ground floor was a slab-on-grade, and elevated floors, if any, were composite steel framing with concrete on metal deck spanning between beams, which in turn were supported on girders and columns or bearing walls. This floor system provided a relatively stiff diaphragm. In accordance with common practice, the roof was untopped steel deck supported by open-web steel joists and wide-flange perimeter beams. This roof system provided a relatively flexible diaphragm.

An important characteristic of the archetypes was the presence of flanged walls. Such walls are common in practice and were deemed necessary if the archetypes were to be representative of the existing building stock. Designs that incorporate flanged wall behavior can be challenging, considering the

need to adhere to maximum reinforcement limits and competing demands for a single flanged wall element that must meet code requirements for design forces in two orthogonal directions. In some cases, provisions of TMS 402/602, *Building Code Requirements and Specification for Masonry Structures* (TMS, 2013), that allow maximum reinforcement requirements to be bypassed under certain conditions were invoked.

Although efficient structural design was a goal, the arrangement and size of the shear walls were selected to represent common buildings and were not optimized to provide the minimum structure necessary to meet code-specified seismic strength or displacement criteria. Instead, the wall configurations were considered as a given architectural constraint. As a result, the shorter archetypes were governed by minimum reinforcement requirements, whereas the taller archetypes were more likely to be governed by drift or strength criteria.

4.2.3 Design of Steel SCBF Archetypes

The archetypes were intended to represent code-compliant modern construction for commercial office occupancies (COM) in Risk Category II that routinely adopt a steel SCBF system. This SFRS is common in high-seismic areas in the western United States. Other occupancies were not studied because occupancy is not believed to have a significant effect on the layout or design of this SFRS. An isometric view of the two-story, high-seismic steel SCBF COM archetype is shown in Figure 4-3.

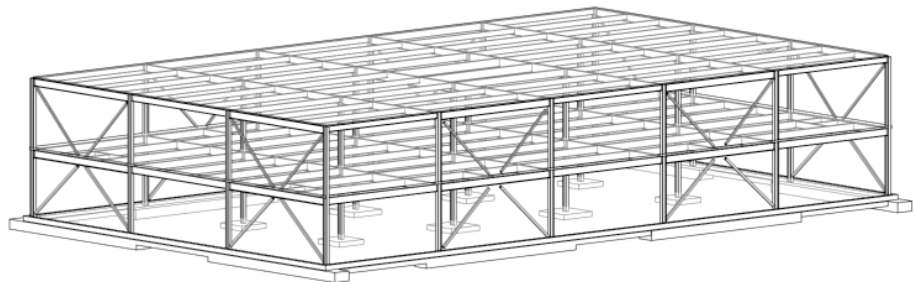


Figure 4-3 Isometric view of the two-story, high-seismic steel SCBF commercial archetype.

The plans for all archetypes shared the following characteristics:

- Rectangular plan: 90 feet \times 150 feet
- Grid spacing: 30 feet \times 30 feet
- Floor-to-floor height: 14 feet
- Structurally symmetrical in each plan direction, with the seismic-force-resisting system on the building faces

- Floors:
 - 3-inch normal-weight concrete over 2-inch, 18-gauge composite deck supported on composite wide-flange beams at 10-feet on center
- Roof:
 - 3-inch roof deck over wide-flange beams at 10-feet on center
 - One full bay at the center of the building was assumed to have a concrete deck and mechanical loading

In practice, different brace shapes and sizes can be selected to satisfy project requirements, including wide-flange sections or square, rectangular, or round hollow structural sections (HSS). For this study, square HSS was chosen to represent a common choice for low-rise building SCBF braces. Square HSS was also chosen because it represents the shape that has been used commonly in research. All HSS shapes were selected to meet the width-to-thickness ratio (b/t) requirements of ANSI/AISC 341-10, *Seismic Provisions for Structural Steel Buildings* (AISC, 2010).

Braces sizes were selected to produce a design demand-to-design capacity ratio (D/C) closest to 1.0. This included using shapes that may not be readily available or used commonly in practice. Selection of the most efficient brace size was done to minimize the inherent overstrength associated with the braced frame systems.

4.3 Summary of Numerical Modeling

This section summarizes the modeling techniques used to analyze the wood light-frame, reinforced masonry, and steel SCBF archetypes. Advancements in modeling features used in this study compared to prior FEMA P-695 studies are also briefly discussed.

4.3.1 Numerical Modeling of Wood Light-Frame Archetypes

The *Timber3D* analysis program (Pang et al., 2012) developed as part of the NEES-Soft project (van de Lindt et al., 2012) was utilized to analyze the nonlinear and inelastic seismic collapse mechanics of wood light-frame archetype models. The ability to analyze three-dimensional wood light-frame models based on co-rotational formulation and large displacement theory represents a significant advancement compared to the prior FEMA P-695 studies using two-dimensional models (Shirazi and Pang, 2012; Christovasilis and Filiatrault, 2013) or pseudo three-dimensional models (Folz and Filiatrault, 2001).

For typical wood light-frame buildings, nonlinear behavior mainly comes from shear walls. Hence, except for the shear walls and vertical soil springs, all components were modeled using elastic elements (Figure 4-4). The horizontal (floor and roof) diaphragms and vertical wall studs were modeled using co-rotational, three-dimensional, two-noded, 12-degree-of-freedom (DOF) elastic frame elements, which account for geometric nonlinearity (P-delta effects). The elastic flexural and axial stiffness of wall studs were modeled using three-dimensional, two-noded, 12-DOF elastic frame elements. The wall panel-to-framing assemblies were modeled using 6-DOF, frame-to-frame (F2F) link elements. Only one (lateral) DOF of the F2F link element was activated to model lateral nonlinear cyclic response of walls sheathed with wood panels and other (nonstructural) materials. For the SSI and foundation flexibility parametric study, additional F2F link elements were activated to consider the inertial effects of SSI. The lateral and vertical behavior of soil was modeled using a series of linear elastic and bilinear inelastic springs, respectively, spaced at 2-feet on center along the concrete foundation beams, which were modeled using 12-DOF elastic frame elements.

The nonlinear lateral cyclic responses of walls were captured using a new residual strength hysteresis model, which was modified from the CUREE hysteretic rule (Folz and Filiatrault, 2001). The original CUREE hysteretic rule, which was used in prior FEMA P-695 studies, assumes very small drift ratios at collapse of wood sheathed walls (approximately 4 percent). The post-capping strength and stiffness were replaced by an S-shaped curve that converged to a pre-determined post-capping residual strength level at large displacements (Figure 4-4).

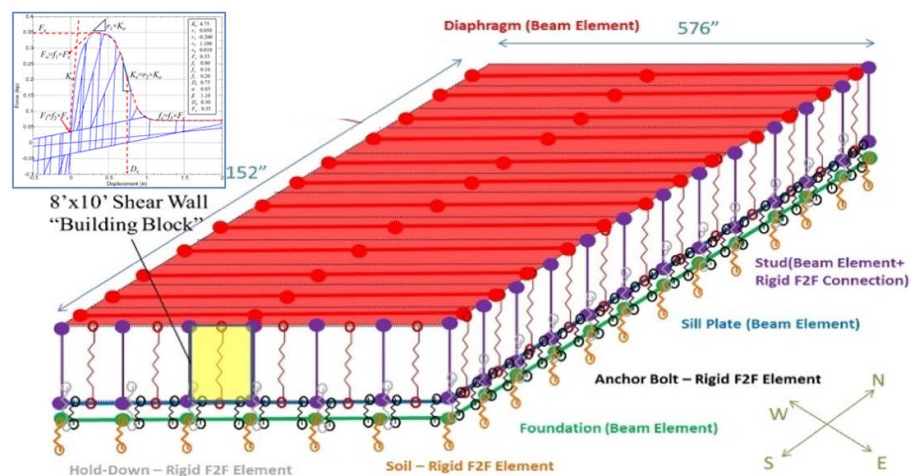


Figure 4-4 Schematic illustration of a three-dimensional one-story wood light-frame archetype model.

To avoid unnecessary detailed modeling of unique wall properties, all walls (structural and nonstructural) were based on 4-foot-long by 10-foot-high and 8-foot-long by 10-foot-high nonlinear wall “building blocks” made of various common sheathing panels and framing materials. The building block has the ability to represent walls with various combinations of sheathing materials (e.g., wood structural panels on one side and gypsum board on both sides) based on the combination rules of FEMA P-807, *Seismic Evaluation and Retrofit of Multi-Unit Wood-Frame Buildings with Weak First Stories* (FEMA, 2012). The baseline archetypes were modeled with the best estimate of wall building-block properties calibrated using available wall test data, including a best-estimate residual post-capping strength of 30 percent of the peak strength.

For each archetype model, free vibration analysis was first performed to evaluate the elastic natural periods and mode shapes. A nonlinear static pushover analysis was also performed in each lateral direction to obtain the peak strength and displacement capacity. Finally, incremental dynamic analysis in accordance with the FEMA P-695 methodology was carried out to determine MCE_R collapse performance.

4.3.2 Numerical Modeling of Reinforced Masonry Archetypes

When subjected to severe seismic forces, shear walls in reinforced masonry buildings can develop inelastic flexure deformations, diagonal shear cracking, shear sliding along horizontal joints between the walls and slabs, or a combination of one or more of these mechanisms. The flexural mechanism can induce tensile cracking and compressive crushing of the masonry and buckling and low-cycle fatigue of the vertical reinforcing bars. The shear sliding and diagonal shear mechanisms can engage the dowel action of the reinforcing bars crossing the cracks. Furthermore, the opening of cracks and the deformations that can be sustained by a cracked wall before the reinforcing bars crossing the cracks fracture in tension strongly depend on the bonding and the amount of slip of the reinforcing bars embedded in the grout. Ultimately, the failure mechanism and the resulting displacement capacity of a reinforced masonry wall system at incipient collapse are strongly affected by the interaction of the wall components with other structural elements, such as the beams and horizontal diaphragms. Hence, to assess the response of the reinforced masonry archetypes to the point of collapse in a reliable manner, all the aforementioned phenomena have to be accounted for in the numerical models. To achieve this goal without sacrificing computational efficiency for IDA, two types of models were developed for each reinforced masonry archetype. One was a finite-element model using the analysis program LS-DYNA (LSTC, 2018) that could

simulate all the aforementioned phenomena. The other was a computationally efficient frame model using the analysis program OpenSees (Mazzoni et al., 2006), which was used for IDA. The latter was calibrated with the finite-element model for each archetype. To obtain numerical results for model calibration, dynamic response-history analyses were performed with the finite-element model using three sets of bi-directional ground-motion records that had different response-spectrum characteristics and time-history profiles. The frame model was calibrated so that its response matched the results from the finite-element model, and the calibration was further validated with a fourth set of ground-motion records.

Figure 4-5a shows a representative finite-element model developed for a two-story reinforced masonry archetype. As shown in Figure 4-5b, the masonry walls were modeled with shell and interface elements, considering both geometric and material non-linearity. A smeared-crack material law was implemented in the shell elements to describe the crushing and cracking behavior of the masonry walls and horizontal concrete diaphragms. For masonry walls in the lower stories, where significant diagonal shear cracks could develop, cohesive crack interface elements were introduced to represent cracks in a discrete fashion, and to model sliding along crack surfaces and joints. The reinforcement in the walls was modeled with beam elements to allow the simulation of bar buckling.

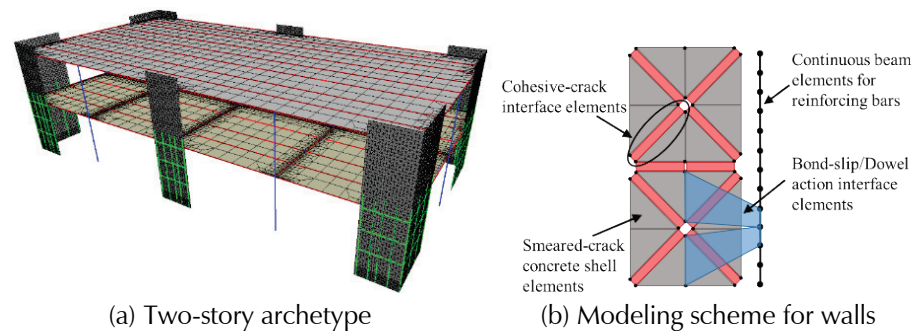


Figure 4-5 Finite-element model for a two-story reinforced masonry archetype.

The bars were connected to the shell elements with interface elements to simulate bond slip and dowel action. The beam elements had a steel material law that accounted for low-cycle fatigue and bar fracture. For walls in the upper stories, where no significant damage was expected, the nonlinear behavior was modeled in a coarser manner, in which only smeared-crack shell elements were used and the reinforcement was modeled in a smeared fashion with a bilinear material law. An element removal strategy (for crushed masonry and fractured bars) was introduced to enhance the

robustness of the numerical computation and the accuracy of the model when the structure approached collapse.

Figure 4-6 shows the frame model for the same two-story reinforced masonry archetype shown in Figure 4-5. The walls in the second story were modeled with elastic beam-column elements for the sake of computational efficiency. To model the inelastic response of the L-shaped walls in the first story, each wall was represented by a rigid bar with two rotational springs at each end. One pair of top and bottom springs were used to model the wall behavior along each direction of the building.

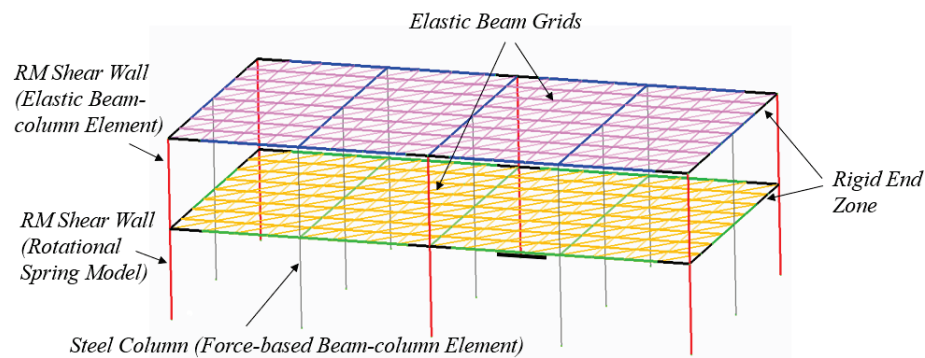


Figure 4-6 Frame model for a two-story reinforced masonry archetype.

The moment-rotation relationship for each spring was represented by a phenomenological hysteretic law. The hysteretic law was calibrated to reproduce the lateral load-lateral displacement response of each wall, as well as the maximum moment developed at the wall base in the finite-element analyses. The steel beams in the floor and roof systems, as well as the steel columns in the gravity frames, were represented by beam-column elements with fiber sections and a bilinear material law. Zero-length springs were used to connect the steel beams to the columns and masonry walls.

To model SSI and foundation flexibility, the foundation around the perimeter of the building was represented by displacement-based beam elements, which had fiber sections that accounted for material nonlinearity. The resistance of the soil was modeled with nonlinear springs and dampers, which were distributed along the foundation. The foundation of each interior column was assumed to have a zero dimension, and the soil resistance was modeled by springs and dampers concentrated at the bases of the columns. To account for kinematic interaction (which includes the effects of base-slab averaging), the free-field ground-motion records were filtered with a transfer function that represented the site properties to obtain the input motion.

Free vibration analyses and pushover analyses were conducted with the finite-element and frame models. For each frame model, incremental

dynamic analysis in accordance with the FEMA P-695 methodology was carried out to determine MCE_R collapse performance.

The models described above were more refined than those used in the previous study on the application of the FEMA P-695 methodology to reinforced masonry structures (NIST, 2010). In that study, only simplified frame models were used. The coupling actions of the floor and roof diaphragms on masonry shear walls were ignored. The frame models did not account for the shear-dominated mechanism of a wall and could not simulate the actual collapse mechanism of the structural system. Rather, collapse was signified by a set of conservative criteria. It was assumed that a building archetype would reach the collapse state when the shear strength of a wall was first reached or when the maximum curvature in a wall reached a critical value at which severe masonry crushing or bar fracture would occur. This modeling approach underestimated the displacement capacity of a masonry structure.

4.3.3 Numerical Modeling of Steel SCBF Archetypes

The steel SCBF archetypes were modeled in three dimensions using the analysis program OpenSees. Recent research on simulating the nonlinear seismic response of steel SCBF systems (e.g., Hsiao et al., 2012 and Sen et al., 2019) was drawn upon to develop the component behaviors that were included in the models. The contribution of all gravity frame members to system response was included. Gravity frame members were modeled using the same method as the beams and columns within the braced frames, including the nonlinear behavior of the beam-to-column connections. Co-rotational element formulations were used in OpenSees to account for nonlinear geometric effects.

The braced frames were modeled considering the nonlinear behavior of the braces, beams, columns, and connections. Figure 4-7 shows an annotated close-up of a steel SCBF model with callouts to the component models that are summarized below.

The brace model was based upon prior research by Hsiao et al. (2012) that has been extended recently by Sen et al. (2019). Braces were modeled with a fiber discretized cross section where a Giuffre-Menegotto-Pinto stress-strain model available in OpenSees was used for the material properties and fracture, as simulated by tracking the maximum strain range for each fiber and comparing that to the maximum strain range at fracture calibrated from more than 60 brace tests in Sen et al. (2019).

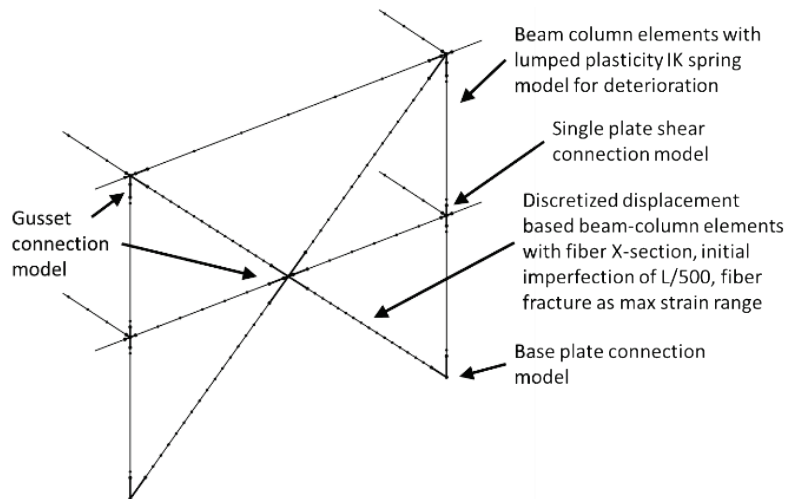


Figure 4-7 Annotated steel SCBF model with callouts for component models.

Gusset plates were assumed to bend out of plane to accommodate brace buckling and were modeled with nonlinear rotational springs with strength and stiffness as proposed by Hsaio et al. (2012). Beams were modeled with displacement-based nonlinear beam-column elements with distributed plasticity and fiber-discretized cross sections. Deterioration of the beams themselves was not considered since all beams met seismic compactness requirements, and the flexural demands were small. Columns, in both the braced frames and the gravity framing, were modeled with elastic beam column elements incorporating discrete nonlinear rotational springs at each end to represent the nonlinear behavior of the columns in both the strong- and weak-axis bending directions, including deterioration.

Beam-to-column connections that were designed with shear tabs, both within the braced frames and within the gravity framing, were modeled with rotational springs with properties based largely on the recommendations in Liu and Astaneh-Asl (2004). Column-base connections within the braced frames were also modeled with rotational springs that accounted for base-plate connections that could not develop the plastic moment capacities of the columns.

Where SSI and foundation flexibility were considered, the footings under the braced frames were modeled explicitly using lumped-plasticity nonlinear beam elements, and the behavior of the soil, including damping, was simulated for all six degrees of freedom using a series of nonlinear spring and damper elements. The effects of kinematic interaction on the ground-motion input were included. A schematic of the model for a single braced frame on a strip footing with soil springs and dampers is shown in Figure 4-8.

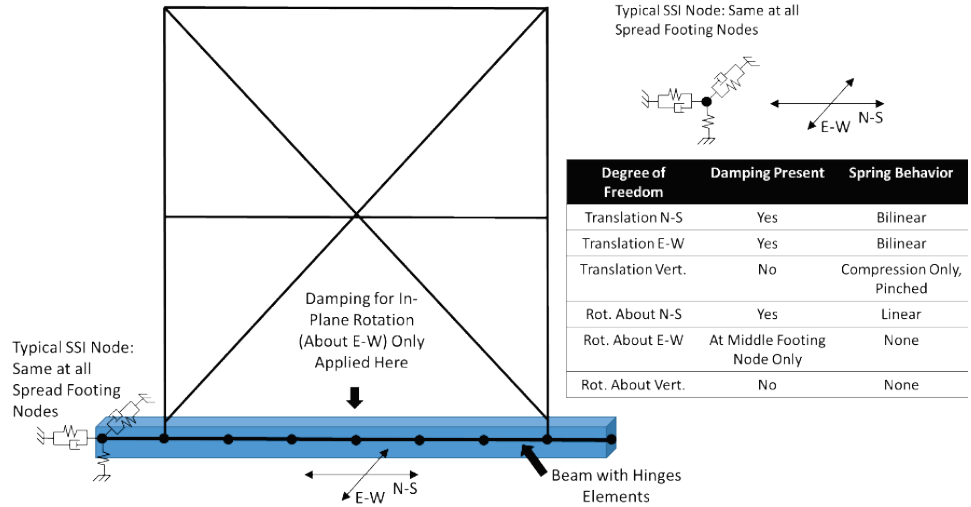


Figure 4-8 Schematic of spread footing with soil springs and dampers.

For each archetype, free vibration and pushover analyses were conducted. Incremental dynamic analysis in accordance with the FEMA P-695 methodology was carried out to determine MCE_R collapse performance.

The modeling described above for the steel building archetypes represents an advancement compared to prior FEMA P-695 studies because it combined for the first time the advanced deterioration models for braces, columns, and gravity frame connections in three-dimensional analyses to collapse. The inclusion of SSI considerations for some models was a further advancement in the three-dimensional simulation of braced frames through collapse.

4.4 Summary of Numerical Results: High-Seismic Baseline Archetypes

This section summarizes the collapse results of the baseline numerical models of high-seismic archetypes and compares them with the results of prior FEMA P-695 studies of short-period archetypes of similar height and seismic design level. Collapse results of these studies and those of prior studies are also compared to the benchmark metrics of Section 3.4 to determine if the analytical collapse results are consistent with observed collapse performance in past earthquakes. Key properties and collapse results of high-seismic baseline archetype models of these studies and those of prior FEMA P-695 studies of wood light-frame (Wood) systems, reinforced masonry (Masonry) systems, and steel SCBF (Steel) systems are summarized in Table 4-2.

Table 4-2 Summary of Key Model Properties and Collapse Results of High-Seismic Baseline Archetype Models and Comparable Archetypes of Prior FEMA P-695 Studies of Short-Period Buildings Designed for High-Seismic Loads

Archetype Model		Model Properties					Collapse Results			
SFRS	Name (Model ID)	No. of Stories	Period T (sec)	Period T_1 (sec)	Strength		Drift Ratio		CMR	P[COL] MCE _R] (%)
					Ω	V_{max}/W	Roof	First Story		
Wood Commercial Building Baseline Archetypes (FEMA P-2139-2)										
Wood	COM1B	1	0.16	0.29	3.6	0.56	0.082	0.082	1.55	7.3
Wood	COM2B	2	0.26	0.36	3.1	0.48	0.035	0.067	1.31	13.4
Wood	COM3B	4	0.45	0.58	2.0	0.31	0.016	0.046	1.15	19.0
Wood Multi-Family Dwelling Baseline Archetypes (FEMA P-2139-2)										
Wood	MFD1B	1	0.16	0.19	8.5	1.30	0.071	0.071	2.43	1.0
Wood	MFD2B	2	0.26	0.28	4.4	0.68	0.046	0.091	1.67	5.5
Wood	MFD3B	4	0.45	0.51	2.4	0.37	0.0164	0.052	1.2	17.2
Wood Single-Family Dwelling Baseline Archetypes (FEMA P-2139-2)										
Wood	SFD1B	1	0.16	0.16	12.1	1.86	0.022	0.022	2.15	1.8
Wood	SFD1BC	1	0.16	0.15	8.3	1.28	0.066	0.066	2.21	1.6
Wood	SFD2B	2	0.26	0.26	5.0	0.77	0.058	0.117	1.99	2.6
Wood	SFD2BC	2	0.26	0.25	4.9	0.76	0.049	0.096	1.92	3.0
PG-1 Wood Archetypes with Low Aspect-Ratio Walls of FEMA P-695 ⁽¹⁾										
Wood	1	1	0.16	0.40	2.0	0.33	≤0.07	≤0.07	1.34	12.4
Wood	5	2	0.26	0.46	2.5	0.42		≤0.07	1.49	9.1
Wood	9	3	0.36	0.58	2.0	0.33		≤0.07	1.45	9.4
Wood	PG-1	All	0.29	0.48	2.2	0.36		≤0.07	1.43	10.1
PG-9 Wood Archetypes with High Aspect-Ratio Walls of FEMA P-695 ⁽¹⁾										
Wood	2	1	0.16	0.29	4.1	0.68	≤0.07	≤0.07	1.94	8.1
Wood	6	2	0.26	0.37	3.8	0.63		≤0.07	2.14	6.1
Wood	10	3	0.36	0.44	3.7	0.62		≤0.07	1.91	8.4
Wood	13	4	0.45	0.53	2.9	0.48		≤0.07	1.73	12.0
Wood	15	5	0.53	0.62	2.6	0.43		≤0.07	1.78	11.4
Wood	PG-9	All	0.37	0.45	3.4	0.57		≤0.07	1.90	8.9
Masonry Commercial Baseline Archetypes (FEMA P-2139-3)										
Masonry	COM1B	1	0.18	0.14	5.6	1.11	0.088	0.088	3.35	0.14
Masonry	COM2B	2	0.26	0.19	3.3	0.66	0.035	0.064	1.90	3.2
Masonry	COM3B	4	0.45	0.31	2.4	0.47	0.015	0.058	1.43	9.9
PG-1S Masonry High-Gravity Archetypes of NIST GCR 10-917-8 ⁽²⁾										
Masonry	S1	1	0.18	0.10	1.84	0.37			0.52	79
Masonry	S2	2	0.26	0.13	2.28	0.46	0.015		1.14	21
Masonry	S3	4	0.45	0.21	1.87	0.37			1.55	8.4
Masonry	PG-1S	All	0.32	0.15	2.00	0.35			1.07	26

Table 4-2 Summary of Key Model Properties and Collapse Results of High-Seismic Baseline Archetype Models and Comparable Archetypes of Prior FEMA P-695 Studies of Short-Period Buildings Designed for High-Seismic Loads (continued)

Archetype Model		Model Properties					Collapse Results			
SFRS	Name (Model ID)	No. of Stories	Period T (sec)	Period T_1 (sec)	Strength		Drift Ratio		CMR	P[COL MCE _R] (%)
					Ω	V_{max}/W	Roof	First Story		
PG-5S Masonry Low-Gravity Archetypes of NIST GCR 10-917-8 ⁽²⁾										
Masonry	S11	1	0.18	0.10	1.84	0.37			0.52	79
Masonry	S12	2	0.26	0.13	1.82	0.36			1.71	5.9
Masonry	S13	4	0.45	0.26	1.73	0.35			1.65	6.8
Masonry	PG-5S	All	0.32	0.16	1.80	0.36			1.29	15.3
Steel Commercial Baseline Archetypes (FEMA P-2139-4)										
Steel	COM1B	1	0.20	0.16	11.0	2.00	0.030	0.030	2.32	1.2
Steel	COM2B	2	0.26	0.27	6.0	1.02	0.033	0.051	1.87	3.4
Steel	COM3B	4	0.45	0.46	3.9	0.66	0.032	0.065	1.83	6.0
PG-1SCB Steel Archetypes of NIST GCR 10-917-8										
Steel	2SCBFDmax	2	0.26	0.40	1.44	0.24		≤ 0.10	1.00	35
Steel	3SCBFDmax	3	0.49	0.58	1.41	0.23		≤ 0.10	1.60	8.6
Steel	PG-1SCB	All	0.38	0.49	1.43	0.24		≤ 0.10	1.30	17

- ⁽¹⁾ Drift ratios at incipient collapse are not provided in the FEMA P-695 report for wood light-frame archetype models. In that study, backbone curves have a relatively steep descending slope beyond a story drift ratio of about 0.03, causing collapse at or before a story drift ratio of about 0.07.
- ⁽²⁾ Drift ratios of non-simulated failure modes are only reported in NIST GCR 10-917-8 for certain reinforced masonry archetype models.
- ⁽³⁾ Drift ratios at incipient collapse are not provided in the NIST GCR 10-917-8 report for steel SCBF archetype models. In that report, the study of steel SCBF building archetypes assumed a story drift ratio of 0.10 for modeling non-simulated collapse failure modes.

In Table 4-2, key model properties include the number of stories, the design period of the archetype ($T = C_u T_a$, Section 12.8.2, ASCE/SEI 7), the fundamental period of the numerical model (T_1), the maximum base shear (or peak strength) of the pushover curve normalized by the weight of the archetype (V_{max}/W), and model overstrength ($\Omega = V_{max}/V_{design}$, where V_{design} is the design base shear for the archetype). Values of the model fundamental period, overstrength, and peak strength given in Table 4-2 represent the average values of these parameters in the two horizontal directions of response. The numerical models of these studies were three dimensional, whereas the numerical models of prior FEMA P-695 studies were two dimensional.

Collapse results include roof and first-story drift ratios at the point of incipient collapse of the numerical models, the collapse margin ratios (CMR), and the corresponding probabilities of collapse given MCE_R ground motions. The CMR parameter is defined as the ratio of the median collapse response spectral acceleration determined through incremental dynamic analysis to the

MCE_R response spectral acceleration ($CMR = S_{CT}/S_{MT}$). The value of the spectral shape factor (SSF), which is used in the calculation of the probability of collapse, is not shown but in all cases is equal to (or only slightly different from) 1.33, the value defined by Table 7-1b of FEMA P-695 for a short-period ($T \leq 0.5$ seconds) system with large ductility capacity ($\mu_T \geq 8$).

In Table 4-2, shading is used to indicate compliance of the collapse results with benchmark values of the MCE_R collapse probability established in Section 3.4 (i.e., 0–2 percent for one-story archetypes, 0–5 percent for archetypes of two stories or more). Green shading indicates compliance of numerical model results with benchmark values, and yellow and red shading indicate non-compliance. In addition to non-compliance with the benchmark values of these studies, red shading also indicates MCE_R collapse probability *greater* than the ASCE/SEI 7 collapse-safety objective of 10 percent probability of collapse given MCE_R ground motions for Risk Category II structures.

Figure 4-9 shows plots of the MCE_R collapse probabilities of Table 4-2 as a function of the design period (T). The design period (T), rather than model period (T_I), is used for consistency with the results of prior FEMA P-695 studies shown in Figure 1-1. The trends of decreasing or increasing values of the MCE_R collapse probability with period (i.e., number of stories) would be the same for any given SFRS if plotted in terms of model period. An added benefit of plotting in terms of the design period is a greater uniformity by building height. In Figure 4-9, results for models with the same number of stories are plotted at about the same design period for all SFRSs (e.g., 0.15 seconds–0.20 seconds for one-story models and about 0.25 seconds for two-story models).

In Figure 1-1, average MCE_R collapse probabilities are plotted for the short-period performance group of the SFRS of interest (which are also included in Table 4-2). The average MCE_R collapse probability can mask the period-dependent variability and trends of MCE_R collapse probabilities of the individual archetypes of the performance group. For example, the average value of the PG-1S short-period performance group of the prior reinforced masonry study of NIST GCR 10-917-8 plotted in Figure 1-1 is 26 percent; whereas the MCE_R collapse probabilities of individual archetypes of this performance group are 79 percent for the one-story archetype, 21 percent for the two-story archetypes, and 8.4 percent for the four-story archetype. Figure 4-9 shows the MCE_R collapse probabilities for individual archetypes of the short-period performance groups of prior studies presented in Table 4-2 to better illustrate period-dependent trends in collapse performance of short-period buildings.

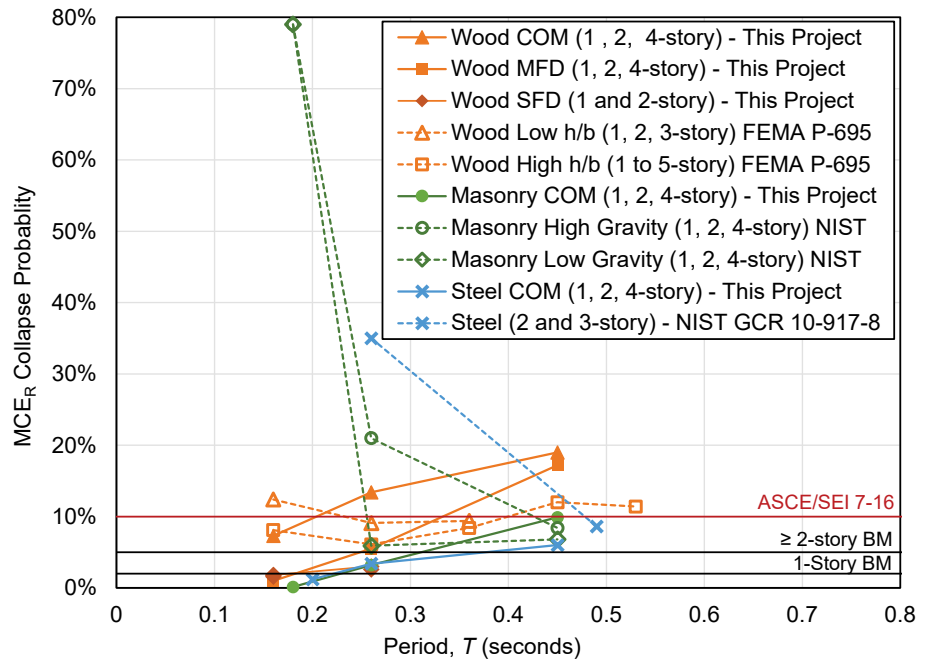


Figure 4-9 MCE_R collapse probabilities of high-seismic baseline archetype models and those of comparable archetype models of prior FEMA P-695 studies plotted as a function of archetype design period (T), and benchmark (BM) values of MCE_R collapse probabilities and the MCE_R collapse-safety objective of ASCE/SEI 7.

In general, the MCE_R collapse probabilities of one-story and two-story wood light-frame, reinforced masonry, and steel SCBF archetypes comply with benchmark metrics. COM wood light-frame archetypes are the notable exception with MCE_R collapse probabilities much greater than benchmark values. The higher values of the MCE_R collapse probabilities of COM wood light-frame archetypes are directly related to the relatively low strengths of these archetypes. In comparison to MFD wood light-frame archetypes, the configurations of COM wood light-frame archetypes have fewer internal walls and a much smaller contribution to archetype strength from nonstructural wall finishes.

Figure 4-10 shows the same MCE_R collapse probabilities as those of Figure 4-9 but plotted as function of the pushover strength of the numerical model normalized by weight (V_{max}/W), instead of the design period (T), of the archetype. COM and MFD wood light-frame archetypes have comparable values of MCE_R collapse probability for comparable values of pushover strength normalized by weight. Figure 4-10 also shows a consistent trend in the values of the MCE_R collapse probability for all archetypes of these studies and, in general, those of prior FEMA P-695 studies for the three SFRSs. This consistent trend is that the stronger the archetype, the better the collapse performance. This is in contrast to the trends shown in Figure 4-9, where

values of the MCE_R collapse probability consistently increase with period for the high-seismic archetypes, whereas values of the MCE_R collapse probability generally decrease with period for archetypes of the prior FEMA P-695 studies.

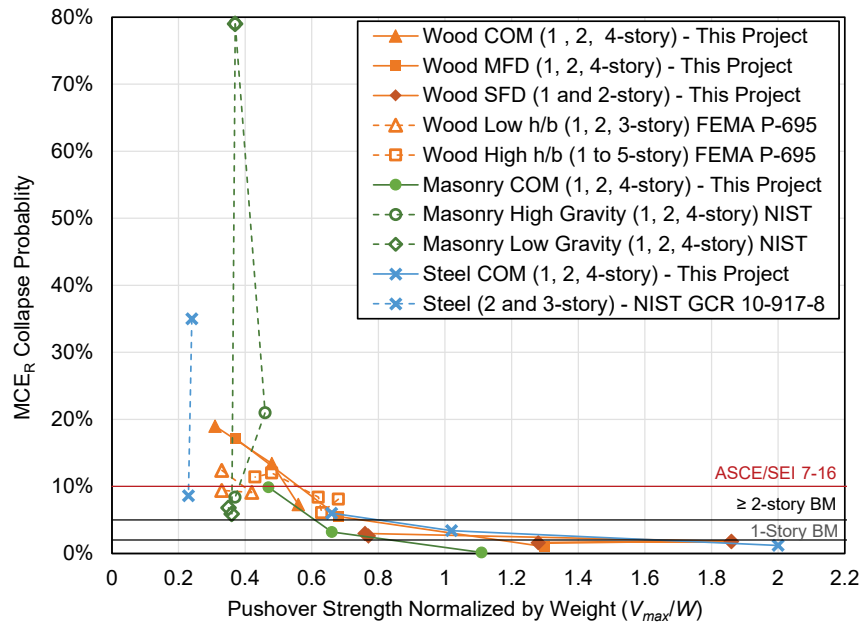
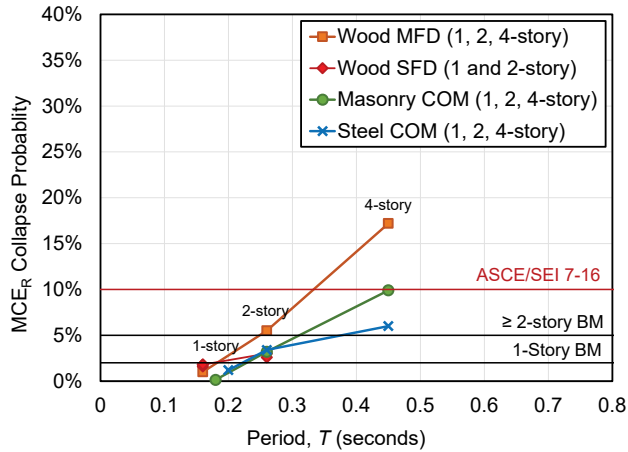
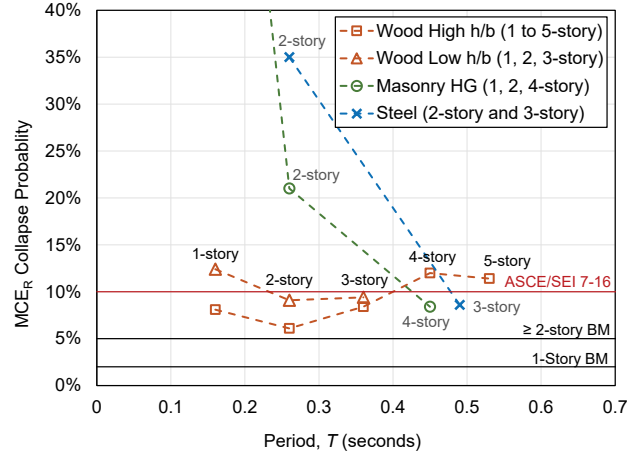


Figure 4-10 MCE_R collapse probabilities of high-seismic baseline archetype models and those of comparable archetype models of prior FEMA P-695 studies plotted as a function of pushover strength normalized by weight (V_{max}/W), and benchmark (BM) values of MCE_R collapse probabilities and the MCE_R collapse-safety objective of ASCE/SEI 7.

Figure 4-11a shows plots of the MCE_R collapse probabilities of high-seismic baseline archetype models as a function of the design period (T), and Figure 4-11b shows plots of the MCE_R collapse probabilities of comparable archetypes of prior FEMA P-695 studies as a function of the design period (T). These are the same plots as those of Figure 4-9 at a different scale, except without the COM wood light-frame archetypes of these studies and the low-gravity archetypes of the prior FEMA P-695 study of reinforced masonry buildings. The COM wood light-frame archetypes of these studies do not comply with the benchmark metrics (i.e., do not match observed performance) and, therefore, are not considered appropriate for resolving the short-period paradox. The MCE_R collapse probabilities of reinforced masonry low-gravity archetypes are largely redundant with those shown in Figure 4-11 for the reinforced masonry high-gravity archetypes and are omitted for clarity. Figure 4-11a shows the results of the improved numerical models of these studies that, along with the observed good collapse performance of short-period buildings in past earthquakes, provide the basis for resolving the short-period building performance paradox in Chapter 6.



(a) High-Seismic Baseline Archetype Models



(b) Archetype Models of Prior FEMA P-695 Studies

Figure 4-11 MCE_R collapse probabilities of (a) high-seismic baseline archetype models and (b) those of comparable archetype models of prior FEMA P-695 studies plotted as a function of archetype design period (T), and benchmark (BM) values of MCE_R collapse probabilities and the MCE_R collapse-safety objective of ASCE/SEI 7.

4.5 Key Findings Applicable to All Three Short-Period Systems

4.5.1 Key Findings of Baseline High-Seismic Studies

The baseline high-seismic parametric studies generated a number of key findings that are common across all three systems investigated in these studies. These common key findings are summarized below.

Failure Mechanism and Collapse Performance

For all high-seismic baseline archetypes, the failure mechanism is characterized by P-delta failure at the first story, which is more critical for taller archetypes.

The one-story and two-story high-seismic MFD and SFD wood light-frame baseline archetypes comply with the collapse benchmarks. COM and four-story MFD wood light-frame archetypes do not comply with the collapse benchmarks, and taller COM and MFD wood light-frame archetypes with overstrength less than approximately 4.0 also do not comply with the ASCE/SEI 7 collapse-safety objective of 10 percent probability of collapse given MCE_R ground motions.

Similarly, the one-story and two-story high-seismic reinforced masonry baseline archetypes comply with the collapse benchmarks. The four-story, high-seismic reinforced masonry baseline archetype does not comply, but this archetype complies with the ASCE/SEI 7 collapse-safety objective of 10 percent probability of collapse given MCE_R ground motions. All the high-

seismic steel SCBF baseline archetypes generally comply with the collapse benchmarks.

The common first-story failure mechanism observed in the high-seismic baseline archetypes indicates the importance of considering P-delta effects in numerical models, in particular for taller (multi-story) archetypes.

Influence of Strength on Collapse Performance

Strength was found to be the most important parameter influencing the collapse performance of the high-seismic baseline archetypes. As shown in Figure 4-10, there is a strong correlation between collapse performance and archetype pushover strength normalized by weight (V_{max}/W), which explains the relatively poor collapse performance of the weaker COM and MFD wood light-frame archetypes. The normalized pushover strength of a given archetype tends to be period dependent. That is, the shorter the period, the greater the normalized pushover strength for archetypes of the same seismic-force-resisting system. The same trends are seen when strength is expressed as overstrength (V_{max}/V_{design}). There is a strong correlation between collapse performance and overstrength (i.e., lower probabilities of collapse for higher values of overstrength), and the shorter the archetype, the greater the overstrength for archetypes of the same seismic-force-resisting system.

4.5.2 Key Findings of Collapse Displacement Capacity Studies

After strength, displacement capacity at the point of incipient collapse was found to be the next most important parameter influencing collapse performance of the wood light-frame and reinforced masonry high-seismic baseline archetypes. The influence of displacement capacity was not investigated for the steel SCBF high-seismic baseline archetypes.

For the wood light-frame archetypes, the displacement capacity, expressed in terms of a residual strength based on a percentage of the model peak strength and maintained to significantly higher drift ratios than previous FEMA P-695 studies, was found to significantly influence their collapse performance. The collapse results show a strong trend of lower collapse probabilities with increased collapse displacement capacity that corresponds directly to increased post-capping residual strength.

For the reinforced masonry archetypes, the displacement capacity, expressed in terms of the modeled post-peak slope of the base shear-vs.-first-story drift curves, also was found to have noticeable influence on the collapse performance. The collapse results show a strong trend of lower collapse probabilities with increased collapse displacement capacity.

It should be noted that the specific value of displacement capacity at the point of incipient collapse to incorporate in a numerical model of a given system is not well understood due to the lack of test data at these very large displacements.

4.5.3 Key Findings of Baseline Very High-Seismic Studies

The key findings described for high-seismic archetypes ($S_{MS} = 1.5g$) also apply to very high-seismic archetypes ($S_{MS} = 2.25g$). In general, however, the collapse performance was worse, often exceeding the ASCE/SEI 7 collapse-safety objective of 10 percent probability of collapse given MCE_R ground motions, for archetypes designed and evaluated for very high-seismic loads (model properties and collapse results for all very high-seismic archetypes can be found in FEMA P-2139-2, FEMA P-2139-3, and FEMA P-2139-4). Although the seismic loads for very high-seismic regions were 50 percent higher than those for high-seismic regions, the normalized pushover strengths for the very high-seismic archetypes were always less than 50 percent greater than the values for the same archetypes designed for high-seismic loads. For example, the one-story, very high-seismic steel SCBF archetype had only a 22 percent larger normalized pushover strength than the one-story, high-seismic steel SCBF archetype, and the two-story, very high-seismic steel SCBF archetype had only a 12 percent larger normalized pushover strength than its high-seismic counterpart. Overstrength for very high-seismic archetypes was also consistently less than that of the same archetypes designed for high-seismic loads. The reasons for the differences in strength between very high-seismic and high-seismic archetypes are different for each SFRS.

The structural walls of the very high-seismic wood light-frame archetypes were designed for 50 percent greater strength than those of the corresponding high-seismic archetypes. However, the strength of the nonstructural walls (e.g., interior gypsum and exterior stucco) was the same for both sets of archetypes, such that the nonstructural wall finishes provided a smaller contribution to the overall strength of the very high-seismic archetypes. As a result, all the COM and two-story and three-story MFD very high-seismic wood light-frame archetypes exceed the ASCE/SEI 7 collapse-safety objective.

The strength of a reinforced masonry system depends heavily on wall cross-sectional areas, which can be controlled to an extent in design and led to smaller differences in overstrength between high-seismic and very high-seismic archetypes compared with the wood light-frame and steel SCBF systems. This might help to explain why none of the reinforced masonry very high-seismic archetypes exceeds the ASCE/SEI 7 collapse-safety objective. For example, the four-story, very high-seismic reinforced

masonry archetype included significantly more wall cross-sectional area than the corresponding four-story, high-seismic archetype, resulting in similar overstrength and collapse performance values for both archetypes.

The strength of a steel SCBF system depends heavily on its brace sections. The lower overstrength for very high-seismic steel SCBF archetypes was the result of their braces having more efficient designs than those of high-seismic archetypes due to the limited availability of brace sizes. As a result, the overstrength of the two-story and four-story very high-seismic steel SCBF archetypes was reduced to the point that they do not meet the ASCE/SEI 7 collapse-safety objective.

4.5.4 Relationship between Strength and Collapse Displacement Capacity

The results of the baseline parametric studies clearly indicate that the strength and displacement capacity at the point of incipient collapse are the two most important parameters influencing the collapse performance of the three SFRSs investigated. This suggests that the probability of collapse of an SFRS can be determined by a collapse surface in which the three axes are defined by: (1) strength; (2) displacement capacity at the point of incipient collapse; and (3) probability of collapse. In other words, the same probability of collapse of an SFRS could be achieved for different combinations of strength and displacement capacity. This concept is discussed in more detail in Chapter 6.

However, the results also suggest that the relationship between strength and displacement capacity may be inherent to each SFRS. As shown in Table 4-2, the first-story drift ratios at incipient collapse of the light-frame wood and reinforced masonry one-story, two-story, and four-story high-seismic COM baseline archetypes increase with increasing values of strength. The trend is opposite for the steel SCBF baseline archetypes, where the first-story drift ratios at incipient collapse reduce with increasing strength. The results indicate that these two key parameters—strength and displacement capacity—may not be adjusted independently for a given SFRS.

4.5.5 Key Findings of SSI and Foundation Flexibility Studies

In general, the results indicate that modeling of SSI and foundation flexibility is not required for accurate calculation of short-period building collapse performance.

Modeling SSI inertial effects and foundation flexibility had a negligible influence on the collapse performance of wood light-frame building archetypes.

SSI kinematic effects had a negligible influence on collapse performance of reinforced masonry archetypes. Modeling SSI inertial effects and foundation flexibility did not significantly impact collapse performance for reinforced masonry archetypes. However, although it was not observed in the modeling, it is recognized that collapse performance could be influenced by SSI inertial effects and foundation flexibility for certain configurations of reinforced masonry archetypes for which lateral loads overcome gravity loads and cause uplift and rocking of spread footings before the walls above fail.

SSI kinematic effects had a negligible influence on collapse performance of steel SCBF archetypes. In contrast, collapse performance of steel SCBF archetypes founded on spread footings was significantly influenced by SSI inertial effects and foundation flexibility. Although collapse probabilities of the archetypes modeled with flexible bases with soil springs and dampers were found to be comparable to those of the baseline archetypes with rigid bases, the collapse failure modes were entirely different. In both cases, collapse was due to P-delta failure. However, rather than first-story brace failure, the steel SCBF archetypes modeled with SSI inertial effects and flexible foundations overcame gravity loads, uplifted, and rocked before brace failure could occur.

The results of the SSI and foundation flexibility studies suggest that code-based allowable reductions in design base shear for typical short-period buildings due to SSI and foundation flexibility may not be justified.

Chapter 5

Generic Collapse Performance

This chapter summarizes an investigation of the generic collapse performance of short-period buildings as characterized by a set of bilinear single-degree-of-freedom (SDOF) models and compares results of these analyses with those of prior SDOF studies. Here, the term “generic” is used in the sense that the investigation was not specific to any seismic-force-resisting system. Results of the SDOF models are then used to illustrate a notional relationship between short-period building collapse performance and the strength, displacement capacity, elastic response period, and failure mode of the building.

The impetus for the SDOF study comes from Section 2.3, which revealed a potential shortcoming with prior SDOF studies that defined collapse in terms of ductility rather than drift. The results of this chapter show that calculated collapse probabilities based on drift-based collapse displacement limits agree more closely with observed collapse behavior than those of ductility-based collapse displacement limits used in prior studies. The short-period seismic performance paradox is therefore explained in part by the simplified definitions of collapse displacement capacity adopted in the past. The results of this chapter augment the key findings of the system-specific studies of detailed models of wood light-frame, reinforced masonry, and steel SCBF systems summarized in Chapter 4.

5.1 SDOF Study Purpose and Methods

5.1.1 Introduction

The generic collapse performance of a set of simple bilinear SDOF models of short-period buildings was evaluated using the FEMA P-695 methodology for comparison with the results of prior SDOF studies, such as those described in NIST GCR 12-917-20.

The collapse evaluations of generic SDOF models were informed by (and complement) those of the detailed nonlinear models of wood light-frame, reinforced masonry, and steel SCBF systems summarized in Chapter 4. Specifically, collapse displacement at failure of the SDOF models was based on a relatively large story-drift ratio representative of that of the detailed nonlinear models of the three system-specific studies. For comparison, collapse displacement based on displacement ductility, the parameter used to

evaluate collapse performance of the SDOF models of prior studies, was also considered. In summary, collapse performance was evaluated for the same set of SDOF models for two different collapse displacement limits: (1) collapse displacement capacity based on an assumed displacement ductility of the SDOF model; and (2) collapse displacement capacity based on an assumed story-drift ratio capacity of the SDOF model.

5.1.2 SDOF Models

The SDOF models had the following characteristics:

- elastic-perfectly plastic hysteretic behavior (no strain hardening),
- the inclusion of P-delta effects,
- 2 percent of critical equivalent viscous damping, and
- nominal seismic weight, W , of 1000 kips.

Two SDOF model heights were considered:

- model height, H , was fixed at 10 feet, regardless of SDOF model period, and
- model height, H , varied with SDOF model period from 10 feet (nominal height of one-story buildings) to about 31 feet. Model height, H , was assumed to be $2/3$ of the total height (h_n) of a building, where total height (h_n) was determined from the elastic period (T) of the SDOF model using the approximate fundamental period formula of Section 12.8.2.1 of ASCE/SEI 7-16 (see Table 5-1).

The two types of model heights represented bounding patterns of the distribution of inelastic story drift over the height of a multi-story building. The SDOF model with the fixed height of 10 feet effectively assumed that all inelastic story drift occurred at the first story of a multi-story building, typical of the failure modes of the detailed models of two-story and four-story archetypes of wood light-frame, reinforced masonry, and steel SCBF systems. In contrast, the SDOF model with varying heights (which varied with model period) effectively assumed that inelastic story drift occurred uniformly at all stories of a multi-story building. The latter model represented a more favorable response mechanism that has distributed damage.

The maximum strengths and periods of the SDOF models were varied over ranges consistent with those of the detailed system-specific models. The SDOF model period, T , range considered was from 0.1 seconds to 0.5 seconds in 0.05-second intervals. Four maximum (pushover) base shear strengths, V_{max} , of SDOF models were used: $0.2W$, $0.4W$, $0.6W$, and $0.8W$.

Given the elastic-perfectly plastic behavior and the inclusion of P-delta effects, the initial elastic stiffness, K_e , and post-yield stiffness, K_p , (which is negative due to P-delta effects) of the SDOF models are given by:

$$K_e = \frac{W}{g} \left(\frac{2\pi}{T} \right)^2 \quad (5-1)$$

$$K_p = -\frac{W}{H} \quad (5-2)$$

where, g is the acceleration of gravity. Note that the relatively minor influence of P-delta effects is neglected in Equation 5-1.

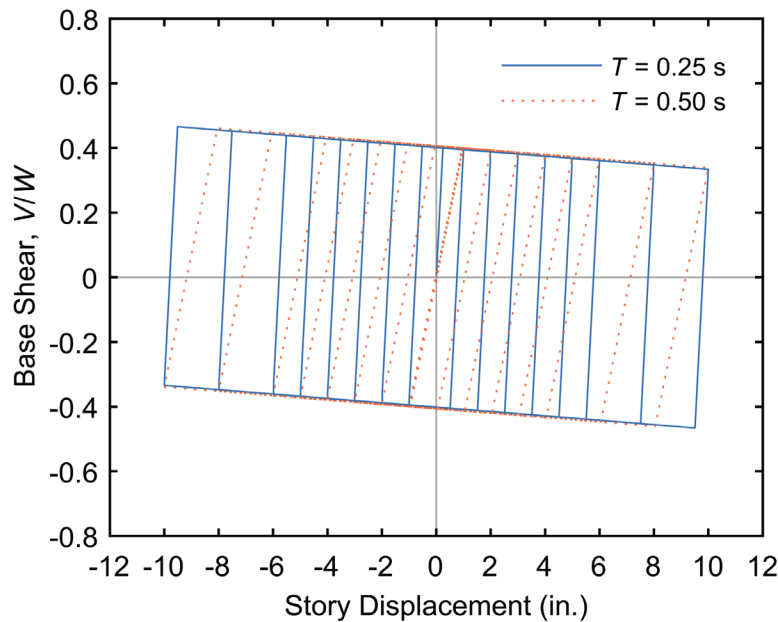


Figure 5-1 Example hysteretic behavior of SDOFs model with periods, $T = 0.25$ seconds and $T = 0.50$ seconds and maximum strength, $V_{max} = 0.4W$.

Elastic-perfectly plastic modeling was selected in order to best match the prior SDOF studies to which comparisons are being made. It is understood that this modeling significantly overestimates retained capacity for post-peak displacements, which results in overestimation of the adjusted collapse margin ratio, $ACMR$, which is obtained by correcting the collapse margin ratio, CMR , by the spectral shape factor, SSF (i.e., $ACMR = SSF \times CMR$). This modeling assumption, however, does not detract from the conceptual results provided by this investigation. An example of the resulting hysteretic behavior of the SDOF model with period, $T = 0.25$ seconds and maximum strength, $V_{max} = 0.4W$ is shown in Figure 5-1. The negative slope beyond peak strength is due to P-delta effects. Notably, because these systems have short periods and small elastic displacements, the stability coefficients calculated for these systems from ASCE/SEI 7-16 are small.

5.1.3 Incremental Dynamic Analysis

Incremental dynamic analysis was performed according to FEMA P-695 using the 22 ground motion pairs (44 individual motions) of the far-field ground motion set. The far-field record set was normalized using the approach described in Appendix A of FEMA P-695. Incremental dynamic analysis was conducted by scaling the record set such that the geometric mean spectral acceleration of the records at the building's period, S_T , ranged from 0.01g to a maximum value of S_T in 0.01g increments, where the maximum value of S_T depended on the SDOF model strength (e.g., from 5.0g for SDOF models with maximum strengths of $V_{max} = 0.2W$ and $V_{max} = 0.4W$ to 7.0g for SDOF models with a maximum strength of $V_{max} = 0.8W$). An example IDA result is shown in Figure 5-2 for the SDOF model with period, $T = 0.25$ seconds and strength, $V_{max} = 0.4W$.

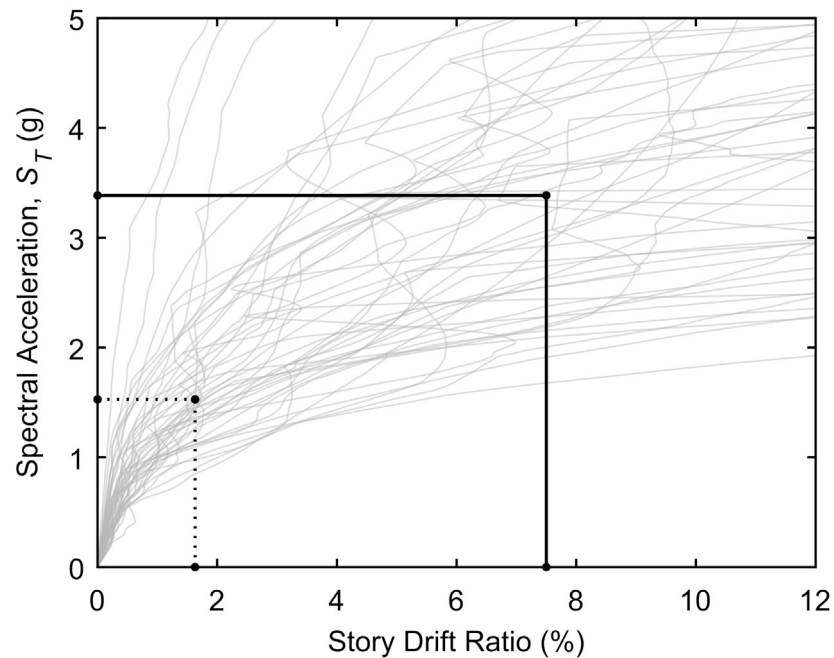


Figure 5-2 Example IDA results for the SDOF model with period, $T = 0.25$ seconds and maximum strength, $V_{max} = 0.4W$ showing median spectral accelerations at a story-drift ratio of 1.6 percent (corresponding to $\mu = 8$) and at a story-drift ratio of 7.5 percent (see Table 5-1).

The results of the incremental dynamic analyses of the SDOF models were saved for subsequent post-processing, including:

- evaluation of collapse performance using the two non-simulated collapse displacement limits described in Section 5.1.4, and
- evaluation of peak inelastic displacement (i.e., extent of peak inelastic displacement exceeding peak elastic displacement at shorter periods of

weaker SDOF models), confirming that trends are similar to those of prior SDOF studies using displacement ductility as the collapse displacement limit (e.g., Figure 2-3(d)).

5.1.4 Collapse Evaluation Criteria

The results of the incremental dynamic analyses were used to evaluate collapse performance of each SDOF model using two non-simulated collapse displacement limits:

1. Ductility-Based Collapse. Collapse was assumed to occur when the peak displacement of the SDOF model reached a maximum ductility demand, μ_{max} , of 8, typical of the ductility of models of prior SDOF studies, where ductility demand, μ , is defined as the ratio of peak story drift at collapse to story drift at yield, δ_y . Peak displacement at collapse is the product of maximum ductility demand, μ_{max} , and the story drift at yield, δ_y , where story drift at yield, δ_y , is a function of the maximum strength, V_{max} , and period of the model, T , i.e., $\delta_y = (g/4\pi^2) T^2 (V_{max}/W)$.
2. Drift-Based Collapse. Collapse was assumed to occur when the peak displacement of the SDOF model reached a drift ratio of 7.5 percent times the height of the model. Collapse performance is sensitive to the assumed value of the drift ratio, as illustrated by the notional collapse surfaces of Section 5.4. A drift ratio of 7.5 percent is typical of the median first-story drift ratio at collapse of the detailed system-specific models, which can vary significantly for different system models but were generally greater than 5 percent and less than 10 percent (see Table 4-2). Unlike the ductility-based collapse limit, the drift-based collapse limit was not a function of SDOF model strength. That is, drift-based collapse failure was assumed to occur at the same story-drift ratio for each model, except that weaker SDOF models were subject to P-delta failure at smaller story drifts than those of stronger SDOF models.

The drift-based and ductility-based collapse displacement limits of the models of the SDOF study are summarized in Table 5-1. At very short periods, ductility-based collapse displacements are unrealistically small (e.g., 0.31 inches for the SDOF model with a maximum strength, $V_{max} = 0.4W$ and a period, $T = 0.1$ seconds), but increase with period and converge on the more realistic drift-based value of collapse displacement for the SDOF model with a period of 0.5 seconds (i.e., 9.0 inches based on first-story failure and a drift ratio of 7.5 percent at collapse). The significant increase in drift-based collapse displacement of taller models assumed to have story drift essentially uniformly distributed over the height of the SDOF model (i.e., multi-story failure) is also shown in Table 5-1.

Table 5-1 Summary of Ductility-Based and Drift-Based Collapse Displacements Used to Evaluate SDOF Study Models

Elastic Period of SDOF Model (sec.)	Ductility-Based Collapse ($\mu = 8.0$)								Drift-Based Collapse (7.5 Percent)			
	$V_{max} = 0.2W$		$V_{max} = 0.4W$		$V_{max} = 0.6W$		$V_{max} = 0.8W$		First-Story Failure ⁽¹⁾		Multi-Story Failure ⁽²⁾	
	Yield Displ. (in.)	Collapse Displ. (in.)	Yield Displ. (in.)	Collapse Displ. (in.)	Yield Displ. (in.)	Collapse Displ. (in.)	Yield Displ. (in.)	Collapse Displ. (in.)	Model Height (ft.)	Collapse Displ. (in.)	Model Height ⁽³⁾ (ft.)	Collapse Displ. (in.)
0.1	0.02	0.16	0.04	0.31	0.06	0.47	0.08	0.63	10	9.0	10	9.0
0.15	0.04	0.35	0.09	0.71	0.14	1.06	0.18	1.41	10	9.0	10	9.0
0.20	0.08	0.63	0.16	1.25	0.24	1.88	0.31	2.5	10	9.0	10	9.0
0.25	0.12	0.98	0.25	1.96	0.37	2.94	0.49	3.9	10	9.0	12.3	11.1
0.30	0.18	1.41	0.35	2.8	0.53	4.2	0.71	5.6	10	9.0	15.7	14.2
0.35	0.24	1.92	0.48	3.8	0.72	5.7	0.96	7.7	10	9.0	19.3	17.4
0.40	0.31	2.5	0.63	5.0	0.94	7.5	1.25	10.0	10	9.0	23.1	20.8
0.45	0.40	3.2	0.79	6.4	1.19	9.6	1.59	12.7	10	9.0	27.0	24.3
0.50	0.49	3.9	0.98	7.8	1.47	11.7	1.96	15.7	10	9.0	31.1	28.0

⁽¹⁾ First-story failure assumed that all inelastic story drift occurred at the first story of a multi-story building represented by the SDOF model, where the height of the first story was $H = 10$ feet.

⁽²⁾ Multi-story failure assumed that inelastic story drift was uniformly distributed over the height of a multi-story building.

⁽³⁾ Model height, H , represented the effective height, which was assumed to be $2/3$ of total height (h_n) of a multi-story building, where the total height (h_n) was calculated from the elastic period (T) of the model using the approximate fundamental period formula of Section 12.8.2.1 of ASCE/SEI 7-16, i.e., $H = 2/3 \exp[\ln(T/1.4(0.02))/0.75]$.

Collapse performance of SDOF models was evaluated separately for the two non-simulated collapse displacement limits in accordance with FEMA P-695 methods, noting the following:

- \hat{S}_{CT} is the median value of the spectral acceleration, S_T , at the fundamental period, T , at which the SDOF model reached or exceeded collapse displacement capacity for one-half of the 44 individual ground motion records.
- For certain ground-motion records, the incremental dynamic analysis results sometimes showed peak displacement response that did not increase monotonically with the incremental increase in spectral acceleration, S_T . In such cases, where there was a “resurrection” of peak displacements across a collapse displacement limit, the median value of S_T of all of the crossings was used in the \hat{S}_{CT} evaluation.
- The value of the collapse margin ratio, CMR , was calculated in accordance with Equation 6-9 of FEMA P-695 for values of S_{MT} that were typically about 1.5g, consistent with the high-seismic (SDC D_{max}) loading criteria used for design of the detailed system-specific models.

- The SDOF models were not designed for S_{MT} (after reduction by $1.5R$), defined as the MCE_R spectral acceleration at the period of the system, as would be typical for FEMA P-695 procedures. Rather model maximum strength was assumed (e.g., $V_{max} = 0.4W$), meaning there was no defined value of S_{MT} for scaling of the ground-motion records. As a result, records were scaled by a factor of 2.0 to approximate the MCE_R level of response (i.e., $S_{MT} = 1.5g$), where a factor of 2.0 is typical of the scaling factors of Table A-3 of FEMA P-695 required for evaluation of SDC D_{max} archetypes with design periods less than or equal to 0.5 seconds. Values of S_{MT} used to calculate the CMR were based on the median spectral response of the scaled record set at the elastic period of interest.
- The value of the spectral shape factor, SSF , was taken as 1.33 for all analyses (i.e., period-based ductility, $\mu_T \geq 8$, Table 7-1a of FEMA P-695), consistent with the typical value of SSF used for collapse evaluation of the detailed system-specific models.
- The value of total system collapse uncertainty, β_{TOT} , was taken as 0.5, consistent with the value of β_{TOT} used for collapse evaluation of the detailed system-specific models.

Example plots of the collapse fragility curves (that include the SSF factor) for the SDOF model with maximum strength, $V_{max} = 0.4W$ and elastic period, $T = 0.25$ seconds and the collapse fractions of the IDAs used to develop these curves are shown in Figure 5-3. In the upper right corner of Figure 5-3 are the collapse probabilities at S_{MT} determined from the fragility curves for the two collapse displacement limits. Shading indicates spectral accelerations at or below the MCE_R ground-motion parameter, $S_{MT} = 1.57g$, and the probabilities of collapse given MCE_R ground motions are shown for the ductility-based and drift-based fragility curves. Figure 5-3 illustrates the significant difference in collapse performance of the same SDOF model evaluated using ductility-based (i.e., $\mu = 8$) and drift-based (i.e., 7.5 percent) collapse displacement limits. Collapse fragility curves shown in Figure 5-3 are based on the drift-based collapse displacement limit that assumes first-story failure; differences in collapse performance would be more significant for the drift-based collapse displacement limit that assumes multi-story failure (see Table 5-1).

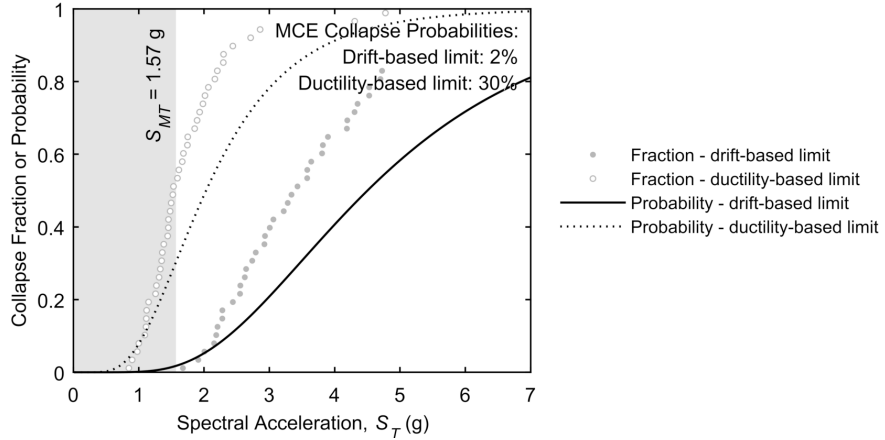


Figure 5-3 Example collapse fragility curves of the SDOF model with maximum strength, $V_{max} = 0.4W$ and period, $T = 0.25$ seconds and corresponding collapse fractions.

5.2 SDOF Study Results

5.2.1 Peak Inelastic Displacement

Peak inelastic drift ratios plotted as a function of the corresponding elastic drift ratio of SDOF models with model maximum strengths, $V_{max} = 0.2W$, $0.4W$, $0.6W$, and $0.8W$ are shown in Figure 5-4a through Figure 5-4d, respectively. In each figure, peak inelastic drift ratios are shown for SDOF models with model period, T , ranging from 0.1 seconds to 0.5 seconds. Circles identify values of peak inelastic response at $S_T = 2/3S_{MT}$, corresponding approximately to design level response. Note that the elastic drift ratios are computed directly from the spectral acceleration of the ground motion and the SDOF period [i.e., $S_T g T^2 / (4\pi^2)$] and that the median peak drift ratios from the elastic-perfectly plastic SDOF models include the displacement up to yield of the SDOF, which was small for the short-period SDOFs considered.

Trends in median peak inelastic displacement relative to peak elastic displacement that are similar to those of prior SDOF studies of short-period models, namely, for weaker models (i.e., $V_{max} \leq 0.4W$) are demonstrated by curves in Figure 5-4a through Figure 5-4d. Peak inelastic displacement is greater than peak elastic displacement at very short periods—the shorter the period, the greater the difference as a ratio. The most significant differences can be seen in Figure 5-4a for SDOF models with model maximum strength, $V_{max} = 0.2W$. The design-level peak inelastic drift ratio of the SDOF model with model period, $T = 0.5$ seconds is about 3 percent, or approximately 50 percent greater than the design-level elastic drift ratio of about 2 percent, whereas the design-level peak inelastic drift ratio of the SDOF model with model period, $T = 0.25$ seconds is about 1.6 percent, or approximately three times the design-level elastic drift ratio of about 0.5 percent.

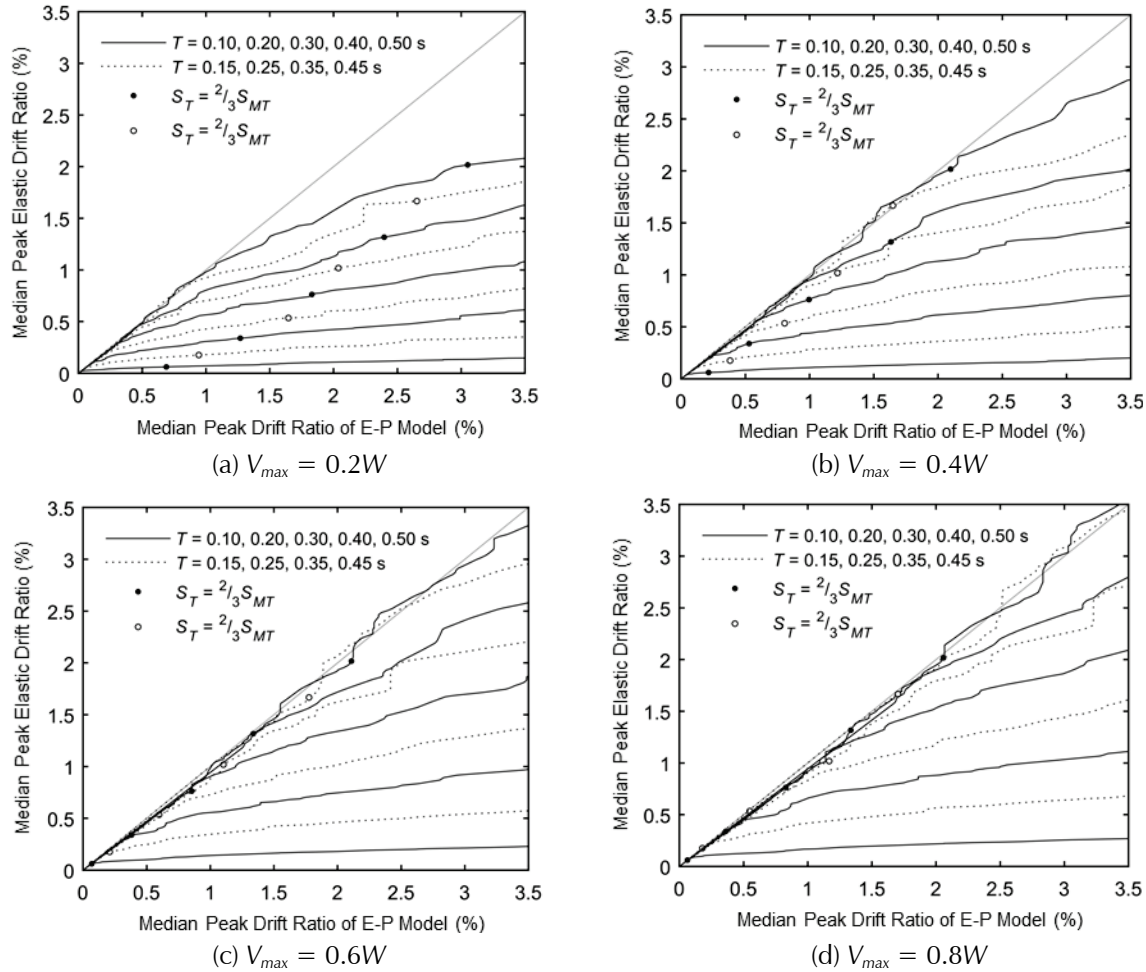


Figure 5-4 Peak elastic drift ratio versus median peak inelastic drift ratio for four SDOF model maximum strengths, where circles indicate design level response ($2/3 \times MCE_R$).

5.2.2 Collapse Fragility Curves

The collapse fragility curves for each SDOF model maximum strength using the ductility-based and drift-based collapse limits are shown in Figure 5-5 through Figure 5-8 (i.e., Figure 5-5 shows plots of fragility curves for the SDOF models with $V_{max} = 0.2W$ and has nine subfigures that correspond to each of the nine SDOF model periods).

In Figure 5-5 through Figure 5-8, drift-based collapse fragility curves assume first-story failure. In each figure, shading indicates spectral accelerations at or below the MCE_R ground-motion parameter, S_{MT} , and the numerical values of the probabilities of collapse given MCE_R ground motions (i.e., value of the collapse fragility curve at $S_T = S_{MT}$) are provided for the ductility-based and drift-based collapse fragility curves. The figures demonstrate that the probability of collapse is lower when the drift-based collapse displacement limit is used, the periods are short, and the strengths are low. As the period

and strength increase, the collapse fragility curves for the drift- and ductility-based collapse displacement limits move closer together. For stronger models at longer periods (e.g., $T = 0.5$ seconds and $V_{max} = 0.6W$), the ductility-based limit leads to lower collapse probabilities than those of the drift-based limit. The collapse probabilities are directly related to the collapse displacements for the two different collapse limits that were shown in Table 5-1.

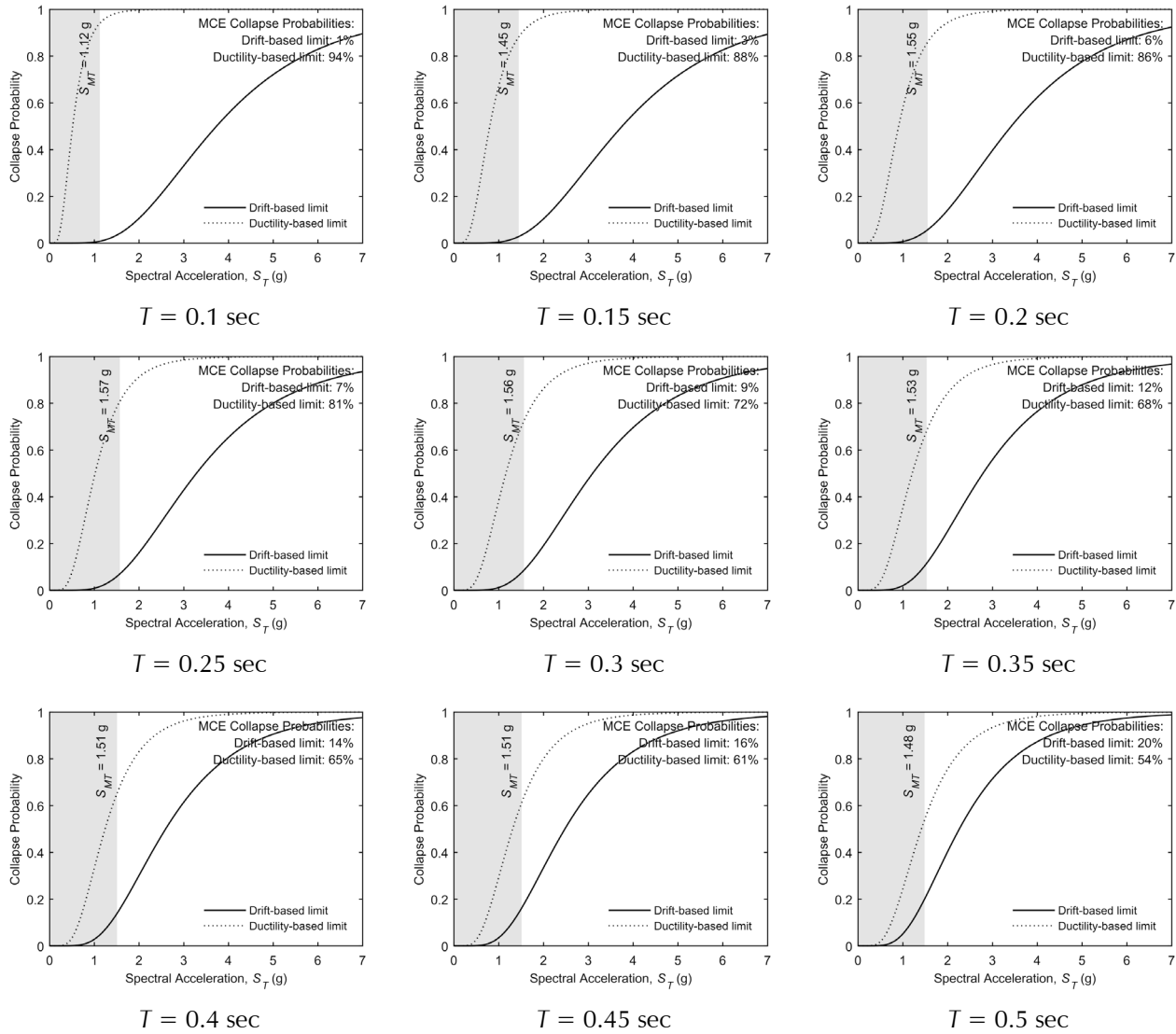


Figure 5-5 Collapse fragility curves for SDOF models with maximum strength, $V_{max} = 0.2W$.

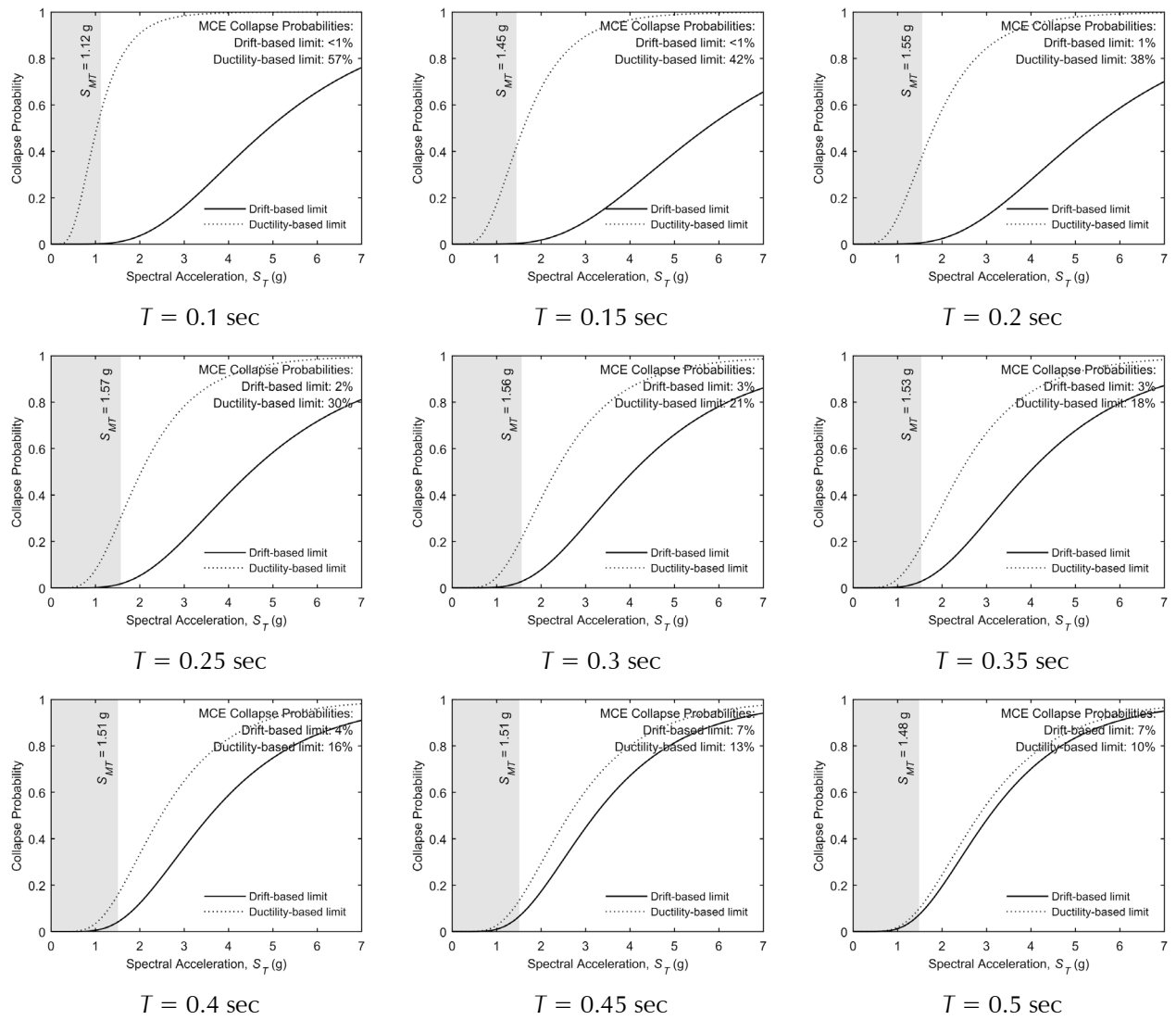


Figure 5-6 Collapse fragility curves for SDOF models with maximum strength, $V_{max} = 0.4W$.

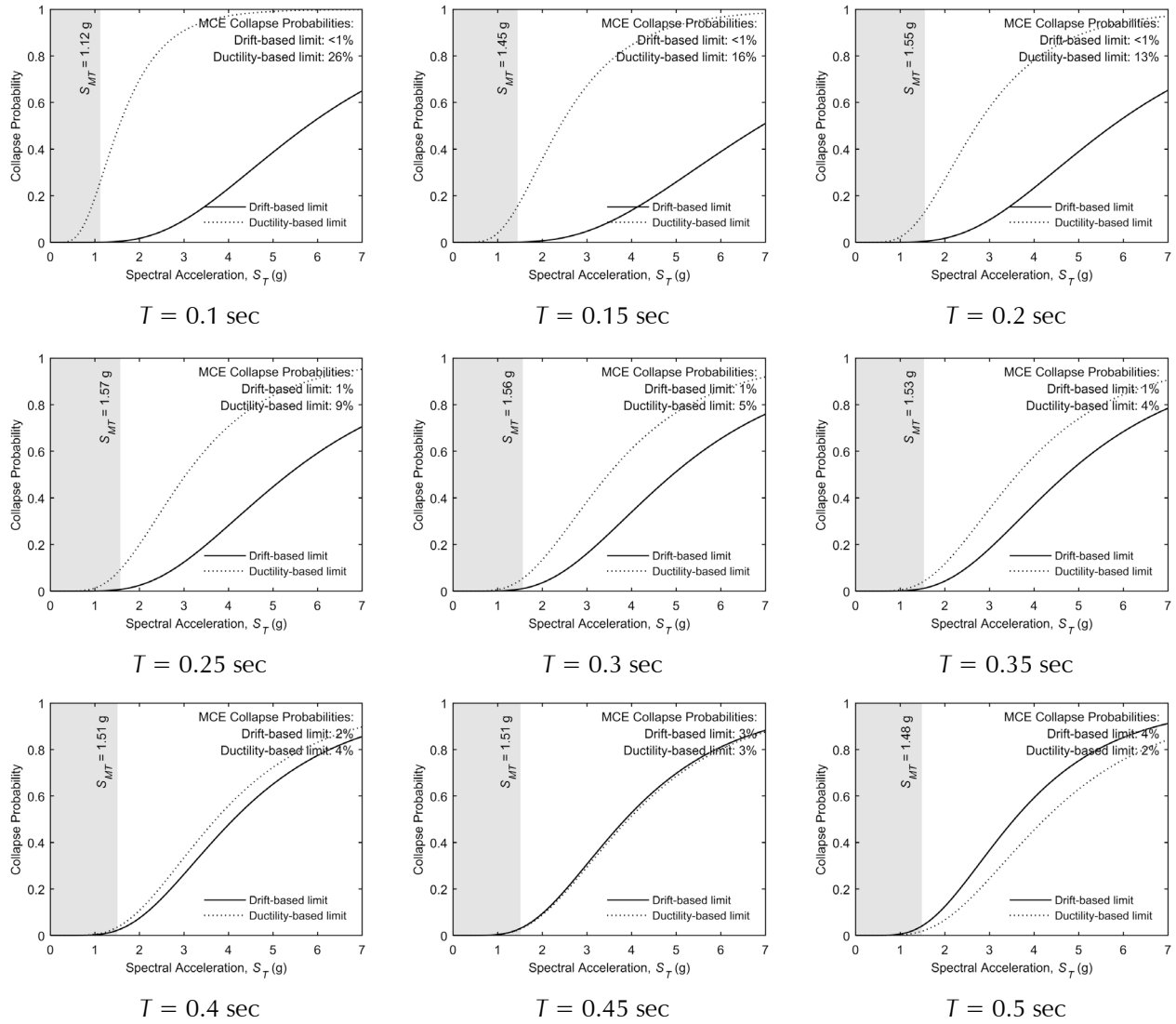


Figure 5-7 Collapse fragility curves for SDOF models with maximum strength, $V_{max} = 0.6W$.

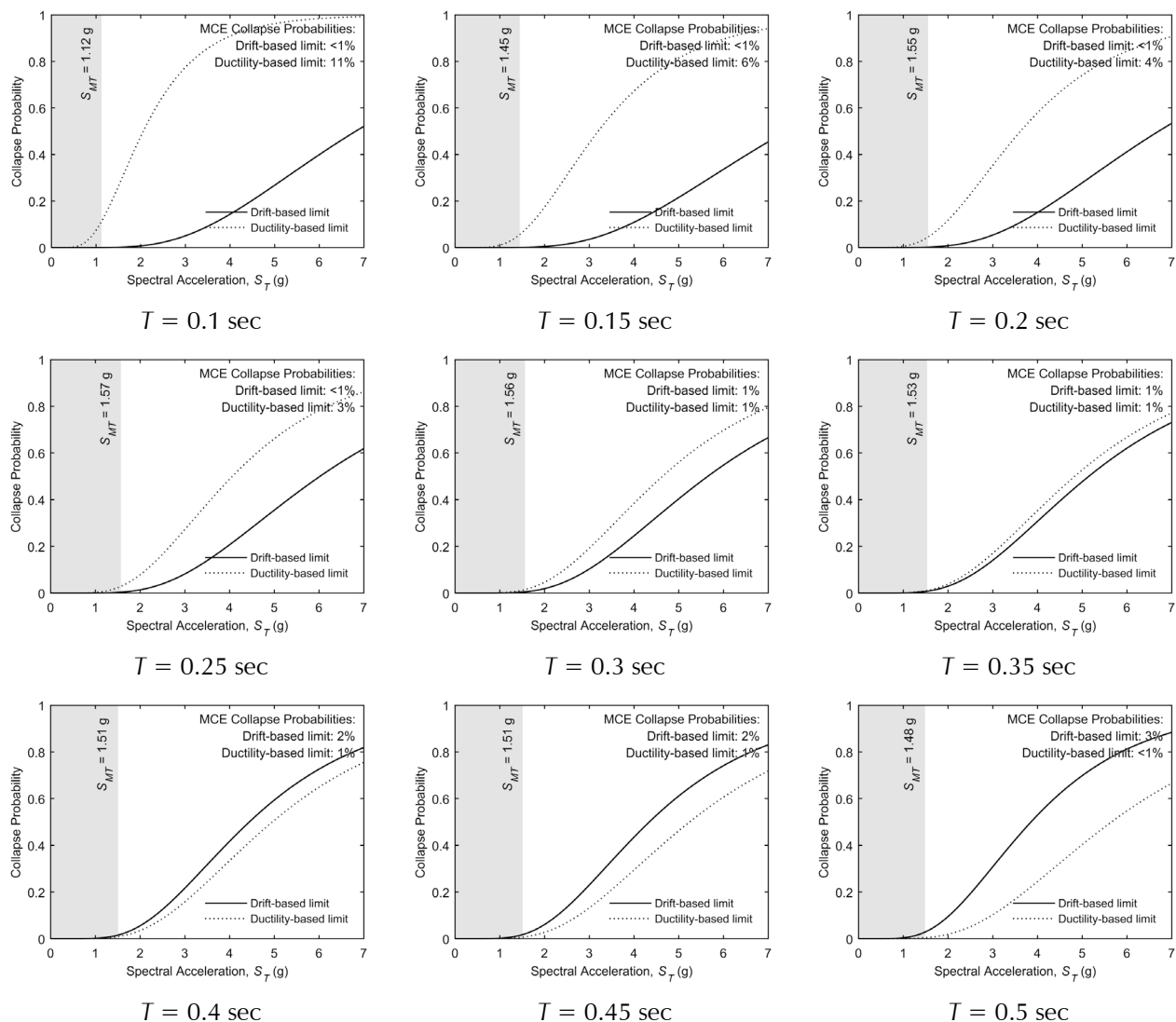


Figure 5-8 Collapse fragility curves for SDOF models with maximum strength, $V_{max} = 0.8W$.

5.2.3 Median Collapse Trends

Trends in the ratios of drift-based \hat{S}_{CT} to ductility-based \hat{S}_{CT} as function of model period for SDOF model maximum strengths, $V_{max} = 0.2W, 0.4W, 0.6W$ and $0.8W$ are shown in Figure 5-9 and Figure 5-10. Ratios shown in Figure 5-9 are calculated using values of drift-based \hat{S}_{CT} that assume first-story failure; ratios shown in Figure 5-10 are calculated using values of drift-based \hat{S}_{CT} that assume multi-story failure.

As shown in Figure 5-9 and Figure 5-10, drift-based and ductility-based collapse displacement limits result in similar \hat{S}_{CT} for periods approaching 0.5 seconds and maximum strengths from $0.4W$ to $0.8W$, which is consistent with the collapse displacements converging as the period approaches 0.5 seconds.

In general, the ratio of drift-based to ductility-based \hat{S}_{CT} for the first-story failure (Figure 5-9) is greater than or equal to 1.0 for periods below 0.40 seconds regardless of strength and for strengths less than $0.6W$ for all periods. For the multi-story failure, the ratio is greater than 1.0 for all strengths and periods considered. For very short periods, the \hat{S}_{CT} ratio can be quite large (i.e., greater than a factor of 4). These and the fragility findings above indicate that the ductility-based collapse displacement limits are overly conservative for short-period buildings, resulting in low estimates of \hat{S}_{CT} and high estimates of collapse probability at S_{MT} .

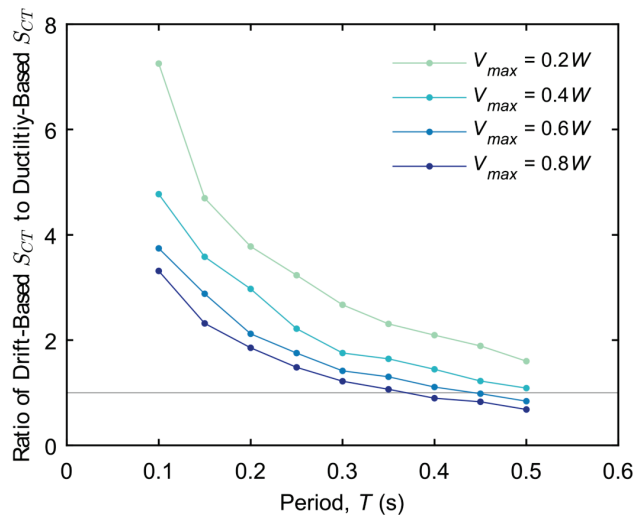


Figure 5-9 Trends in the ratios of drift-based \hat{S}_{CT} to ductility-based \hat{S}_{CT} as function of model period for SDOF model maximum strengths, $V_{max} = 0.2W$, $0.4W$, $0.6W$, and $0.8W$ assuming first-story failure for evaluation of drift-based \hat{S}_{CT} .

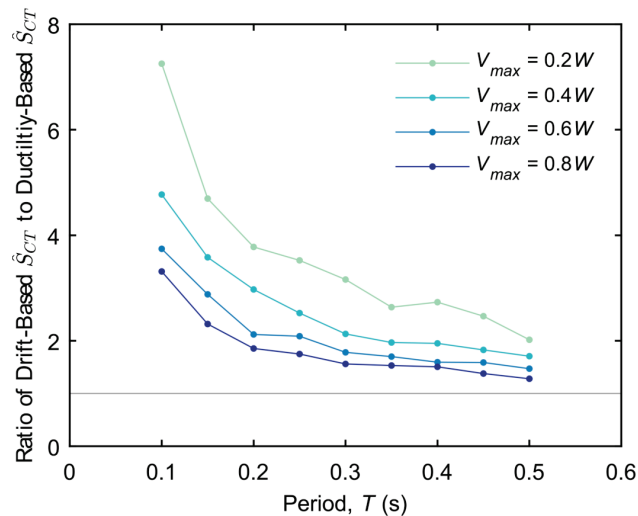


Figure 5-10 Trends in the ratios of drift-based \hat{S}_{CT} to ductility-based \hat{S}_{CT} as function of model period for SDOF model maximum strengths, $V_{max} = 0.2W$, $0.4W$, $0.6W$, and $0.8W$ assuming multi-story failure for evaluation of drift-based \hat{S}_{CT} .

5.2.4 ACMR and $ACMR/ACMR_{10\%}$

Plots of $ACMR$ and the ratio of $ACMR/ACMR_{10\%}$ as a function of the model period of SDOF models evaluated using either (1) ductility-based collapse displacement limits or (2) drift-based collapse displacement limits of Table 5-1 are shown in Figure 5-11. Ratios of $ACMR/ACMR_{10\%}$ greater than or equal to 1.0 indicate MCE_R collapse probabilities less than or equal to 10 percent. $ACMR_{10\%}$ is taken as the value of $ACMR$ resulting in an MCE_R collapse probability of 10 percent for each model. Also shown in Figure 5-11 is a plot $ACMR/ACMR_{10\%}$ as a function of model period of SDOF models of comparable maximum strength taken from Figure 3-1 of NIST GCR 12-917-20. Drift-based values of $ACMR$ are shown for SDOF models evaluated assuming (1) first-story failure and (2) multi-story failure as defined in Table 5-1. Values of $ACMR$ shown in Figure 5-11 are provided in Table 5-2.

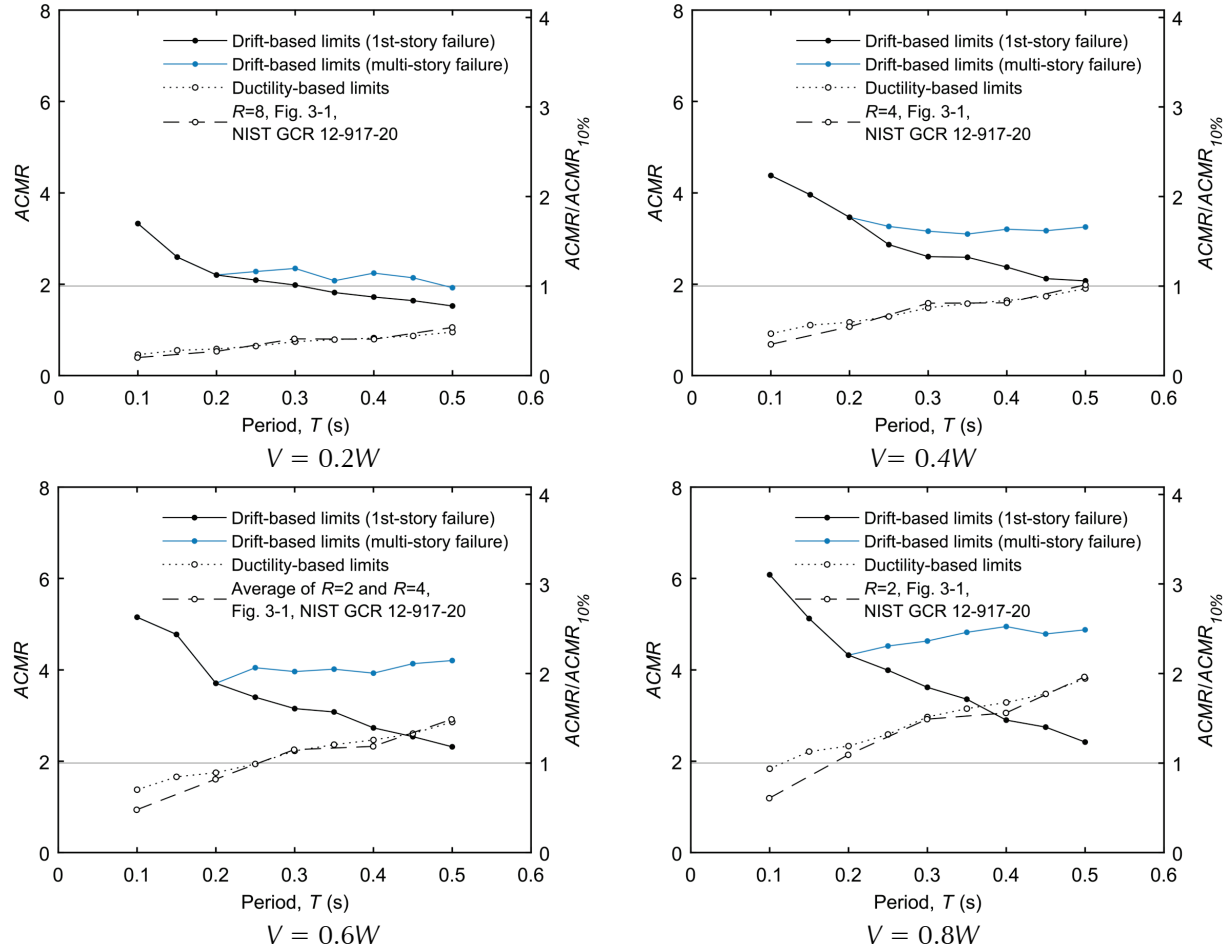


Figure 5-11 Plots of $ACMR$ and the ratio of $ACMR/ACMR_{10\%}$ as a function of the model period of SDOF models evaluated using drift-based and ductility-based collapse displacement limits. Drift-based values of $ACMR$ are shown for SDOF models evaluated assuming (1) first-story failure and (2) multi-story failure. Also shown is a plot of $ACMR/ACMR_{10\%}$ as a function of model period of SDOF models of comparable maximum strengths taken from Figure 3-1 of NIST GCR 12-917-20.

Table 5-2 Summary of Adjusted Collapse Margin Ratios (ACMRs) of SDOF Models Evaluated for the Ductility-Based ($\mu = 8$) and Drift-Based (drift ratio, $DR = 0.075$) Collapse Displacements of Table 5-1

SDOF Model Properties		MCE _R Ground Motions S_{MT} (g)	Adjusted Collapse Margin Ratio (ACMR)		
Strength V_{max}/W	Period T (s)		Ductility Based ($\mu = 8$)	Drift Based ($DR = 0.075$)	
		First-Story Failure		Multi-Story Failure	
0.2	0.10	1.12	0.46	3.33	3.33
0.2	0.15	1.45	0.55	2.59	2.59
0.2	0.20	1.55	0.58	2.20	2.20
0.2	0.25	1.57	0.65	2.09	2.28
0.2	0.30	1.56	0.74	1.98	2.35
0.2	0.35	1.53	0.79	1.82	2.08
0.2	0.40	1.51	0.82	1.72	2.24
0.2	0.45	1.51	0.87	1.64	2.14
0.2	0.50	1.48	0.95	1.52	1.92
0.4	0.10	1.12	0.92	4.38	4.38
0.4	0.15	1.45	1.11	3.96	3.96
0.4	0.20	1.55	1.17	3.46	3.46
0.4	0.25	1.57	1.29	2.87	3.26
0.4	0.30	1.56	1.48	2.60	3.16
0.4	0.35	1.53	1.58	2.59	3.10
0.4	0.40	1.51	1.64	2.37	3.20
0.4	0.45	1.51	1.74	2.12	3.17
0.4	0.50	1.48	1.91	2.07	3.25
0.6	0.10	1.12	1.38	5.15	5.15
0.6	0.15	1.45	1.66	4.77	4.77
0.6	0.20	1.55	1.75	3.71	3.71
0.6	0.25	1.57	1.94	3.40	4.05
0.6	0.30	1.56	2.23	3.15	3.96
0.6	0.35	1.53	2.36	3.08	4.01
0.6	0.40	1.51	2.46	2.73	3.93
0.6	0.45	1.51	2.60	2.54	4.13
0.6	0.50	1.48	2.86	2.32	4.20
0.8	0.10	1.12	1.84	6.08	6.08
0.8	0.15	1.45	2.21	5.12	5.12
0.8	0.20	1.55	2.33	4.32	4.32
0.8	0.25	1.57	2.59	3.99	4.52
0.8	0.30	1.56	2.97	3.62	4.63
0.8	0.35	1.53	3.15	3.36	4.82
0.8	0.40	1.51	3.29	2.90	4.95
0.8	0.45	1.51	3.47	2.75	4.79
0.8	0.50	1.48	3.81	2.42	4.88

The SDOF models of the prior NIST study used to develop the ratios of $ACMR/ACMR_{10\%}$ shown in Figure 5-11 are somewhat different from those of this study in that they included 10 percent post-yield strain hardening, assumed a collapse ductility of 10, and ignored the effects of P-delta. Nonetheless, the ratios of $ACMR/ACMR_{10\%}$ are quite similar to those of this study for models with comparable maximum strengths. The “R” factor of the prior NIST study represented the ductility component (R_d) of the R factor of ASCE/SEI 7 (i.e., no overstrength). Hence, the SDOF models of this study have comparable maximum strengths to those of the prior NIST study when $V_{max} = (S_{MS}/R)W = 1.5W/R$ for $S_{MS} = 1.5g$, where R is the “R” factor of the prior study. For example, for the $R = 4$, SDOF model of the prior NIST study, the SDOF model of this study of comparable maximum strength would have $V_{max} = 1.5W/4 = 0.375W$, or approximately, $V_{max} = 0.4W$.

5.3 Comparison of $ACMR$ Results with those of Prior SDOF Studies

Similar to the prior SDOF study of the NIST GCR 12-917-20 report, this SDOF study evaluated collapse performance of bilinear SDOF models using the same set of earthquake records and incremental dynamic analysis methods of FEMA P-695. Despite some differences in the modeling, this SDOF study found remarkably similar collapse results to those of the prior NIST study when the bilinear SDOF models were evaluated using a ductility-based collapse displacement limit.

Similarly, this SDOF study found the same trend as the prior NIST study of an increase in the ratio of inelastic displacement to elastic displacement as period decreases. Finding the same trend in the ratio of inelastic-to-elastic displacement is expected since peak nonlinear response (calculated by incremental dynamic analysis) is not influenced by collapse displacement capacity (i.e., either drift-based or ductility-based). Finding the same trend (i.e., same inelastic displacement) also confirms that the nonlinear response calculations of this SDOF study are consistent with those of the prior NIST study and other prior SDOF system studies, including the original theoretical work of Veletsos and Newmark (1960).

With respect to collapse performance, entirely different results and trends as a function of model period were found for bilinear SDOF models evaluated using drift-based collapse limits compared with the same set of bilinear SDOF models evaluated using ductility-based collapse limits, as illustrated in Figure 5-11. Trends are reversed for the same set of models of this SDOF study when the $ACMR$ is evaluated using the Table 5-1 drift-based collapse limits that assume first-story failure (i.e., failure mode typical of the detailed models of

wood light-frame, reinforced masonry, and steel SCBF archetypes). That is, the ratio of $ACMR/ACMR10\%$ increases as the period decreases, indicating improved collapse performance at shorter periods of SDOF models with the same yield strength. Similarly, individual values of the ratio $ACMR/ACME10\%$ are generally much greater than 1.0, corresponding to MCE_R collapse probabilities substantially less than the 10 percent collapse-safety objective of ASCE/SEI 7-16 for Risk Category II structures.

Where drift-based collapse limits are applied to the SDOF models with the multi-story failure mode, the ratio of $ACMR/ACMR10\%$ is approximately the same for periods greater than about 0.2 seconds (and greater at shorter periods), as shown in Figure 5-11. This finding supports period-independent values of the R factor for those systems that distribute inelastic story drift over the height of the structure (i.e., rather than only at the first story). Even for very weak SDOF models (e.g., $V_{max} = 0.2W$), the values of the ratio $ACMR/ACME10\%$ are generally greater than 1.0, corresponding to MCE_R collapse probabilities less than the 10 percent collapse-safety objective of ASCE/SEI 7-16 for Risk Category II structures.

The results of the SDOF study when collapse is evaluated using drift-based collapse displacement limits based on first-story failure are contrary to the findings of prior studies of bilinear SDOF models of short-period buildings, where collapse was evaluated using ductility-based collapse limits, and refute the long-standing notion that the shorter the period, the worse the collapse performance. The results of this SDOF study are limited and should not be considered conclusive, but provide a theoretical basis for understanding why short-period buildings have been observed to perform well in past earthquakes (Chapter 3) and why analytical studies of improved numerical models of short-period buildings (Chapter 4) have found better collapse performance than the results of prior analytical studies.

5.4 Notional Collapse Surfaces

During the course of these studies, the concept of a “collapse surface” was developed to describe the interaction of primary building response properties affecting collapse performance of particular classes of structures. Data from the generic collapse performance investigation of SDOF models have been used to develop examples of notional collapse surfaces. This concept of collapse surfaces appears to be a potentially useful tool and worthy of further development. The following sections describe the approach, details of the parameters used, and the resulting example notional collapse surfaces.

5.4.1 Approach

Conceptually, a collapse surface describes the value of a collapse metric (e.g., *ACMR*) as a function of key building response properties (e.g., strength, collapse displacement capacity) that significantly influence collapse performance. Collapse surfaces could be used to either estimate collapse performance given building strength and collapse displacement capacity or, conversely, be used to determine the amount of strength and collapse displacement capacity required to achieve a specific collapse performance objective (e.g., 10 percent probability of collapse given MCE_R ground motions). In this study, notional collapse surfaces were developed for short-period systems, although the collapse surface concept applies to buildings of any height.

To illustrate the collapse surface concept, the simple bilinear SDOF models of this study were used to calculate large sets of collapse data. Ideally, the collapse results of detailed nonlinear models of building archetypes, such as those of wood light-frame, reinforced masonry, and steel SCBF systems described in Chapter 4, would be used either directly to develop collapse surfaces or indirectly to validate collapse surfaces developed from simpler models. The detailed system-specific studies, although collectively quite extensive, do not have sufficient collapse data broadly distributed over the full range of possible values of key building response properties to directly develop collapse surfaces. Notional collapse surfaces developed from SDOF model collapse data illustrate the concept but may not accurately represent collapse surfaces of more detailed nonlinear models of building archetypes that have fundamentally different hysteretic behavior (e.g., nonlinear models that incorporate cyclic degradation).

5.4.2 Collapse Surface Metrics

Conceptually, collapse surfaces are a function of building strength, collapse displacement capacity, period, and the mode of failure. As discussed in Chapter 4, the detailed numerical models of wood light-frame, reinforced masonry, and steel SCBF building archetypes found strength and collapse displacement capacity to be the two primary building response properties influencing collapse performance. As discussed in Section 5.3 (and illustrated in Figure 5-11), the period of the SDOF model and the mode of failure can also significantly influence collapse performance.

The collapse metric of the notional collapse surfaces of this SDOF study is the *ACMR* parameter of FEMA P-695. The building response properties that define the *ACMR* surface are the: (1) the strength of the SDOF model, characterized by the ratio Ω/R ; (2) the story-drift ratio, *DR*, corresponding to

median peak inelastic displacement at incipient collapse; (3) the elastic period, T , of the SDOF model; and (4) implicitly, the mode of failure (i.e., either first-story or multi-story failure). The rationale for choosing these collapse metrics is discussed in the following paragraphs.

Collapse Metric: $ACMR$. $ACMR$ was deemed the most appropriate collapse metric for defining the collapse surface, although other collapse metrics could be used, such as the CMR or the probability of collapse. $ACMR$ incorporates the spectrum shape factor, SSF (i.e., $ACMR = SSF \times CMR$), which has the same value ($SSF = 1.33$) for all short-period buildings (i.e., $T \leq 0.5$ s) that have large ductility (i.e., period-based ductility, $\mu_T \geq 8$). This is the case for most of the SDOF models of this study and virtually all of the detailed models of wood light-frame, reinforced masonry, and steel SCBF building archetypes described in Chapter 4. In this sense, $ACMR$ provides no advantage over CMR . However, for collapse data of SDOF models with different collapse displacement capacities (i.e., where SSF values can be less than 1.33), $ACMR$ better characterizes the relative susceptibility of SDOF models to collapse.

The probability of collapse is not the preferred collapse metric since it necessarily incorporates the total system uncertainty factor, β_{TOT} , the value of which is determined by judgmental criteria (see Section 7.3 of FEMA P-695) rather than by analysis (i.e., β_{TOT} is not a response property of the SDOF models). As a reminder, the probability of collapse is directly related to $ACMR$ for a given value of the total system uncertainty factor, β_{TOT} .

Strength Ratio: Ω/R . The strength ratio is the ratio of overstrength (Ω) to the value of the response modification factor (R) selected for design of the system of interest. The strength ratio, Ω/R , provides a system-independent (i.e., R -factor independent) measure of the maximum strength, i.e., pushover strength (V_{max}) normalized by the weight (W) of the system of interest, V_{max}/W , relative to the seismic demand, $S_{MS}/1.5$, required for design at the site of interest:

$$\Omega/R = 1.5(V_{max}/W)/S_{MS} \quad (5-3)$$

This relationship is derived from: (1) Equation 6-5 of FEMA P-695, which defines overstrength, $\Omega = V_{max}/V_{design}$; (2) Equation 12.8-1 and Equation 12.8-2 of ASCE/SEI 7-16, which define the base shear, $V = C_s W$, and the seismic design coefficient, $C_s = S_{DS}/R$ (for Risk Category II structures); and (3) Equation 11.4-3 of ASCE/SEI 7-16, which relates short-period design ground motions to short-period MCE_R ground motions, $S_{DS} = 2/3 S_{MS}$. The strength ratio, Ω/R , is the preferred strength parameter since it provides a measure of system strength (e.g., SDOF model strength) that is independent of system-specific design requirements and site-specific seismic criteria.

Overstrength, Ω , is not the preferred strength parameter since overstrength, defined in terms of design base shear (V_{design}), incorporates the R factor. Similarly, pushover strength normalized by weight, V_{max}/W , is not the preferred strength metric since pushover strength (V_{max}) is influenced by the level of ground motions ($S_{MS}/1.5$) required for design. Conceptually, the collapse surface based on the strength ratio, Ω/R , is generically applicable to different systems designed for different values of the R factor and different levels of MCE_R ground motions.

Since the SDOF models of this study were not designed per se (i.e., for base shear, V_{design} , defined in terms of an R factor), the value of the strength ratio, Ω/R , was taken as $1.5(V_{max}/W)/S_{MS}$.

Collapse Displacement Drift Ratio: DR . The collapse displacement drift ratio, DR , is the median peak inelastic displacement of the story governing collapse divided by the height of that story. Story-drift ratio, rather than roof drift ratio, is the preferred collapse displacement parameter since, in general, it relates directly to the failure of elements of the structural system governing collapse. It should be noted that stronger models (i.e., a larger strength ratio, Ω/R) do not necessarily have larger collapse displacement drift ratios.

Typically, first-story failure governs collapse, which was found to be the case for virtually all of the detailed models of light-frame wood, reinforced masonry, and steel SCBF archetype buildings. For those system-specific models, inelastic drifts were typically concentrated at the first story, and median peak first-story drifts at failure were much larger than the story drifts of upper floors for multi-story models. This mode of failure may not always be the case, as discussed below.

Elastic Period: T_l . The elastic period, T_l , is the elastic, fundamental period in the direction of interest of complex models, such as the detailed models of wood light-frame, reinforced masonry, and steel SCBF building archetypes described in Chapter 4.

For the SDOF models of this study, the elastic period (T) was based on the elastic stiffness and 100 percent of model weight. As illustrated in Figure 5-11, collapse performance can be period dependent.

Collapse Failure Mode. The mode of failure, as characterized by the distribution of peak inelastic displacement at the point of incipient collapse over the height of the building (displaced shape), can significantly influence collapse performance, as shown in Figure 5-11 for two very different modes of failure (i.e., first-story failure and multi-story failure). Although concentration of inelastic demands and failure at the first story was typical of

the detailed system-specific models, this was not always the case, as was shown by the rocking response of the steel SCBF archetypes modeled with flexible foundations (see Section 4.5.5), for which story drifts (and story-drift ratios) at failure were found to be approximately equal at all stories.

An appropriate collapse metric to account for the mode of failure is not obvious but might involve modification of the collapse displacement drift ratio (DR) parameter to account for the distribution over height of peak inelastic displacement at incipient collapse. As an alternative concept, a different set of collapse surfaces could be developed for different modes of failure for which collapse performance ($ACMR$) is found to be significantly different. As an example of this alternative concept, two sets of collapse surfaces are developed from the SDOF models of this study. The first set includes $ACMR$ data based on the first-story failure, and the second set includes $ACMR$ data based on the multi-story failure.

The collapse failure modes of the SDOF models of this example are inherently limited by the bilinear force-deflection properties and non-degrading hysteretic response characteristics of these relatively simple nonlinear models. The collapse failure modes of complex 3-D nonlinear models would necessarily be influenced by more realistic numerical modeling of hysteretic behavior and cyclic degradation (e.g., based on laboratory test data). As such, the collapse failure modes of complex 3-D models would, in general, be different for SFRSs that have different backbone curve shapes and hysteretic response characteristics.

5.4.3 SDOF Model Analysis and Collapse Results

The results of the incremental dynamic analyses of the SDOF models were used to evaluate collapse performance of each model, where collapse displacements were defined by the drift-based limits given in Table 5-3. Collapse was assumed to occur when the peak displacement of the SDOF model reached the specified drift ratio, DR , where values of DR were 0.02, 0.04, 0.06, 0.08, and 0.10. Except for the value of the drift ratio, DR , the collapse evaluation methods were the same as those described in Section 5.1.

Model properties, MCE_R ground motions, values of the strength ratio parameter ($\mathcal{Q}R$) of the 36 SDOF models (i.e., SDOF models with one of nine different periods and one of four different maximum strengths), and the 180 values of $ACMR$, where the 36 SDOF models are each evaluated for one of the five first-story failure collapse displacements of Table 5-3, are summarized in Table 5-4. The same information for the 36 SDOF models evaluated using the five multi-story failure collapse displacements of Table 5-3 is summarized in Table 5-5.

Table 5-3 Summary of Drift-Based Collapse Displacements as a Function of the Drift Ratio, DR , Used to Evaluate SDOF Models for Development of Notional Collapse Surfaces

Elastic Period of Model (sec.)	First-Story Failure ⁽¹⁾						Multi-Story Failure ⁽²⁾					
	Model Height (ft.)	Collapse Displacement (in.)					Model Height ⁽³⁾ (ft.)	Collapse Displacement (in.)				
		$DR = 0.02$	$DR = 0.04$	$DR = 0.06$	$DR = 0.08$	$DR = 0.10$		$DR = 0.02$	$DR = 0.04$	$DR = 0.06$	$DR = 0.08$	$DR = 0.10$
0.1	10	2.4	4.8	7.2	9.6	12.0	10	2.4	4.8	7.2	9.6	12.0
0.15	10	2.4	4.8	7.2	9.6	12.0	10	2.4	4.8	7.2	9.6	12.0
0.20	10	2.4	4.8	7.2	9.6	12.0	10	2.4	4.8	7.2	9.6	12.0
0.25	10	2.4	4.8	7.2	9.6	12.0	12.3	3.0	5.9	8.9	11.8	14.8
0.30	10	2.4	4.8	7.2	9.6	12.0	15.7	3.8	7.5	11.3	15.1	18.8
0.35	10	2.4	4.8	7.2	9.6	12.0	19.3	4.6	9.3	13.9	18.5	23.2
0.40	10	2.4	4.8	7.2	9.6	12.0	23.1	5.5	11.1	16.6	22.2	27.7
0.45	10	2.4	4.8	7.2	9.6	12.0	27.0	6.5	13.0	19.4	25.9	32.4
0.50	10	2.4	4.8	7.2	9.6	12.0	31.1	7.5	14.9	22.4	29.9	37.3

⁽¹⁾ First-story failure assumes that all inelastic story drift occurs at the first story of a multi-story building represented by the SDOF model, where the height of the first story is $H = 10$ feet.

⁽²⁾ Multi-story failure assumes that inelastic story drift is uniformly distributed over the height of a multi-story building.

⁽³⁾ Model height, H , represents the effective height, which is assumed to be 2/3 of total height (h_n) of a multi-story building, where the total height (h_n) is calculated from the elastic period (T) of the model using the approximate fundamental period formula of Section 12.8.2.1 of ASCE/SEI 7-16, i.e., $H = 2/3 \exp[\ln(T/1.4(0.02))/0.75]$.

Table 5-4 Summary of SDOF Model Properties, MCE_R Ground Motions, Strength Parameter (Ω/R), and 180 Values of $ACMR$ of SDOF Models Assuming First-Story Failure

SDOF Model Properties		MCE_R Ground Motions S_{MT} (g)	Strength Parameter (Ω/R)	Adjusted Collapse Margin Ratio ($ACMR$) of SDOF Models Evaluated for First-Story Failure				
Strength V_{max}/W	Period T (s)			Drift Ratio (DR) Defining Drift-Based Collapse				
				$DR = 0.02$	$DR = 0.04$	$DR = 0.06$	$DR = 0.08$	$DR = 0.10$
0.2	0.10	1.12	0.27	1.55	2.39	2.96	3.44	3.80
0.2	0.15	1.45	0.21	1.30	2.05	2.31	2.64	2.93
0.2	0.20	1.55	0.19	1.12	1.77	2.02	2.25	2.54
0.2	0.25	1.57	0.19	1.02	1.45	1.84	2.16	2.36
0.2	0.30	1.56	0.19	0.94	1.36	1.59	2.07	2.28
0.2	0.35	1.53	0.20	0.87	1.33	1.54	1.84	1.98
0.2	0.40	1.51	0.20	0.76	1.22	1.50	1.84	1.97
0.2	0.45	1.51	0.20	0.72	1.12	1.40	1.67	1.88
0.2	0.50	1.48	0.20	0.65	1.06	1.35	1.55	1.78

Table 5-4 Summary of SDOF Model Properties, MCE_R Ground Motions, Strength Parameter (Ω/R), and 180 Values of $ACMR$ of SDOF Models Assuming First-Story Failure (continued)

SDOF Model Properties		MCE_R Ground Motions S_{MT} (g)	Strength Parameter (Ω/R)	Adjusted Collapse Margin Ratio ($ACMR$) of SDOF Models Evaluated for First-Story Failure				
Strength V_{max}/W	Period T (s)			Drift Ratio (DR) Defining Drift-Based Collapse				
				$DR = 0.02$	$DR = 0.04$	$DR = 0.06$	$DR = 0.08$	$DR = 0.10$
0.4	0.10	1.12	0.54	2.08	3.10	3.75	4.79	5.51
0.4	0.15	1.45	0.41	1.81	2.59	3.41	4.10	4.28
0.4	0.20	1.55	0.39	1.62	2.23	2.90	3.53	3.84
0.4	0.25	1.57	0.38	1.42	2.05	2.60	2.90	3.41
0.4	0.30	1.56	0.38	1.31	1.87	2.33	2.72	3.10
0.4	0.35	1.53	0.39	1.15	1.73	2.37	2.66	2.69
0.4	0.40	1.51	0.40	0.99	1.53	2.12	2.43	2.54
0.4	0.45	1.51	0.40	0.89	1.44	1.90	2.24	2.55
0.4	0.50	1.48	0.40	0.77	1.30	1.77	2.10	2.37
0.6	0.10	1.12	0.80	2.64	3.48	4.66	5.36	6.12
0.6	0.15	1.45	0.62	2.32	3.19	3.89	4.89	5.37
0.6	0.20	1.55	0.58	1.96	2.76	3.35	4.05	4.54
0.6	0.25	1.57	0.57	1.68	2.48	3.07	3.50	4.21
0.6	0.30	1.56	0.58	1.44	2.29	2.81	3.34	3.70
0.6	0.35	1.53	0.59	1.26	2.05	2.60	3.24	3.69
0.6	0.40	1.51	0.60	1.01	1.77	2.29	2.82	3.36
0.6	0.45	1.51	0.60	0.98	1.50	2.16	2.61	3.03
0.6	0.50	1.48	0.61	0.73	1.39	1.95	2.46	2.89
0.8	0.10	1.12	1.07	3.20	4.17	5.40	6.21	6.87
0.8	0.15	1.45	0.83	2.84	3.62	4.43	5.19	6.06
0.8	0.20	1.55	0.77	2.27	3.23	3.87	4.47	4.94
0.8	0.25	1.57	0.76	1.86	2.85	3.47	4.09	4.53
0.8	0.30	1.56	0.77	1.61	2.63	3.22	3.74	4.20
0.8	0.35	1.53	0.78	1.32	2.30	2.95	3.46	4.07
0.8	0.40	1.51	0.80	1.09	1.97	2.56	3.05	3.64
0.8	0.45	1.51	0.79	0.90	1.78	2.14	2.88	3.38
0.8	0.50	1.48	0.81	0.68	1.55	2.12	2.60	3.09

Table 5-5 Summary of SDOF Model Properties, MCE_R Ground Motions, Strength Parameter (Ω/R), and 180 Values of $ACMR$ of SDOF Models Assuming Multi-Story Failure

SDOF Model Properties		MCE_R Ground Motions S_{MT} (g)	Strength Parameter (Ω/R)	Adjusted Collapse Margin Ratio ($ACMR$) of SDOF Models Evaluated for Multi-Story Failure				
Strength V_{max}/W	Period T (s)			Drift Ratio (DR) Defining Drift-Based Collapse				
				$DR = 0.02$	$DR = 0.04$	$DR = 0.06$	$DR = 0.08$	$DR = 0.10$
0.2	0.10	1.12	0.27	1.55	2.39	2.96	3.44	3.80
0.2	0.15	1.45	0.21	1.30	2.05	2.31	2.64	2.93
0.2	0.20	1.55	0.19	1.12	1.77	2.02	2.25	2.54
0.2	0.25	1.57	0.19	1.12	1.67	2.02	2.32	2.39
0.2	0.30	1.56	0.19	1.20	1.70	2.28	2.40	2.41
0.2	0.35	1.53	0.20	1.30	1.83	2.05	2.08	2.11
0.2	0.40	1.51	0.20	1.26	1.93	2.19	2.25	2.25
0.2	0.45	1.51	0.20	1.29	1.96	2.13	2.14	2.14
0.2	0.50	1.48	0.20	1.40	1.84	1.92	1.92	1.92
0.4	0.10	1.12	0.54	2.08	3.10	3.75	4.79	5.51
0.4	0.15	1.45	0.41	1.81	2.59	3.41	4.10	4.28
0.4	0.20	1.55	0.39	1.62	2.23	2.90	3.53	3.84
0.4	0.25	1.57	0.38	1.57	2.24	2.86	3.34	3.66
0.4	0.30	1.56	0.38	1.63	2.40	3.10	3.33	3.45
0.4	0.35	1.53	0.39	1.70	2.60	2.83	3.11	3.30
0.4	0.40	1.51	0.40	1.75	2.51	3.02	3.26	3.46
0.4	0.45	1.51	0.40	1.75	2.57	2.99	3.18	3.21
0.4	0.50	1.48	0.40	1.80	2.68	3.07	3.28	3.42
0.6	0.10	1.12	0.80	2.64	3.48	4.66	5.36	6.11
0.6	0.15	1.45	0.62	2.32	3.19	3.89	4.89	5.37
0.6	0.20	1.55	0.58	1.96	2.76	3.35	4.05	4.54
0.6	0.25	1.57	0.57	1.93	2.79	3.36	4.20	4.40
0.6	0.30	1.56	0.58	2.02	2.89	3.60	4.19	4.58
0.6	0.35	1.53	0.59	2.02	3.14	3.90	4.16	4.33
0.6	0.40	1.51	0.60	1.96	3.28	3.77	4.09	4.38
0.6	0.45	1.51	0.60	2.00	3.16	3.85	4.25	4.65
0.6	0.50	1.48	0.61	2.05	3.26	3.84	4.30	4.45
0.8	0.10	1.12	1.07	3.20	4.17	5.40	6.21	6.87
0.8	0.15	1.45	0.83	2.84	3.62	4.43	5.19	6.06
0.8	0.20	1.55	0.77	2.27	3.23	3.87	4.47	4.94
0.8	0.25	1.57	0.76	2.13	3.14	3.82	4.48	5.39
0.8	0.30	1.56	0.77	2.09	3.27	4.10	4.80	5.22
0.8	0.35	1.53	0.78	2.27	3.41	4.78	5.13	5.35
0.8	0.40	1.51	0.80	2.15	3.51	4.54	5.01	5.14
0.8	0.45	1.51	0.79	2.01	3.50	4.50	4.83	5.03
0.8	0.50	1.48	0.81	2.17	3.61	4.34	4.93	5.31

5.4.4 Development of Notional Collapse Surfaces

Notional collapse surfaces were developed from the collapse data of Table 5-4 representing first-story collapse failure and from the collapse data of Table 5-5 representing multi-story collapse failure, as defined in Table 5-3. To facilitate the construction of the collapse surfaces, the collapse data of Table 5-4 and Table 5-5 were regressed to develop smooth mathematical relationships defining $ACMR$ as a function of SDOF model strength, Ω/R , collapse displacement capacity, DR , and elastic period, T . For this example, $ACMR$ was assumed to be related to the SDOF model response parameters, Ω/R , DR , and T , in accordance with the following functional form:

$$ACMR = A(\Omega/R)^a + B(T+b2)^{b1} + C(DR)^c + D(\Omega/R)^a (DR)^c + E(\Omega/R)^a (T+b2)^{b1} + F(DR)^c (T+b2)^{b1} + G \quad (5-4)$$

where the coefficients, a , $b1$, $b2$, c , A , B , C , D , E , F and G , are determined by regression analysis. The assumed functional form includes three terms of individual building response properties and three terms that are products of pairs of these three properties. There is no physical significance to the assumed functional form of Equation 5-4; rather, it is simply a mathematical scheme used in this example to illustrate the concept of a collapse surface. Similarly, Equation 5-4 is not unique and other functional forms could be used to characterize $ACMR$.

The values of the coefficients of Equation 5-4 were developed in two stages. First, the exponents and the period bias factor (a , $b1$, $b2$ and c) were estimated individually for each of the three $ACMR$ parameters (Ω/R , DR , and T) based on trends in the average value of $ACMR$ as a function of the building property of interest. Building response properties, as modified by these exponents and the period bias factor, were then treated as independent variables and linearly regressed to determine values of the coefficients A , B , C , D , E , F , and G . The intent of this statistical effort was to demonstrate that a mathematical relationship of $ACMR$ could be developed that reasonably represents the collapse data of Table 5-4 and Table 5-5 for all possible values of SDOF model response parameters, Ω/R , DR , and T .

Values of the coefficients of Equation 5-4 are given in Table 5-6, along with selected regression results for three sets of $ACMR$ data corresponding to: (1) first-story failure data of Table 5-4 for all 180 values of $ACMR$; (2) first-story failure data of Table 5-4, excluding data for SDOF models with periods, $T = 0.1$ seconds and 0.15 seconds (140 data); and (3) multi-story failure data of Table 5-5, excluding data for SDOF models with periods, $T = 0.1$ seconds and 0.15 seconds (140 data). Short-periods ($T = 0.1$ seconds and 0.15 seconds) were excluded from the second data set for comparison of

results with those of the first data set (which is the set used to characterize first-story failure). Short periods ($T = 0.1$ seconds and 0.15 seconds) were excluded from the third data set to improve the correlation at longer periods of interest to multi-story failure. Regression results provide a measure of how well the mathematical function of *ACMR* matched the underlying SDOF model collapse data.

Table 5-6 Summary of Coefficients Describing Notional *ACMR* Collapse Surfaces and Related Results of Multi-Linear Regression Analyses of SDOF Model Data

<i>ACMR</i> Collapse Surface		Value of <i>ACMR</i> Surface Collapse Coefficient		
Associated Parameter or Regression Variable	Coefficient	First-Story Failure of SDOF Models		Multi-Story Failure of SDOF Models $T \geq 0.2$ s
		All Model Periods	Model Periods $T \geq 0.2$ s	
Ω/R	a	0.45	0.45	0.5
T	b1	-1.0	-1.0	0.05
T	b2	0.2	0.2	0
DR	c	0.6	0.6	0.5
$(\Omega/R)^a$	A	-3.658	-5.469	-20.80
$(T+b2)^{b1}$	B	-0.668	-1.067	1.927
DR^c	C	-9.253	-7.178	51.09
$(\Omega/R)^a DR^c$	D	21.55	20.92	26.80
$(\Omega/R)^a (T+b2)^{b1}$	E	1.459	2.519	20.17
$(T+b2)^{b1} DR^c$	F	3.660	2.750	-60.53
Intercept	G	1.861	2.509	-0.4843
Multi-Linear Regression Analysis Results				
No. of Data	n	180	140	140
Correlation	R	99.2%	99.6%	98.8%
No. of Residuals	> 15%	0/180	0/140	3/140
No. of Residuals	> 10%	5/180	3/140	5/140
No. of Residuals	> 5%	12/180	14/140	15/140

For each of the three data sets, regression results include the correlation coefficient (R) and number of times that a predicted value of *ACMR* exceeds the target value of *ACMR* (i.e., so-called residual) by either 5 percent, 10 percent, or 15 percent for values of *ACMR* between 1.5 and 3.0 (i.e., the range of *ACMR* values of primary interest to MCE_R collapse performance). For the first data set, the correlation coefficient is 99.2 percent, and the collapse surface does not overpredict the target value of *ACMR* by more than

15 percent for any of the 180 combinations of SDOF model strength (Ω/R), elastic period (T), and collapse displacement drift ratio (DR). The collapse surface for the first data set is also within 5 percent of the target value of $ACMR$ in all but 12 of the 180 combinations of the three $ACMR$ parameters. Plots of predicted values of $ACMR$ and the underlying $ACMR$ target data of the SDOF models with maximum strengths, $V_{max} = 0.2W$ and $0.4W$ and a collapse drift ratio, $DR = 0.075$ (i.e., $ACMR$ data of Figure 5-11) showing reasonably good fit of predicted values to target values of the $ACMR$ are shown in Figure 5-12.

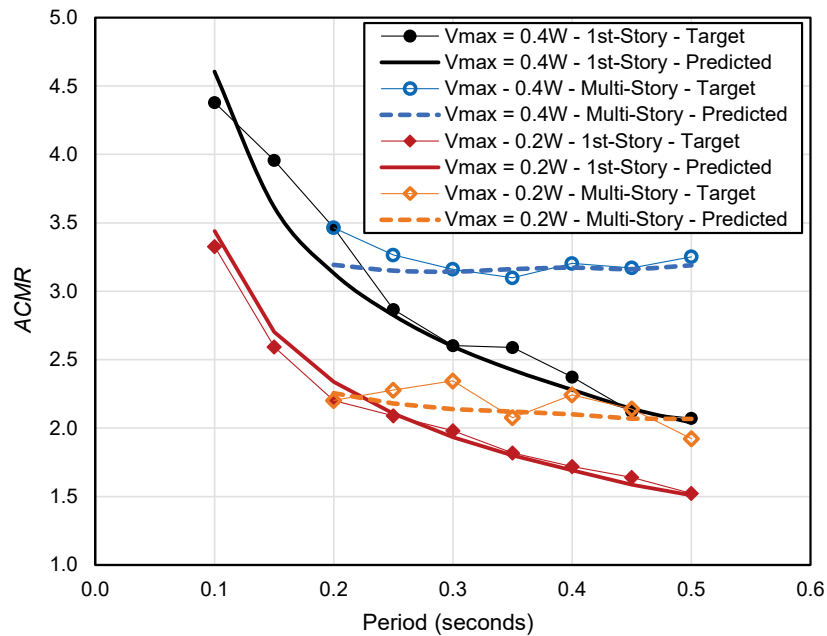


Figure 5-12 Plots of $ACMR$ target data as a function of the model period of SDOF models evaluated using drift-based collapse displacement limits ($DR = 0.075$) assuming either (1) first-story failure or (2) multi-story failure and the corresponding predicted values of $ACMR$ excluding values for $T \leq 0.2$ seconds.

Notional collapse surfaces are shown in Figure 5-13 for SDOF models with elastic periods of $T = 0.15$ seconds, 0.25 seconds, 0.35 seconds, and 0.45 seconds, where $ACMR$ is calculated using Equation 5-4 and the coefficients of the first data set of Table 5-6, which assume first-story failure. The same set of surfaces for SDOF models that assume multi-story failure (i.e., third data set of Table 5-6) are shown in Figure 5-14. Notional collapse surfaces are shown as a function of the two primary building response properties, strength (Ω/R) and displacement capacity (DR), for each of four elastic response periods of interest. In these examples, maximum strength of the SDOF model is expressed in terms of V_{max} , rather than Ω/R , to better relate the collapse surface to the SDOF models used to develop the collapse data; corresponding values of Ω/R are given in Table 5-4. In Figure 5-13 and

Figure 5-14, each collapse surface is shown as a 3-D surface plot and as a 2-D contour plot, with shading indicating the noted ranges of *ACMR* (e.g., yellow shading indicates values of the *ACMR* between 2.0 and 2.5).

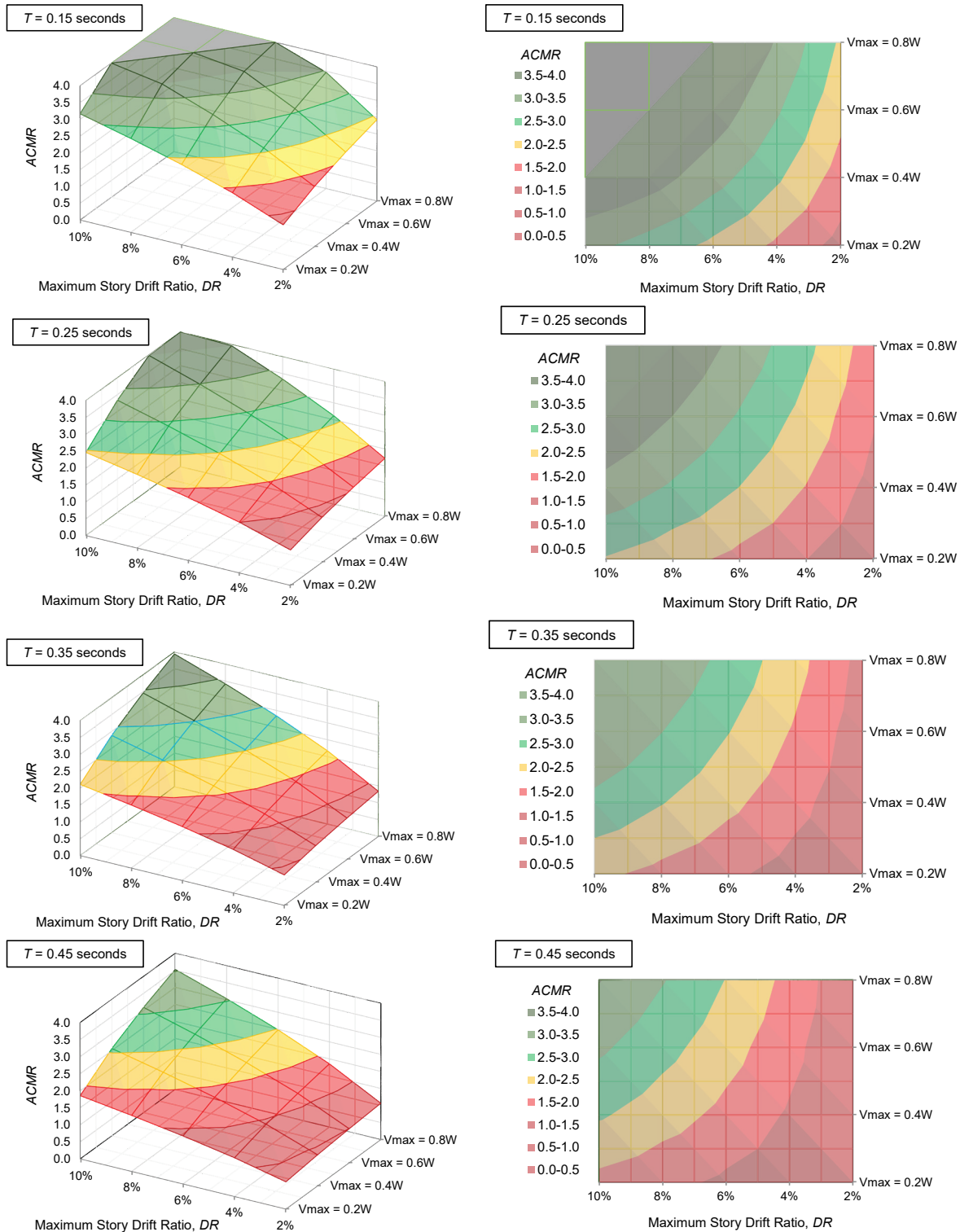


Figure 5-13 Plots of notional collapse surfaces for SDOF models with periods, $T = 0.15$ seconds, $T = 0.25$ seconds, $T = 0.35$ seconds, and $T = 0.45$ seconds assuming first-story failure.

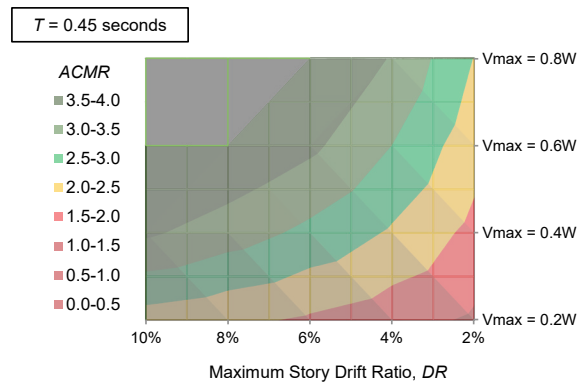
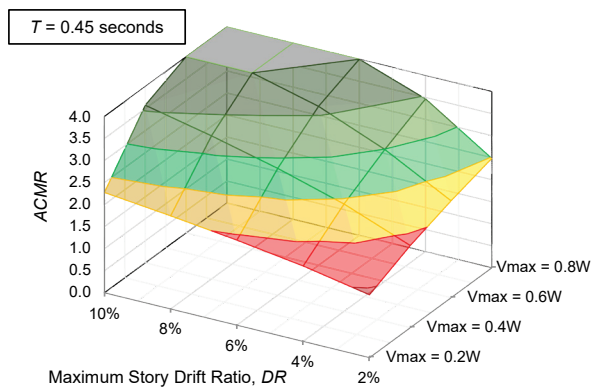
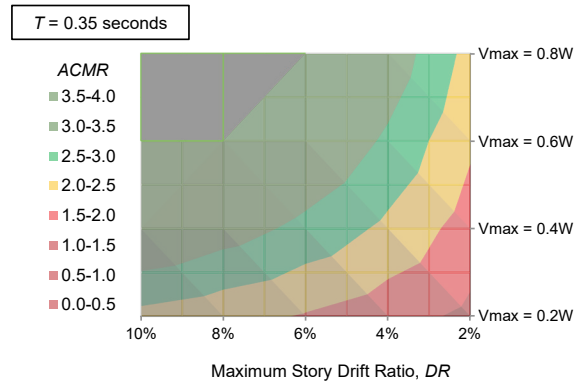
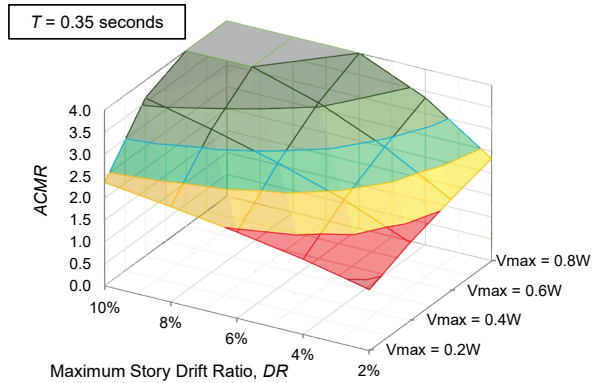
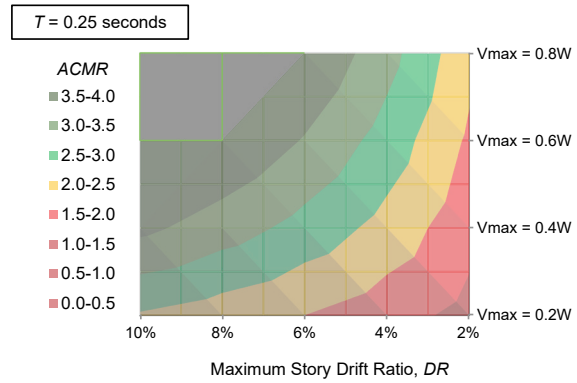
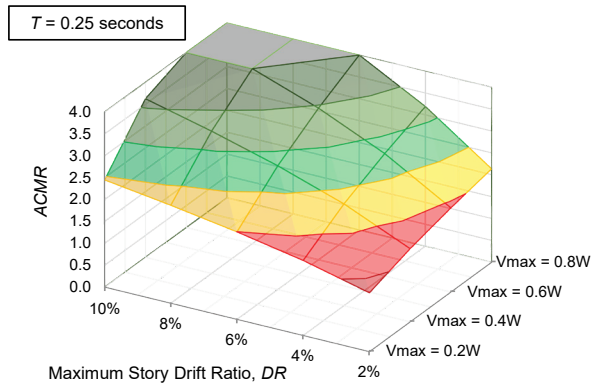
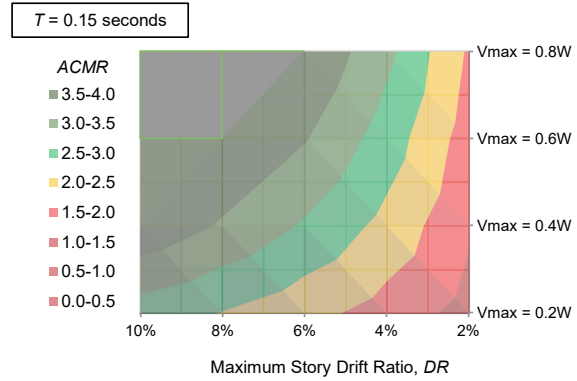
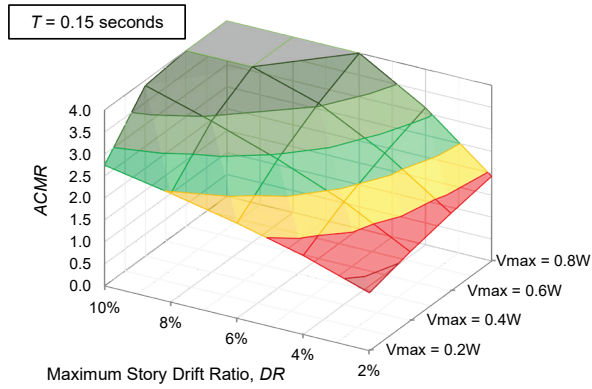


Figure 5-14 Plots of notional collapse surfaces for SDOF models with periods, $T = 0.15$ seconds, $T = 0.25$ seconds, $T = 0.35$ seconds, and $T = 0.45$ seconds assuming multi-story failure.

For reference, Table 5-7 provides example values of the MCE_R collapse probability for values of $ACMR$ ranging from 1.0 to 4.0 and values of the total system uncertainty factor, β_{TOT} , ranging from 0.5 to 0.7. For reference, a value of $\beta_{TOT} = 0.50$ was used to evaluate the collapse performance of the detailed models of light-frame wood, reinforced masonry, and steel SCBF building archetypes. A value of $\beta_{TOT} = 0.525$ is typical of values used to evaluate collapse performance of proposed new SFRSs with “good” quality ratings of test data, design requirements, and numerical models (Table 7.2b of FEMA P-695). A value of $\beta_{TOT} = 0.6$ is the value required by Section 21.2.1 of ASCE/SEI 7-16 for determination of probabilistic MCE_R ground motions.

Table 5-7 Example Values of the MCE_R Collapse Probability for Values of $ACMR$ Ranging from 1.0 to 4.0 and Values of the Total System Uncertainty Factor, β_{TOT} , Ranging from 0.5 to 0.7

<i>ACMR</i>	Total System Uncertainty Factor, β_{TOT}				
	0.50	0.55	0.60	0.65	0.70
1.0	50%	50%	50%	50%	50%
1.5	21%	23%	25%	27%	28%
2.0	8%	10%	12%	14%	16%
2.5	3.3%	4.8%	6.3%	7.9%	10%
3.0	1.4%	2.3%	3.4%	4.5%	5.8%
3.5	0.6%	1.1%	1.8%	2.7%	3.7%
4.0	0.3%	0.6%	1.0%	1.6%	2.4%

The notional collapse surfaces of Figure 5-13, which are based on SDOF models that assume a first-story failure, show a strong period dependence. For example, $ACMR$ is more than 2.5 (i.e., MCE_R collapse probability of about 3 percent, $\beta_{TOT} = 0.50$) for the SDOF model with a maximum strength, $V_{max} = 0.4W$, a maximum story-drift ratio, $DR = 0.04$, and an elastic period, $T = 0.15$ seconds; whereas $ACMR$ is less than 1.5 (i.e., MCE_R collapse probability of more than 20 percent, $\beta_{TOT} = 0.50$) for the SDOF model with the same strength and displacement capacity but an elastic period, $T = 0.45$ seconds.

In contrast, the notional collapse surfaces of Figure 5-14, which are based on SDOF models that assume multi-story failure, show insignificant differences in collapse performance with change in period. Figure 5-14 indicates collapse performance that is in almost all cases acceptable (i.e., values of $ACMR$ corresponding to MCE_R collapse probabilities less than the 10 percent collapse-safety objective of ASCE/SEI 7-16 for Risk Category II structures), except for very weak models with limited displacement capacity.

The notional collapse surfaces demonstrate the relationship between collapse performance ($ACMR$) and building response properties that can be determined by engineering analysis, i.e., the strength ratio ($\Omega/R = 1.5V_{max}/S_{MS}$), the elastic period (T) and the collapse displacement drift ratio (DR), where the value of DR could also be determined by engineering judgment informed by available test data. The collapse surfaces could be used to either estimate collapse performance ($ACMR$) given values of the strength ratio (Ω/R), the elastic period (T), and the collapse displacement drift ratio (DR). Conversely, the collapse surfaces could be used to determine, for example, the amount of maximum strength (V_{max}) required to achieve a specific collapse performance objective (e.g., 10 percent probability of collapse given MCE_R ground motions) given the elastic response period (T) and the collapse displacement drift ratio (DR) of the individual building (or SFRS) of interest and the inherent uncertainty in response properties, as characterized by the total system uncertainty factor, β_{TOT} .

Simple, computationally efficient, SDOF models were used in this study to populate $ACMR$ data describing the notional collapse surfaces. These surfaces are hypothetical and likely underestimate the probabilities of collapse (i.e., predict higher values of $ACMR$) of real buildings, as characterized by the $ACMR$ results of the FEMA P-695 evaluations of the detailed numerical models of wood light-frame, reinforced masonry, and steel SCBF building archetypes, which more accurately modeled hysteretic behavior and cyclic degradation based on laboratory test data.

For example, Figure 5-15 is a plot of the values of $ACMR$ derived from Equation 5-4 using the first-story failure coefficients of Table 5-6 versus the values of $ACMR$ determined directly from FEMA P-695 collapse evaluations for wood light-frame commercial (COM), multi-family dwelling (MFD), and two-story single-family dwelling (SFD) building archetypes presented in Chapter 4. Figure 5-15 indicates that some adjustment would be needed on the results from the hypothetical SDOF models for them to reliably predict building response properties. Figure 5-15 also indicates that the values of $ACMR$ of detailed models of wood light-frame buildings are systematically well correlated (i.e., as a function of strength, period, and displacement capacity), suggesting that there is likely a well-defined set of collapse surfaces for the wood light-frame system (i.e., just not the same set as those derived from the simple SDOF models of this study).

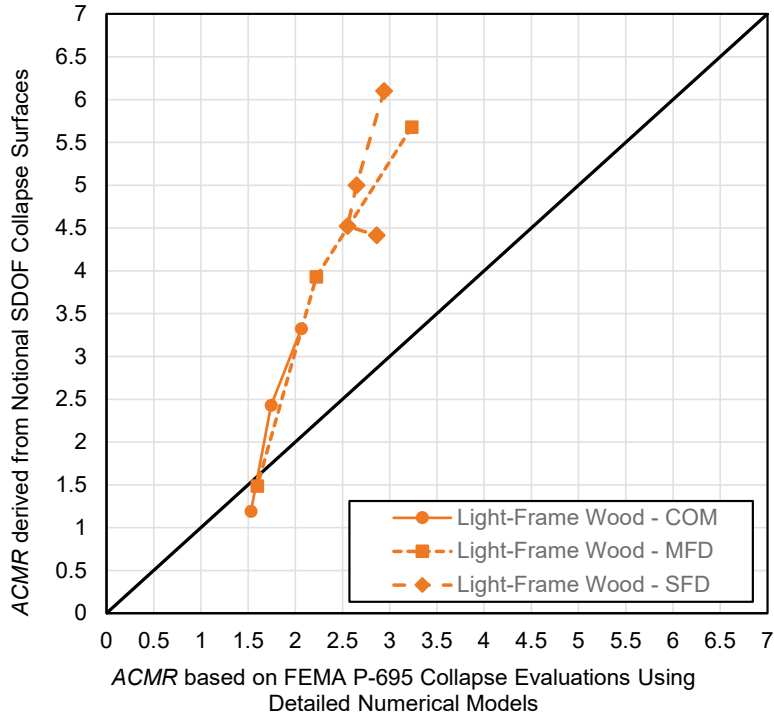


Figure 5-15 Values of *ACMR* derived from Equation 5-4 using the first-story failure coefficients of Table 5-6 versus the values of *ACMR* determined directly from FEMA P-695 collapse evaluations using detailed numerical models for wood light-frame commercial (COM), multi-family dwelling (MFD), and two-story single-family dwelling (SFD) building archetypes.

This chapter addresses the resolution of the short-period building seismic performance paradox based on the collapse evaluations of detailed models of wood light-frame, reinforced masonry, and steel SCBF systems, summarized in Chapter 4, and the generic collapse trends of simple bilinear SDOF models, described in Chapter 5. The applicability of these findings to other seismic-forces-resisting systems of ASCE/SEI 7 are discussed. The chapter closes with a conceptual extrapolation of the system-specific findings of Chapter 4 and the generic collapse trends of Chapter 5 to the prediction of short-period building collapse probability as a function of key building response properties (fundamental period, strength, collapse displacement capacity, and failure mode).

6.1 Resolution of the Short-Period Building Seismic Performance Paradox

6.1.1 Collapse Trends with Period Reversed

Prior FEMA P-695 collapse performance studies on a variety of structural systems over a range of periods have suggested that, for systems with design periods less than about 0.5 seconds, the probability of collapse given MCE_R ground motions increases significantly as the design period decreases. Trends in observed earthquake damage of short-period buildings, however, do not support the high collapse probabilities predicted by numerical analysis. The apparent discrepancy between analytical prediction of collapse performance and the opinions and observations of structural engineers has been designated the short-period building seismic performance paradox.

With improved numerical modeling and representative building archetypes, the detailed studies of short-period wood light-frame, reinforced masonry, and steel SCBF systems have shown that MCE_R collapse probabilities decrease as the design period decreases, which is a reversal of the trend observed in prior FEMA P-695 studies. This is illustrated in Figure 4-11a.

The detailed models of wood light-frame, reinforced masonry, and steel SCBF building archetypes, summarized in Chapter 4, better characterize the relatively large collapse displacements of short-period buildings than those prior FEMA P-695 studies of short-period building archetypes (FEMA,

2009b; NIST, 2010). Similarly, simple SDOF models that assume relatively large collapse displacements also show a reversal of MCE_R collapse probability trends with period, as illustrated by the values of $ACMR$ shown in Figure 5-11.

Key modeling improvements of the detailed system-specific models (summarized in Chapter 4) include: (1) a more realistic characterization of drift displacement at collapse (consistent with observed behavior in earthquakes and shake-table tests) which, in all cases, improves collapse performance; (2) certain SFRS-specific modeling improvements (e.g., including the stiffness and strength of nonstructural wall finishes in wood light-frame models) that improve collapse performance; and (3) the explicit consideration of P-delta effects, which are essential for reliably modeling archetypes prone to first-story failure (i.e., the most common failure mode of multi-story short-period buildings observed in past earthquakes) and can adversely affect the collapse performance of taller short-period archetypes, especially those that have relatively low strength.

The archetypes used in the detailed system-specific studies were configured to be realistic and representative of actual buildings in terms of size and proportion and were designed accordingly. In contrast, the archetypes of prior FEMA P-695 studies were designed to the minimum seismic requirements of ASCE/SEI 7, often using unrealistic configurations that led to an overstatement of collapse risk. For example, the implausible MCE_R probability of collapse of 79 percent of the one-story reinforced masonry (big box) building of the prior FEMA P-695 study (NIST, 2010) resulted from an assumed shear wall length of only 24 feet (of a total wall length of 204 feet) of the archetype that would seldom, if ever, be found in an actual one-story (big box) masonry building.

As shown in Table 4-2, the archetypes that represent real building configurations consistently have more overstrength for shorter archetype configurations (e.g., one-story archetypes are always stronger than the two-story archetypes, which are always stronger than the four-story archetypes of a given SFRS). Additional strength of shorter archetype configurations is often due to practical design considerations. For example, due to the limited number of brace sizes, bracing of the one-story steel SCBF archetype has more capacity margin on seismic design loads, and hence more overstrength, than the two-story steel SCBF archetype, which has more margin and overstrength than the four-story steel SCBF.

The reversal of previously established MCE_R collapse probability trends with period can be largely attributed to the consistently greater overstrength of

shorter archetypes of real building configurations modeled with realistic collapse displacement capacities. There are other factors that also contribute to an improved understanding of the collapse performance of short-period buildings, as shown by the study of SDOF models in Chapter 5. As described in Section 2.4, prior theoretical studies of SDOF models dating to the original work of Veletsos and Newmark (1960) show that: (1) inelastic displacements are greater than elastic displacements for short-period models; and (2) the shorter the period, the worse the collapse performance for models of comparable strength (Chapter 3 of NIST, 2012), where collapse performance is defined by a maximum ductility demand regardless of model period. Defining collapse failure in terms of a ductility-based collapse displacement limit is fundamentally flawed and inappropriate for evaluating the collapse performance of short-period buildings, as shown in Chapter 5. Use of this definition in prior SDOF studies has led to a fundamental misunderstanding of trends in collapse performance with period. Where collapse performance is defined by realistic drift-based collapse capacity, the shorter the period, the better the collapse performance for models of comparable strength. As a result, shorter (e.g., one-story) archetypes of the detailed system-specific models were found to perform better than multi-story archetypes (with longer periods) because they are typically stronger, but even if they had the same strength, they still would have performed better.

6.1.2 MCE_R Collapse Performance

Although it was essential to show a reversal in the collapse trends with period, this alone would not have been sufficient to fully resolve the short-period building seismic performance paradox. As documented in Chapter 3, modern short-period buildings have performed well in past earthquakes, generally with collapse rates much less than the 10 percent collapse-safety objective of ASCE/SEI 7-16 for Risk Category II structures where MCE_R ground motions are defined by high-seismic criteria ($S_{MS} = 1.5g$). Consistent with observed performance, the improved system-specific numerical models demonstrated good collapse performance, in contrast to the sometimes-poor collapse performance of those of prior FEMA P-695 studies, as summarized below for one-story, two-story and four-story archetypes.

One-Story Archetypes. As shown in Figure 4-9 (and Table 4-2), none of the one-story models of prior FEMA P-695 studies meets the 2 percent benchmark collapse probability, with collapse probabilities ranging from 8.1 percent and 12.4 percent for wood light-frame archetypes to 79 percent for the reinforced masonry archetype. In contrast, all of the improved, system-specific, one-story models shown in Figure 4-9 meet the 2 percent

benchmark collapse probability, with collapse probabilities of 1.0 percent (MFD), 1.8 percent (SFD), and 1.6 percent (conventional construction SFD) for wood light-frame archetypes; 0.14 percent for the reinforced masonry archetype; and 1.2 percent for the steel SCBF archetype. It is particularly meaningful that the improved system-specific numerical models meet the benchmark collapse probability (i.e., observed collapse performance) for one-story archetypes since one-story buildings comprise the vast majority of all short-period buildings.

Two-Story Archetypes. As shown in Figure 4-9 (and Table 4-2), none of the two-story models of prior FEMA P-695 studies meets the 5 percent benchmark collapse probability with collapse probabilities of 6.1 percent and 9.4 percent for wood light-frame archetypes, 21 percent for the reinforced masonry archetype, and 35 percent for the steel SCBF archetype. In contrast, all of the improved, system-specific, two-story models shown in Figure 4-9 meet (or almost meet) the 5 percent benchmark collapse probability, with collapse probabilities of 5.5 percent (MFD), 2.6 percent (SFD), and 3.0 percent (conventional construction SFD) for wood light-frame archetypes; 3.2 percent for the reinforced masonry archetype; and 3.4 percent for the steel SCBF archetype. It is particularly meaningful that the improved, system-specific numerical models meet the benchmark collapse probability (i.e., observed collapse performance) for two-story archetypes since two-story buildings are the most common height of multi-story short-period buildings.

Four-Story Archetypes. As shown in Figure 4-9 (and Table 4-19), none of the improved, system-specific, four-story models or those of prior FEMA P-695 studies meets the 5 percent benchmark collapse probability. Collapse probabilities of the four-story archetypes of prior FEMA P-695 studies are 12.0 percent for wood light-frame archetypes, 8.4 percent for the reinforced masonry archetype, and 8.6 percent for the three-story steel SCBF archetype. Collapse probabilities of the improved, system-specific, four-story archetypes are 17.2 percent for the MFD wood light-frame archetype, 9.9 percent for the reinforced masonry archetype, and 6.0 percent for the steel SCBF archetype.

Although potentially important in terms collapse safety, it is less meaningful for resolution of the paradox that the improved, system-specific numerical models of four-story archetypes exceed the benchmark collapse probability (i.e., observed collapse performance). That is because four-story buildings represent a relatively uncommon height of short-period buildings (e.g., at the time of the 1994 Northridge earthquake, there were few, if any, wood light-frame buildings over three stories in height represented in the collapse

performance data of Chapter 3). Due to limited data on the performance of four-story buildings in past earthquakes, it is difficult to assign much reliability to the 5 percent benchmark collapse probability for buildings of this height.

6.2 Applicability to Other SFRSs of Short-Period Buildings

The following sections describe the applicability of key findings of the studies of the detailed numerical models of wood light-frame, reinforced masonry, and steel SCBF buildings to other SFRSs of short-period buildings and, in particular, to the collapse performance of other SFRSs of ASCE/SEI 7.

6.2.1 Conceptual Relationship

The generic collapse surfaces described in Chapter 5 provide a notional relationship between collapse performance and key building response properties, which are used conceptually to relate the key findings of the detailed numerical models to other SFRSs of short-period buildings. The premise of these relationships is that SFRSs of different materials and configurations will have comparable collapse performance (e.g., similar values of $ACMR$) when subjected to MCE_R ground motions, if these SFRSs have the same, or similar, values of each of following building response properties:

1. strength (e.g., the overstrength ratio, $\Omega/R = 1.5(V_{max}/W)/S_{MS}$),
2. collapse displacement capacity (e.g., median first-story drift ratio at incipient collapse, DR),
3. elastic fundamental period (e.g., model period, T_l), and
4. collapse failure mode.

The first three building response properties are determined by engineering analysis of numerical models of building archetypes of the SFRS of interest, where collapse displacement capacity could also be based on engineering judgment informed by available test data. The fourth building response property is a direct result of the numerical model of the building, which is influenced by both the configuration and design of the building archetype, as well as the numerical modeling methods used to characterize the nonlinear dynamic behavior of the SFRS.

For example, as shown in Figure 5-15, the values of $ACMR$ of the detailed models of wood light-frame building archetypes would be overestimated by the $ACMR$ values of simple bilinear SDOF models that do not incorporate the more realistic post-yield cyclic strength degradation, and other features, of the detailed models. In contrast, values of $ACMR$ of the detailed models of

wood light-frame building archetypes are essentially the same for different (COM, MFD, and SFD) configurations and designs of these archetypes, where the archetypes have the same strength, collapse displacement capacity, elastic period and, implicitly, the same collapse failure mode (i.e., since the wood light-frame archetypes were modeled with the same nonlinear response behavior).

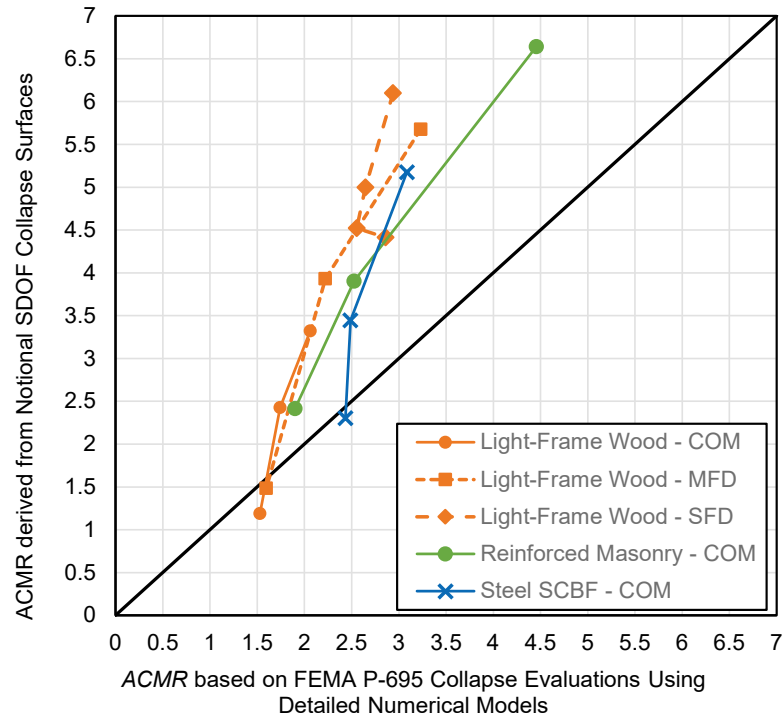


Figure 6-1 Values of *ACMR* derived from Equation 5-4 using the first-story failure coefficients of Table 5-6 versus the values of *ACMR* determined directly from FEMA P-695 collapse evaluations using detailed numerical models for wood light-frame COM, MFD, and SFD archetypes; reinforced masonry COM archetypes; and steel SCBF COM archetypes.

In general, the detailed studies found similar trends and values of *ACMR* as a function of building response properties for each of the three SFRSs investigated. For example, the comparisons of *ACMR* of wood light-frame archetypes from Figure 5-15 are shown in Figure 6-1, along with similar comparisons of *ACMR* of reinforced masonry COM building archetypes and steel SCBF COM building archetypes. In Figure 6-1 (and Figure 5-15), values of *ACMR* derived from notional collapse surfaces (i.e., from Equation 5-4 using the first-story failure coefficients of Table 5-6) are plotted as a function of the values of *ACMR* determined directly from FEMA P-695 collapse evaluations (i.e., the values of *CMR* of Table 4-2 increased by $SSF = 1.33$) using detailed numerical models of wood light-frame, reinforced masonry, and

steel SCBF archetypes. The similarity of the trends and values of *ACMR* for the three SFRSs suggests that values of *ACMR* could be reasonably well predicted by the same generic function of building response properties (i.e., same set of collapse surfaces), where the archetypes of the SFRSs of interest have similar hysteretic response characteristics and, implicitly, the same collapse failure mode.

The values of *ACMR* of the detailed models of all three SFRSs would be overestimated by the *ACMR* values of simple bilinear SDOF models, as shown in Figure 6-1. Overestimation of *ACMR* values compared to those from the detailed models is reasonable considering that the values of *ACMR* derived from Equation 5-4 using coefficients of Table 5-6 are based on simple SDOF models that do not incorporate the more realistic post-yield cyclic strength degradation and other features of the detailed models.

6.2.2 SFRSs of ASCE/SEI 7-16

ASCE/SEI 7-16 (Table 12.2-1) permits 30 SFRSs for design of short-period buildings in high-seismic regions (Table 2-1). The three systems—wood light-frame, reinforced masonry, and steel SCBF—that were the focus of detailed studies represent about 85 percent (by square footage) of all short-period buildings of modern construction subject to building-code requirements (Table 2-2). Residential buildings are the most common use (occupancy) of short-period building, and wood light-frame is by far the most common SFRS used for residential construction. Other SFRSs commonly used for short-period buildings include: (1) special reinforced concrete shear walls; (2) intermediate pre-cast shear walls; (3) cold-formed steel (CFS) walls and frames; (4) steel special (and intermediate) moment frames; and (5) special reinforced concrete moment frames. It should be noted that moment frame buildings are inherently flexible, and, to stay within the short-period building range, where $T \leq 0.5$ seconds, they are generally limited to one-story and two-story configurations.

A listing of the 30 SFRSs permitted in high-seismic regions by ASCE/SEI 7-16 are repeated in Table 6-1, along with a judgmental assignment of the corresponding studied SFRS (wood light-frame, A.15; reinforced masonry, A.7; or steel SCBF, B.2) that is deemed “equivalent” in terms of collapse performance. The corresponding FEMA Model Building Types, MBTs, from FEMA P-155 are also included. In some cases, one of the three SFRSs is considered directly applicable and is thus noted as such; whereas in other cases, one of three SFRSs (shown in parentheses) is considered to be informative, but not directly applicable, and would require further investigation to determine applicability. Where none of the three systems is

Table 6-1 SFRSs Permitted in High-Seismic Regions by ASCE/SEI 7-16 and the Corresponding Studied SFRS Deemed Equivalent in Terms of Collapse Performance and the Corresponding FEMA Model Building Type (MBT) from FEMA P-155

SFRS No.	Description	Equivalent SFRS No.	FEMA MBT
Bearing Wall Systems			
A.1	Special reinforced concrete shear walls	(A.7)	C2
A.5	Intermediate precast shear walls	(A.7)	PC1, PC2
A.7	Special reinforced masonry shear walls	A.7	RM1, RM2
A.15	Light-frame (wood) walls with rated wood structural panels	A.15	W1, W1A, W2
A.16	Light-frame (CFS) walls with rated wood structural panels	(A.15)	W1, W1A, W2
A.17	Light-frame walls with shear panels of all other materials	(A.15)	W1, W1A, W2
A.18	Light-frame (CFS) walls with flat strap bracing	(B.2)	S3
Building Frame Systems			
B.1	Steel eccentrically braced frames	(B.2)	S2
B.2	Steel special concentrically braced frames	B.2	S2
B.3	Steel ordinary concentrically braced frames	(B.2)	S2
B.4	Special reinforced concrete shear walls	(A.7)	C2
B.8	Intermediate precast shear walls	(A.7)	PC1, PC2
B.10	Steel/concrete composite eccentrically braced frames	(B.2, A.7)	S2, C2
B.11	Steel/concrete composite special concentrically braced frames	(B.2, A.7)	S2, C2
B.13	Steel/concrete composite plate shear walls	-	
B.14	Steel/concrete composite special shear walls	-	
B.16	Special reinforced masonry shear walls	A.7	RM1, RM2
B.22	Light-frame wood with rated-wood sheathed shear walls	A.15	W1, W1A, W2
B.23	Light-frame (CFS) with rated-wood or steel sheet shear walls	(A.15)	W1, W1A, W2
B.24	Light-frame walls with other sheathing materials	(A.15)	W1, W1A, W2
B.25	Steel Buckling-restrained braced frames	(B.2)	S2
B.26	Steel special plate shear walls	-	
Moment-Resisting Frame Systems			
C.1	Steel special moment frames	(B.2)	S1
C.2	Steel special truss moment frames	(B.2)	S1
C.3	Steel intermediate moment frame	(B.2)	S1
C.5	Special reinforced concrete moment frames	(A.7)	C1
C.8	Steel/concrete composite special moment frames	(B.2, A.7)	S1, C1
C.9	Steel/concrete composite intermediate moment frames	(B.2, A.7)	S1, C1
C.10	Steel/concrete composite partially restrained moment frames	-	
C.12	Cold-formed steel – special bolted moment frame	(B.2)	S3

considered applicable, no equivalent SFRS is shown. Applicability tacitly assumes collapse is due to first-story failure and that nonlinear dynamic response characteristics are similar, which may not always be the case. Collapse failure modes due to failure of the gravity system prior to that of the SFRS, out-of-plane failure of walls (e.g., of tilt-up construction), and rocking and uplift of foundations (rather than failure of walls or braced frames above) are presumed to not govern collapse performance. These other failure modes, such as those due to rocking and uplift of foundations, are not necessarily detrimental to collapse performance, but they were not incorporated into the baseline models of the three system-specific studies.

6.3 Extrapolation to Other SFRSs of Short-Period Buildings

The collapse evaluations of the three studied SFRSs are sufficient (along with other information) to solve the short-period building seismic performance paradox. However, the collapse results (e.g., values of *ACMR*) are not sufficient to fully define collapse (i.e., collapse surfaces) for all possible combinations of building response properties of interest. The significant amount of effort required to develop detailed numerical models and perform nonlinear analyses of the three SFRSs (Chapter 4) necessarily restricted the number of building archetypes that could be developed and evaluated for collapse. Hence, the sets of collapse data from these studies are not large, even for the studies of wood light-frame building archetypes (i.e., the SFRS with the most extensive set of numerical models and collapse analyses). Relatively large sets of collapse results (i.e., several hundred *ACMR* data), such as those developed from analyses of simple bilinear SDOF models in Chapter 5, would be required to fully define the collapse surfaces for the three studied SFRSs, as well as those for other SFRSs of short-period buildings (Table 6-1).

Computationally efficient SDOF models could be used in combination with limited analyses of complex nonlinear 3D models to develop collapse surfaces, where it would otherwise not be practical to use complex nonlinear 3D models alone. These so-called “calibrated” SDOF models would have dynamic response properties (e.g., elastic period, model height, and nonlinear hysteretic characteristics) that are informed by detailed models of the SFRS of interest. Additionally, values of *ACMR* (i.e., points on the collapse surface) calculated using calibrated SDOF models would be validated by comparison with a limited number of *ACMR* values of the detailed models. The process used to develop large sets of collapse data would be similar to that used in Chapter 5 to develop notional collapse surfaces, except that more sophisticated nonlinear SDOF models (calibrated SDOF models) would be used in lieu of simple bilinear SDOF models. Calibrated SDOF models

would have elastic stiffnesses based on the fundamental periods of the detailed models and post-yield hysteretic behavior that emulates the post-yield hysteretic behaviors of the detailed models of the systems of interest.

Computational efficiency provides several potential advantages, one of which would be the opportunity to explicitly evaluate the variability in collapse performance (i.e. variability of the value of $ACMR$) due to the uncertainty in building response properties, namely, the uncertainty of the shape of the backbone curve and associated post-yield hysteretic properties of the system of interest. The notional collapse surfaces of Chapter 5 are based on a single value of $ACMR$ (i.e., point on the collapse surface) for each combination of building response properties (i.e., strength, collapse displacement capacity, and elastic period). For the same set of building response properties, the process could be repeated for different assumptions of backbone curve shape and post-yield hysteretic properties (e.g., residual strength, cyclic-degradation) to produce a set of $ACMR$ values characterizing the variation in collapse performance due to uncertainty in the building response properties. In this manner, collapse data (collapse surfaces) could be developed that incorporate uncertainty in the value of $ACMR$ due to modeling assumptions (i.e., one of the parameters governing the total uncertainty in collapse, β_{TOT} , of FEMA P-695).

Another potential advantage of computational efficiency would be the opportunity to explicitly evaluate systematic differences in response and collapse performance (i.e. value of $ACMR$) due to different seismic hazard settings (e.g., western U.S. near-source sites, Pacific Northwest sites, central and eastern U.S. sites) and different site conditions for which frequency content, transient shaking characteristics, and duration of strong ground motions are known to be inherently different from those of the far-field record set of FEMA P-695. In this case, the same ensemble of calibrated SDOF models (based on the detailed models) of the SFRS of interest would be evaluated for a different set of ground motions from those of the far-field record set of FEMA P-695.

Collapse surfaces of SFRSs could provide the technical basis for seismic-code committees to re-evaluate and perhaps streamline the judgmental values of seismic performance factors of short-period buildings (in particular the value of the R factor) now defined in Table 12.2-1 of ASCE/SEI 7-16. As shown in Table 2-1, there are 13 different values of the R factor ranging from $R = 2$ to $R = 8$ that imply a level of accuracy and precision not warranted by observation or analysis. Re-evaluating R factors could be accomplished directly by performing FEMA P-695 analyses on the SFRSs of interest. However, the acceptance criteria of FEMA P-695 are based on a pass-fail concept of

evaluating the collapse performance of representative sets of building archetypes for a defined collapse objective (i.e., 10 percent MCE_R collapse probability) such that archetypes with a 9.9 percent probability of collapse are effectively deemed to be just as safe as those with a 1.0 percent probability of collapse. By relating collapse performance to strength, collapse displacement capacity, and elastic period, collapse surfaces provide a more nuanced description of collapse performance that can be used to determine the specific values of building response properties required to achieve a given collapse objective (e.g., strength ratio, Ω/R , required to meet the collapse objective for a given collapse displacement capacity and fundamental period).

Similarly, collapse surfaces could be a benefit to performance-based design methods by providing a convenient means for determining the amount of strength, collapse displacement capacity, or both required to achieve a specific collapse performance objective, or conversely, to verify adequate collapse performance given building strength and displacement capacity. Collapse surfaces could be of particular benefit to the seismic retrofit requirements of ASCE/SEI 41, which are based on nonlinear analysis methods using realistic building response properties (e.g., yield strength) similar to those required by FEMA P-695 for modeling and analysis of building archetypes. As shown in Chapter 5, collapse surfaces can be significantly influenced by the failure mode (e.g., first story versus height distributed), as characterized by the nonlinear response properties of the SDOF models. Likewise, for performance-based design, collapse surfaces would necessarily be a function of failure mode, where calibrated SDOF models would be based on sophisticated modeling criteria (e.g., modeling parameters of ASCE/SEI 41), rather than the crude assumption of bilinear (elasto-plastic) behavior used to model SDOF systems in Chapter 5.

7.1 Introduction

The goal of this chapter is to identify and document recommendations that are common to all three of the seismic-force-resisting systems (wood light-frame, reinforced masonry, and steel SCBF) that were the focus of detailed studies. Most of these recommendations can be found in Chapter 6 of the three reports summarizing these studies (FEMA P-2139-2, FEMA P-2139-3, and FEMA P-2139-4). Some new recommendations have been included based on a review of the key findings and conclusions of all three reports, as well as insights gleaned from the SDOF study described in Chapter 5.

The recommendations are organized under the following topics:

- Improved Seismic Design Codes and Standards
- Advanced Seismic Design and Analysis Practice
- Enhanced Modeling, Testing, and Data Collection

Although there is considerable overlap, the recommendations for seismic design codes and standards are intended primarily for seismic-code-development committees; the recommendations for seismic design and analysis practice are intended primarily for engineering practitioners; and the recommendations for modeling, testing, and data collection are intended primarily for research engineers and academicians.

7.2 Recommendations for Improved Seismic Design Codes and Standards

This section describes topics and provides recommendations considered applicable to seismic-code-development committees, including the Provisions Update Committee of the Building Seismic Safety Council, the Seismic Subcommittee of ASCE/SEI 7, the ASCE/SEI 41 Standards Committee on Seismic Evaluation and Retrofit of Existing Buildings, and material-specific standards committees, such as the Wood Design Standards Committee of the American Wood Council, the TMS 402/602 Standards Committee of The Masonry Society, and the AISC Committee on Specifications of the American Institute of Steel Construction. Seismic-code committees have limited resources and studies would, in most cases, require

a funded project to develop the requisite technical basis of any proposals to improve existing codes and standards.

Performance-Based Design Criteria (Collapse Surface). The collapse results of the detailed studies of baseline archetype models of wood light-frame, reinforced masonry, and steel SCBF buildings show consistent and similar trends of the combined influence of strength and displacement capacity on collapse performance of short-period buildings. Collapse surfaces, defined in Section 5.4, characterize these trends by relating collapse performance in terms of the adjusted collapse margin ratio (*ACMR*) to building response properties, namely, strength, displacement capacity, and elastic fundamental period. Notional collapse surfaces based on simple bilinear SDOF models are illustrated in Figure 5-13 and Figure 5-14. Collapse surfaces could be a benefit to performance-based design methods by providing a convenient means of determining the amount of strength, collapse displacement capacity, or both required to achieve a specific collapse performance objective, or conversely, to verify adequate collapse performance given building strength and displacement capacity (Section 6.3). Such surfaces could address performance objectives other than collapse, such as building downtime or others related to the “resilience” of structures.

A study is recommended to develop collapse surfaces following the approach described in Section 6.3, which would comprehensively characterize collapse performance (or other performance objectives) of short-period buildings in terms of building response properties, namely, strength, collapse displacement capacity, elastic fundamental period, and the mode of collapse failure.

Strength and Displacement Capacity. The collapse study results from both detailed archetype models and SDOF models demonstrated the significant influence of model maximum strength normalized by weight (expressed as a ratio of V_{max}/W) and post-peak displacement capacity, as well as period, on the resulting collapse probabilities. The combined influence of these parameters was further illustrated in the notional collapse surfaces presented in Chapter 5 for the SDOF models. It is recommended that collapse studies that are used to inform future code and standard development (using FEMA P-695 or similar methods) explicitly consider the real strength and displacement capacity of the archetype building numerical models and address the influence of these parameters on the resulting reported probabilities of collapse.

Overstrength. The analyses in the detailed system-specific studies confirmed that increasing overstrength (i.e., $\Omega = V_{max}/V_{design}$) decreases the probability of collapse. In this context, the term “overstrength” refers only to

real strength greater than the design strength and not to the overstrength factor (Ω_0) defined in Chapter 11 of ASCE/SEI 7-16.

Buildings in the detailed system-specific studies generally had undesigned sources of overstrength, but the sources varied between the different types of systems. For example, in wood light-frame building archetypes, the overstrength derived from the presence of materials not considered part of the SFRS. In reinforced masonry building archetypes, overstrength resulted from architectural configuration of structural elements and minimum reinforcement requirements. For steel SCBF building archetypes, the combination of slender tension and compression elements with different capacities in post-yield and post-buckling configurations resulted in overstrength that was a natural consequence of material and structural configuration.

Historically, the effectiveness of design codes and standards has been evaluated to some degree by looking at the seismic performance of the buildings designed using the previous codes and standards. Those buildings all had inherent overstrength, and that affected their performance. It is recommended that code-and-standard writing bodies be aware that future refinements in design and construction techniques can affect the amount of inherent overstrength in a system, and thus the probability of collapse.

Deformation Compatibility of Components not Part of the SFRS. The nonlinear models in all three system-specific studies had large displacement capacities (e.g., median first-story drift ratios as large as 10 percent at incipient collapse) that are significantly larger than those currently used for ASCE/SEI 7 to check deformation compatibility of components not part of the seismic-force-resisting system. This is of possible concern because the collapse probabilities determined by these studies assumed that the gravity systems could support gravity loads out to the drift at incipient collapse.

A study is recommended to determine whether current ASCE/SEI 7 provisions for deformation compatibility checks are adequate given the new drift information available from these studies.

Very High-Seismic Collapse Potential. Each system studied showed an increased probability of collapse at the highest ground motions investigated. An increase in the probability of collapse with stronger ground motions is contrary to the target reliability of Table 1.3-2 of ASCE/SEI 7-16, which defines the maximum conditional probability of failure (e.g., 10 percent for Risk Category II structures) independent of the level of MCE_R ground motions. The results from these studies indicate that objective not being fulfilled.

All archetypes of very high-seismic loads were designed and evaluated for very high-seismic loads (i.e., $1.5 \times$ high seismic, SDC $D_{\max} = 2.25g$ criteria of FEMA P-695). In both the wood light-frame and steel SCBF studies, the collapse probabilities of two-story and four-story baseline archetypes exceed the 10 percent collapse-safety objective of ASCE/SEI 7 for Risk Category II structures, often by a substantial amount. Although the collapse probabilities of the very high-seismic reinforced masonry archetypes do not exceed 10 percent, collapse performance is, in all cases and all systems studied, worse for an archetype designed and evaluated for very high-seismic criteria compared to the same archetype designed and evaluated for high-seismic criteria. An increase in the probability of collapse given MCE_R ground motions also was observed in a study documented in FEMA P-695 for reinforced concrete moment frame archetypes. There is a consistent trend of collapse probabilities exceeding the 10 percent collapse-safety objective of ASCE/SEI 7 in regions of very high seismicity.

A study is recommended to quantify the potential increase in the conditional probability of collapse given MCE_R ground motions (i.e., above the 10 percent target of ASCE/SEI 7 for Risk Category II structures) and the associated increase in collapse risk (i.e., annual probability of collapse) of building archetypes of common seismic-force-resisting systems for sites located in very high-seismic regions (i.e., $S_{MS} \geq 1.5g$).

Target Collapse Probability. ASCE/SEI 7 targets a conditional probability of collapse given the occurrence of MCE_R ground motion of 10 percent for Risk Category II structures. That level was selected because it represented reasonably well the computed probabilities of collapse for a limited set of seismic-force-resisting systems involved in past FEMA P-695 studies. Those systems had extensive testing and well-established design requirements, as well as at least some successful performance in past earthquakes. The 10 percent level was not based on empirical data from historical earthquakes. As documented in these studies, that 10 percent value is substantially in excess of the observed rate of failure for short-period structures found in historical U.S. earthquakes.

The FEMA P-695 methodology for estimation of collapse probabilities includes several important constraints. One is that the strengths of elements not designed as part of the seismic-force-resisting system are not to be included in the analytical model for nonlinear response. As demonstrated in these studies, inclusion of such elements for some systems can significantly impact computed probabilities of collapse. These studies also showed that the use of more realistic archetype designs and realistic displacement capacity assumptions can result in more realistic collapse estimates.

The detailed system-specific studies also found that computed conditional probabilities of collapse increased as the number of stories increased and as the design ground-motion levels became very high, in some cases exceeding the 10 percent target of ASCE/SEI 7. There is much less empirical data for performance of four-story short period buildings, and there is little empirical data for performance under very high-seismic ground motions.

It is recommended that committees responsible for seismic-code development consider the following observations from this study of short-period buildings in their deliberations:

1. Empirical data suggest that collapse rates for high-seismic ground motions (i.e., $S_{MS} = 1.5g$) are substantially less than 10 percent. Public expectations for collapse rates may understandably be more in line with empirical experience than with the 10 percent target of ASCE/SEI 7.
2. Advanced modeling techniques can lead to smaller computed probabilities of collapse than are found using methods more like those used in establishing the 10 percent target.
3. Incorporation of strength from elements not considered part of the designed seismic-force-resisting system has a significant effect on the computed probability of collapse for some systems, and is likely more realistic but more difficult to control in design and in building regulation in any systematic fashion. This challenge would be further complicated when design and construction practices change in the future. Should such trends reduce the contribution of non-SFRS elements to collapse resistance, they are likely to affect previously established collapse probabilities.
4. Computed probabilities of collapse for structures designed for and subjected to very high-seismic ground motions (i.e., $S_{MS} = 2.25g$) are typically higher than structures designed for and subjected to high-seismic ground motions (i.e., $S_{MS} = 1.5g$).
5. Computed probabilities of collapse increase as the number of stories increase for building archetypes with the same seismic-force-resisting system.

Furthermore, it is recommended that additional research be undertaken to support code-development committees concerned with the following questions:

1. Should the target for conditional probability of collapse be revised to be more in line with empirical experience? If so, what changes would be needed in the FEMA P-695 methodology to accommodate the revised target collapse probabilities?

2. Should the methodologies for estimating collapse probability be revised to explicitly consider strength from elements not a formal part of the seismic-force-resisting system, and, if yes, how would their contribution be controlled in design?
3. Should the target conditional probability of collapse be different for very high-seismic (i.e., near fault) sites than for other sites? If no, are more rigorous design rules needed for very high-seismic sites in order to achieve the target conditional probability of collapse?
4. Do the observations identified in item 4 and item 5 above hold true for longer-period structures?

FEMA P-695 Seismic Criteria Update. The seismic criteria of FEMA P-695 are based on the “Zone 4” seismic criteria of the 1994 version of the *Uniform Building Code* (ICBO, 1994), as embodied in the deterministic-lower-limit seismic criteria of Section 21.2.2 of ASCE/SEI 7-05 (ASCE, 2005). The seismic criteria of FEMA P-695 are out-of-date with respect to the current seismic criteria of ASCE/SEI 7-16 and ASCE/SEI 7-22, as proposed. At short periods (i.e., the acceleration domain), the seismic criteria of FEMA P-695 are either the same as the deterministic lower limit of ASCE/SEI 7-16 or only about 10 percent less than those proposed for ASCE/SEI 7-22. In the velocity domain (i.e., periods greater than 1.0 second for Site Class D site conditions), the seismic criteria of FEMA P-695 are only about 60 percent of those of ASCE/SEI 7-16 (and somewhat less for ASCE/SEI 7-22, as proposed). Updating the seismic criteria of FEMA P-695 would not significantly affect the collapse evaluation of short-period building archetypes (or the findings of the system-specific studies presented in Chapter 4), but could be of importance to the collapse evaluation of taller building archetypes with longer periods.

As per the original “Zone 4” approach of FEMA P-695, all of the ground motions represent “far-field” sites and purposely ignore higher levels of ground shaking typical of sites closer to the fault(s) governing site seismic hazard. Accordingly, FEMA P-695 implicitly permits MCE_R collapse probabilities greater than 10 percent for structures at sites where ground motions are greater than those of the “far-field” SDC D_{max} seismic criteria; whereas, the 10 percent collapse objective of Section 1.3.1.3 (Performance-Based Procedures) and Section 12.2.1.1 (Alternate Structural Systems) of ASCE/SEI 7-16 applies to all sites, regardless of their proximity to fault rupture, noting that the commentary to Section 12.2.1.1 identifies FEMA P-695 as the preferred methodology for verifying compliance with the 10 percent collapse objective. As shown by comparison of the collapse

performance of high-seismic and very high-seismic baseline archetype models of the system-specific studies, very different conclusions could be reached if the MCE_R ground motions greater than those of the “far-field” SDC D_{max} of FEMA P-695 were required for collapse evaluation. The fundamental question is simply: Does the 10 percent collapse-safety objective of ASCE/SEI 7-16 apply to buildings at all possible sites or only to those sites that are not “near-source”?

A study is recommended to determine what if any updates to FEMA P-695 should be made to: (1) incorporate current ASCE/SEI 7-16 and forthcoming ASCE/SEI 7-22 ground-motion criteria; and (2) address the apparent discrepancy between the acceptance criteria of FEMA P-695 and those of Section 12.2.1.1 of ASCE/SEI 7-16.

Soil-Structure Interaction and Foundation Flexibility. Parametric studies performed for all three building systems evaluated showed that when a building underwent significant inelastic displacement, soil-structure interaction (SSI) and foundation flexibility did not consistently reduce the probability of collapse. In two out of the three systems evaluated (wood light-frame and reinforced masonry), SSI and foundation flexibility essentially had no impact on the probability of collapse. It is recommended that committees involved in the development of ASCE/SEI 7 and ASCE/SEI 41 revisit the rules for use of SSI and foundation flexibility in the design of short-period buildings. Specifically, the findings of the SSI and foundation flexibility parametric studies suggest that allowing design base shear to be reduced when SSI and foundation flexibility are considered in design could lead to worse collapse performance and may not be justified.

7.3 Recommendations for Advanced Seismic Design and Analysis

This section describes topics and provides recommendations considered applicable to engineering practitioners, especially those who are interested in performance-based design of new buildings or seismic retrofit of existing buildings. It is recognized that the recommendations may not be practical for implementation by practitioners and would likely require funded projects to fully develop the requisite methods.

Overstrength. All three system-specific studies identified sources of undesigned overstrength in the seismic-force-resisting systems. Although the sources of overstrength were not the same, they were all consequences of common design or building practices, as described in Section 7.2. It is reasonable to expect that this observation is not unique to the building types in these studies.

Designers should be aware that undesigned overstrength can result in unintentional failure modes that are inconsistent with the capacity design principles that underlie the building code. For example, a shear wall that is much stronger than necessary may remain effectively elastic (i.e., $R = 1$) and will not limit design forces in other elements, such as diaphragms and their connections, to design-level forces. A study is recommended to examine the full effect of overstrength on collapse behavior to extend the observations and conclusions of these studies.

Rocking Failure Modes. One possible consequence of the observed overstrength is that foundation rocking can occur before the strength capacity of the intended seismic-force-resisting system is reached. This behavior was observed explicitly in the steel SCBF studies but could occur for other building systems. The observed rocking response behavior was not found to adversely affect collapse performance for the limited number of SCBF archetypes investigated; however, the rocking response represents an entirely different collapse failure mode from that assumed by codes and standards that develop seismic loads and design requirements.

Further study is recommended to first determine if there is a collapse safety issue due to rocking (i.e., identify building configurations or design conditions for which collapse performance could be made worse due to rocking) and if so, develop appropriate code changes to remedy the potential collapse safety deficiency. Second, it is recommended that additional study investigate and determine feasible code changes that would explicitly incorporate rocking response in the design of all buildings.

7.4 Recommendations for Enhanced Modeling, Testing, and Data Collection

This section describes topics and provides recommendations considered applicable to engineers and academicians interested in research studies of wood light-frame, reinforced masonry, or steel SCBF buildings. In this context, the modeling recommendations apply to sophisticated modeling, such as that described in Chapter 4, and the testing recommendations apply to monotonic- and cyclic-load testing or shake-table testing of structures investigated within the scopes of these studies.

Cyclic-Load Testing Protocol. Experimental data of component and system behavior through collapse are critical for calibration of numerical models. Such test data are rare. There are a number of available cyclic-load testing protocols that have been used to develop hysteretic backbone characterizations of structural and nonstructural elements of buildings, including the CUREE Publication No. W-02, *Development of a Testing*

Protocol for Woodframe Structures (CUREE, 2001) and FEMA 461, *Interim Testing Protocols for Determining the Seismic Performance Characteristics of Structural and Nonstructural Components* (FEMA, 2007), which are not necessarily appropriate for measuring nonlinear behavior at very large displacements.

A study is recommended to develop test protocols that quantify necessary component and system deformation demands through collapse such that experiments can be systematically conducted through the large deformations necessary for accurate collapse simulations. The protocol should address the seismic hazard and tectonic region that is meant to be captured. This protocol would also address the need for tests to include quantification of the residual capacity of components after significant deterioration.

Shake-Table Testing to Collapse. All three system-specific studies identified a need for experimental data from shake-table tests taken to the verge of collapse, in order to calibrate and validate numerical models. Each study identified needs particular to the system. For wood light-frame buildings, there is a need for testing of taller configurations that were found to be more vulnerable than shorter configurations. For masonry buildings, there is a need for testing with bi-axial earthquake ground motions. For steel SCBF structures, there is a need for testing that captures rocking behavior and the behavior of diaphragms, collectors, and connections. Common to each system was the need to take tests to large displacements and to (or near to) collapse.

It is recommended that experimental research utilizing shake-table testing to investigate the behavior of structures under seismic loads consider:

(1) protocols that take structures to large displacements at the verge of collapse; and (2) the importance of multi-direction loading.

Building Assembly Testing. These studies identified the importance of the interaction of multiple building components and realistic boundary conditions in the modeling and analysis of full building systems. Individual component tests, although informative, cannot capture these important effects. In the absence of resources or funds for shake-table testing, quasi-static testing of realistic assemblies of components to validate complex models is critical to the accurate determination of collapse probabilities of building systems. It is recommended that emphasis be placed on testing of realistic assemblies.

Post-Earthquake Data Collection. The efficacy of projects that seek to validate seismic design criteria, investigate probability of collapse, and

contribute to the establishment of realistic performance objectives depends critically on the accuracy and completeness of post-earthquake surveys of building performance. To be effective, such surveys must be sufficiently broad to include a large population of (if not all) buildings or building systems in an affected area, including both damaged and undamaged buildings. For buildings that are damaged, data collection protocols should be of sufficient depth to be useful in calibrating analytical studies. Response data from instrumented buildings are also valuable.

It is recommended that appropriate agencies put plans in place to support such surveys to be conducted rapidly and completely immediately after significant seismic events, which is to say that funding mechanisms and protocols should be established prior to an event.

References

- AIJ, 1995a, *Preliminary Reconnaissance Report of the 1995 Hyogoken-Nanbu Earthquake*, English Edition, Architectural Institute of Japan, Tokyo, Japan.
- AIJ, 1995b, *Reconnaissance Report on Damage to Steel Building Structures Observed from the 1995 Hyogoken-Nanbu (Hanshin /Awaji) Earthquake*, Steel Committee of Kinki Branch, Architectural Institute of Japan (in Japanese with Abridged English Edition), Tokyo, Japan.
- AISC, 2010, *Seismic Provisions for Structural Steel Buildings*, ANSI/AISC 341-10, American Institute of Steel Construction, Chicago, Illinois.
- ASCE, 2005, *Minimum Design Loads for Buildings and Other Structures*, ASCE/SEI 7-05, American Society of Civil Engineers, Reston, Virginia.
- ASCE, 2010, *Minimum Design Loads for Buildings and Other Structures*, ASCE/SEI 7-10, American Society of Civil Engineers, Reston, Virginia.
- ASCE, 2016, *Minimum Design Loads and Associated Criteria for Buildings and Other Structures*, ASCE/SEI 7-16, American Society of Civil Engineers, Reston, Virginia.
- ASCE, 2017, *Seismic Evaluation and Retrofit of Existing Buildings*, ASCE/SEI 41-17, American Society of Civil Engineers, Reston, Virginia.
- ATC, 1989, *Procedures for Postearthquake Safety Evaluation of Buildings*, ATC-20, Applied Technology Council, Redwood City, California
- ATC, 2000, *Database on the Performance of Structures near Strong-Motion Recordings: 1994 Northridge, California, Earthquake*, ATC-38, Applied Technology Council, Redwood City, California.
- ATC, 2005, *Field Manual: Postearthquake Safety Evaluation of Buildings Second Edition*, ATC-20-1, Applied Technology Council, Redwood City, California.

- ATC, 2015, *Roadmap for Solutions to the Issue of Short Period Building Performance*, ATC-116 Report, Applied Technology Council, Redwood City, California.
- AWC, 2008, *Special Design Provisions for Wind and Seismic, 2008 Edition*, ANSI/AF&PA SDPWS-2008, American Wood Council, American Forest & Paper Association, Washington, D.C.
- Baker, J.W., 2015, "Efficient analytical fragility function fitting using dynamic structural analysis," *Earthquake Spectra*, Vol. 31, No.1, pp. 579-599.
- Brady, A.G., Etheredge, E.C., and Porcella, R.L., 1988, "The Whittier Narrows, California earthquake of October 1, 1987 – preliminary assessment of strong ground motion records," *Earthquake Spectra*, Vol. 4, No. 1, pp. 55-74.
- CEN, 2004, *Eurocode 8: Design of Structures for Earthquake Resistance - Part 1: General Rules, Seismic Actions and Rules for Buildings*, European Committee for Standardization, Brussels, Belgium.
- Cheng, J., Koutras, A.A., and Shing, P.B., 2020, "Evaluation of collapse resistance of reinforced masonry wall systems by shake-table tests," *Earthquake Engineering and Structural Dynamics* (published online).
- Chopra, A., and Chintanapakdee, C., 2004, "Inelastic deformation ratios for design and evaluation of structures: single-degree-of-freedom bilinear systems," *Journal of Structural Engineering*, Vol. 130, No. 9, pp. 1309-1319.
- Christovasilis, I.P., and Filiatrault, A., 2013, "Numerical framework for non-linear analysis of two-dimensional light-frame wood structures," *Ingegneria Sismica: International Journal of Earthquake Engineering*, No. 4, pp. 5-25.
- CUREE, 2001, *Development of a Testing Protocol for Woodframe Structures*, CUREE Publication No. W-02, Consortium of Universities for Research in Earthquake Engineering, Richmond, California.
- Dizhur, D., Ingham, J., Moon, L., Griffith, M., Schultz, A., Senaldi, I., Magenes, G., Dickie, J., Lissel, S., Centeno, J., Ventura, C., Leite, J., and Lourenco, P., 2011, "Performance of masonry buildings and churches in the 22 February 2011 Christchurch earthquake," *Bulletin of the New Zealand Society of Earthquake Engineering*, Vol. 44, No. 4, pp. 279-296.

- EERI, 1978, *Reconnaissance Report, Miyagi-Ken-oki, Japan Earthquake, June 12, 1978*, Earthquake Engineering Research Institute, Oakland, California.
- FEMA, 1997, *NEHRP Guidelines for the Seismic Rehabilitation of Buildings*, FEMA 273, prepared by the Applied Technology Council for the Federal Emergency Management Agency for the Building Seismic Safety Council, Washington, D.C.
- FEMA, 2000, *Prestandard and Commentary for the Seismic Rehabilitation of Buildings*, FEMA 356, Federal Emergency Management Agency, Washington, D.C.
- FEMA, 2003, *Multi-hazard Loss Estimation Methodology, Earthquake Model*, HAZUS[®]MH MR4, Technical Manual, prepared by the National Institute of Building Sciences for the Federal Emergency Management Agency, Washington, D.C.
- FEMA, 2005, *Improvement of Nonlinear Static Analysis Procedures*, FEMA 440, prepared by the Applied Technology Council for the Federal Emergency Management Agency, Washington, D.C.
- FEMA, 2007, *Interim Testing Protocols for Determining the Seismic Performance Characteristics of Structural and Nonstructural Components*, FEMA 461, prepared by the Applied Technology Council for the Federal Emergency Management Agency, Washington, D.C.
- FEMA, 2009a, *NEHRP Recommended Seismic Provisions for New Buildings and Other Structures*, FEMA P-750, prepared by the Building Seismic Safety Council of the National Institute of Building Sciences for the Federal Emergency Management Agency, Washington, D.C.
- FEMA, 2009b, *Quantification of Building Seismic Performance Factors*, FEMA P-695, prepared by the Applied Technology Council for the Federal Emergency Management Agency, Washington, D.C.
- FEMA, 2009c, *Effects of Strength and Stiffness Degradation on Seismic Response*, FEMA 440A, prepared by the Applied Technology Council for the Federal Emergency Management Agency, Washington, D.C.
- FEMA, 2012, *Seismic Evaluation and Retrofit of Multi-Unit Wood-Frame Buildings with Weak First Stories*, FEMA P-807, prepared by the Applied Technology for the Federal Emergency Management Agency, Washington, D.C.

- FEMA, 2015, *Rapid Visual Screening of Buildings for Potential Seismic Hazards: Supporting Documentation, Third Edition*, FEMA P-155, prepared by the Applied Technology Council for the Federal Emergency Management Agency, Washington, D.C.
- FEMA, 2020a, *Short-Period Building Collapse Performance and Recommendations for Improving Seismic Design, Volume 2 – Study of One-to-Four Wood Light-Frame Buildings*, FEMA P-2139-2, prepared by the Applied Technology Council for the Federal Emergency Management Agency, Washington, D.C.
- FEMA, 2020b, *Short-Period Building Collapse Performance and Recommendations for Improving Seismic Design, Volume 3 – Study of One-to-Four Story Special Reinforced Masonry Shear Wall Buildings*, FEMA P-2139-3, prepared by the Applied Technology Council for the Federal Emergency Management Agency, Washington, D.C.
- FEMA, 2020c, *Short-Period Building Collapse Performance and Recommendations for Improving Seismic Design, Volume 4 – Study of One-to-Four Story Steel Special Concentrically Braced Frame Buildings*, FEMA P-2139-4, prepared by the Applied Technology Council for the Federal Emergency Management Agency, Washington, D.C.
- Folz, B., and Filiatrault, A., 2001, “Cyclic analysis of wood shear walls,” *Journal of Structural Engineering*, Vol. 127, No. 4, pp. 433-441.
- Hart, G.C., Kariotis, J., and Noland, J.L., 1988, “The Whittier Narrows, California earthquake of October 1, 1987 – masonry building performance survey,” *Earthquake Spectra*, Vol. 4, No. 1, pp. 181-196.
- Hsiao, P.-C., Lehman, D.E., and Roeder, C.W., 2012, “Improved analysis model for special concentrically braced frames,” *Journal of Constructional Steel Research*, Vol. 73, pp 80-94.
- HUD, 1994, *Assessment of Damage to Residential Buildings Caused by the Northridge Earthquake*, prepared by the National Association of Home Builders for the U.S. Department of Housing and Urban Development, Office of Policy Development and Research, Washington, D.C.
- ICBO, 1994, *Uniform Building Code*, International Conference of Building Officials, Whittier, California.

- ICC, 2015a, *International Building Code*, International Code Council, Inc., Country Club Hills, Illinois.
- ICC, 2015b, *International Residential Code*, International Code Council, Inc., Country Club Hills, Illinois.
- ICC, 2018a, *International Building Code*, International Code Council, Inc., Country Club Hills, Illinois.
- ICC, 2018b, *International Residential Code*, International Code Council, Inc., Country Club Hills, Illinois.
- Isoda, I., Filiatrault, A., and Christovasilis, I.P., 2008, “Collapse analysis of Japanese wood houses,” *Proceedings of the 10th World Conference on Timber Engineering*, Miyazaki, Japan, 7 p.
- Kato, B., Tanaka, A., Yamanouchi, H., 1980, “A field work investigation of steel building damage due to the 1978 Miyagiken-Oki earthquake,” *Proceedings of the 7th World Conference on Earthquake Engineering*, Istanbul, Turkey.
- Kircher, C.A., Seligson, H., Bouabid, J., and Morrow, G., 2006a, “When the big one strikes again – estimated losses due to a repeat of the 1906 San Francisco earthquake,” *Earthquake Spectra*, Vol. 22., Issue S2, pp. 297-339.
- Kircher, C.A., Whitman, R.V., Holmes, W.T., 2006b, “HAZUS earthquake loss estimation methods,” *Natural Hazards Review*, Vol. 7, No. 2, pp. 45-59.
- Krawinkler, H., and Nasser, A.A., 1992, “Seismic design based on ductility and cumulative damage demands and capacities,” *Nonlinear Seismic Analysis and Design of Reinforced Concrete Buildings*, edited by P. Fajfar and H. Krawinkler, Elsevier Applied Science, pp. 95-104, New York, New York.
- Krawinkler, H., Anderson, J.C., and Bertero, V.V., 1996, “Northridge earthquake of January 17, 1994: Reconnaissance report, Part 2,” *Earthquake Spectra*, Vol. 11, Suppl. C, pp. 25-47.
- Liu, J., and Astaneh-Asl, A., 2004, “Moment-rotation parameter for composite shear tab connections,” *Journal of Structural Engineering*, Vol. 130, No. 9, pp. 1371-1380.
- LSTC, 2018, *LS-DYNA Theory Manual, Release 11*, Livermore Software and Technology Corporation, Livermore, California.

- Mazzoni, S., McKenna, F., Scott, M.H., and Fenves, G.L., 2006, *OpenSees Command Language Manual*, University of California, Berkeley, Berkeley, California.
- Miranda, E., 2000, “Inelastic displacement ratios for structures on firm sites,” *Journal of Structural Engineering*, Vol. 126, No. 10, pp 1150-1159.
- Miranda, E., and Bertero, V.V., 1994, “Evaluation of strength reduction factors for earthquake resistant design,” *Earthquake Spectra*, Vol. 2, No. 10, pp. 357-379.
- Newmark, N.M., and Hall, W.J., 1982, *Earthquake Spectra and Design*, Earthquake Engineering Research Institute, Oakland, California.
- NIST, 2010, *Evaluation of the FEMA P-695 Methodology for Quantification of Building Seismic Performance Factors*, NIST GCR 10-917-8, prepared by the NEHRP Consultants Joint Venture, a partnership of the Applied Technology Council and the Consortium for Universities for Research in Earthquake Engineering, for the National Institute of Standards and Technology, Gaithersburg, Maryland.
- NIST, 2012, *Tentative Framework for Development of Advanced Seismic Design Criteria for New Buildings*, NIST GCR 12-917-20, prepared by the NEHRP Consultants Joint Venture, a partnership of the Applied Technology Council and the Consortium for Universities for Research in Earthquake Engineering, for the National Institute of Standards and Technology, Gaithersburg, Maryland.
- NOAA, 1973, *San Fernando, California, Earthquake of February 9, 1971*, National Oceanic and Atmospheric Administration, Washington, D.C.
- OES, 1995, *The Northridge Earthquake of January 17, 1994: Report of Data Collection and Analysis, Part A: Damage and Inventory Data*, The Governor’s Office of Emergency Services of the State of California, Sacramento, California.
- Pang, W., Ziaei, E., and Filiatrault, A., 2012, “A 3D model for collapse analysis of soft-story light-frame wood buildings,” *Proceeding of the World Conference on Timber Engineering*, Auckland, New Zealand.
- Porter, K., Jones, L., Cox, D., Goltz, J., Hudnut, K., Mileti, D., Perry, S., Ponti, D., Reichle, M., Rose, A.Z., Scawthorn, C.R., Seligson, H.A., Shoaf, K.I., Treiman, J., Wein, A., 2011, “The ShakeOut scenario: A hypothetical M_w 7.8 earthquake on the Southern San Andreas Fault,” *Earthquake Spectra*, Vol. 27, No. 2, pp. 239-261.

- Qi, X., and Moehle, J., 1991, *Displacement Design Approach for Reinforced Concrete Structures Subjected to Earthquakes*, Report No. UCB/EERC-91/02, University of California, Berkeley, Berkeley, California.
- Ruiz-Garcia, J., and Miranda, E., 2003, “Inelastic displacement ratios for evaluation of existing structures,” *Earthquake Engineering & Structural Dynamics*, Vol. 32, No. 8, pp. 1237-1258.
- Ruiz-Garcia, J., and Miranda, E., 2004, “Inelastic displacement ratios for design of structures on soft soil sites,” *Journal of Structural Engineering*, Vol. 130, No. 12, pp 2051-2061.
- SAC, 1995, *Characterization of Ground Motions during the Northridge Earthquake of January 17, 1994*, SAC 95-03, prepared by the SAC Joint Venture, a partnership of the Structural Engineers Association of California (SEAOC), Applied Technology Council (ATC), and California Universities for Research in Earthquake Engineering (CUREE).
- Schierle, G.G., 2003, *Northridge Earthquake Field Investigations: Statistical Analysis of Woodframe Damage*, CUREE Publication No. W-09, Consortium of Universities for Research in Earthquake Engineering, Richmond, California.
- Sen, A.D., Roeder, C.W., Lehman, D.E., and Berman, J.W., 2019, “Nonlinear modeling of concentrically braced frames,” *Journal of Constructional Steel Research*, Vol. 157, pp. 103-120.
- Shirazi, S.M.H., and Pang, W., 2012, “Seismic performance variability of wood-frame shear walls designed in accordance to the National Design Specification (NDS),” *Proceedings, ASCE Structures Congress 2012*, Chicago, Illinois, pp. 1721-1732.
- Simpson, B.G., Mahin, S.A., and Lai, J-W., 2017, *Experimental Investigation of the Behavior of Vintage and Retrofit Concentrically Braced Steel Frames under Cyclic Loading*, PEER Report No. 2017/12, Pacific Earthquake Engineering Research Center, University of California, Berkeley, Berkeley, California.
- Tanaka A., Morita K., and Yamanouchi H., 1980, “Damage of braced steel frames due to the 1978 Miyagiken-Oki earthquake,” *Proceedings of the 7th World Conference on Earthquake Engineering*, Istanbul, Turkey.

- TMS, 1994, *Performance of Masonry Structures in the Northridge, California Earthquake of January 17, 1994*, a report by the Investigating Disasters Reconnaissance Team, The Masonry Society, Longmont, Colorado.
- TMS, 2013, *Building Code Requirements and Specifications for Masonry Structures*, TMS 402/602, The Masonry Society, Longmont, Colorado.
- Tremblay, R., Filiatrault, A., Bruneau, M., Nakashima, M., Prion, H.G.L., and DeVall, R., 1996, "Seismic design of steel buildings: lessons from the 1995 Hyogo-ken Nanbu earthquake," *Canadian Journal of Civil Engineering*, Vol. 23, No. 3, pp. 727-756.
- Tremblay, R., Filiatrault, A., Timler, P., and Bruneau, M., 1995, "Performance of steel structures during the 1994 Northridge earthquake," *Canadian Journal of Civil Engineering*, Vol. 22, No. 2, pp. 338-360.
- van de Lindt, J., Symans, M.D., Pang, W., Shao, X., and Gershfeld, M., 2012, "Seismic risk reduction for soft-story woodframe building: the NEES-soft project," *Proceedings of the World Conference on Timber Engineering*, Auckland, New Zealand, pp. 237-243.
- Veletsos, A.S., and Newmark, N.M., 1960, "Effect of inelastic behavior on the response of simple systems to earthquake motion," *Proceedings of the 2nd World Conference of Earthquake Engineering*, Tokyo, Japan, Vol. 2, pp. 895-912.
- Veletsos, A.S., Newmark, N.M., and Chelapati, C.V., 1965, "Deformation spectra for elastic and elastoplastic systems subjected to ground shock and earthquake motions," *Proceedings of the 3rd World Congress on Earthquake Engineering*, Auckland and Wellington, New Zealand.
- Wald, D., Somerville, P.G., and Burdick, L.J., 1988, "The Whittier Narrows, California earthquake of October 1, 1987 – simulation of recorded accelerations," *Earthquake Spectra*, Vol. 4, No. 1, pp. 139-156.
- Yamaguchi, N., and Yamazaki, F., 2000, "Fragility curves for buildings in Japan based on damage surveys after the 1995 Kobe Earthquake," Paper No. 2451, *Proceedings of the 12th World Conference of Earthquake Engineering*, Auckland, New Zealand.
- Yamazaki, F., and Murao, O., 2000, "Vulnerability functions for Japanese buildings based on damage data due to the 1995 Kobe earthquake," *Implications of Recent Earthquakes on Seismic Risk*, Series on Innovation in Structures and Construction, Vol. 2., Imperial College Press, London, United Kingdom.

Project Participants

Federal Emergency Management Agency

Mai (Mike) Tong (Project Officer)
Federal Emergency Management Agency
500 C Street, SW, Room 416
Washington, DC 20472

Robert D. Hanson (Technical Advisor)
Federal Emergency Management Agency
5885 Dunabbey Loop
Dublin, Ohio 43017

Applied Technology Council

Jon A. Heintz (Project Executive)
Applied Technology Council
201 Redwood Shores Parkway, Suite 240
Redwood City, California 94065

Scott D. Schiff (Associate Project Manager)
Applied Technology Council
201 Redwood Shores Parkway, Suite 240
Redwood City, California 94065

Justin Moresco (Project Manager)
Applied Technology Council
201 Redwood Shores Parkway, Suite 240
Redwood City, California 94065

Project Technical Committee

Charles A. Kircher (Project Technical Director)
Kircher & Associates
1121 San Antonio Road, Suite D-202
Palo Alto, California 94303

Andre Filiatrault
University at Buffalo
Department of Civil, Structural and Environmental
Engineering
134 Ketter Hall
Buffalo, New York 14260

Jeffrey W. Berman
University of Washington
Dept. of Civil & Environmental Engineering
201 More Hall, Box 352700
Seattle, Washington 98195

James R. Harris
J. R. Harris & Company
1175 Sherman Street, Suite 2000
Denver, Colorado 80203

Kelly Cobeen
Wiss, Janney, Elstner Associates, Inc.
2000 Powell Street, Suite 1650
Emeryville, California 94608

Gregory Kingsley
KL&A, Inc.
1717 Washington Avenue, Suite 100
Golden, Colorado 80401

J. Daniel Dolan
Washington State University
Department of Civil and Environmental
Engineering
P.O. Box 642910
Pullman, Washington 99164

Dawn Lehman
University of Washington
Dept. of Civil & Environmental Engineering
201 More Hall, Box 352700
Seattle, Washington 98195

Weichiang Pang
Clemson University
Glenn Department of Civil Engineering
312 Lowry Hall
Clemson, South Carolina 29634

P. Benson Shing
University of California, San Diego
Department of Structural Engineering
9500 Gilman Drive
La Jolla, California 92093

Project Review Panel

Anthony Court (ATC Board Contact)
A.B. Court & Associates
4340 Hawk Street
San Diego, California 92103

Phil Line
American Wood Council
222 Catoctin Circle SE, Suite 201
Leesburg, Virginia 20175

William T. Holmes
Structural Engineer
2600 La Cuesta Avenue
Oakland, California 94611

James O. Malley
Degenkolb Engineers
375 Beale Street, Suite 500
San Francisco, California 94105

Larry Kruth
American Institute of Steel Construction
130 E. Randolph Street, Suite 2000
Chicago, Illinois 60601

Steve Pryor
Simpson Strong-Tie
5956 W. Las Positas Boulevard
Pleasanton, California 94588

Onder Kustu
OAK Structural (retired)
P.O. Box 2074
Danville, California 94526

Jason Thompson
National Concrete Masonry Association
13750 Sunrise Valley Drive
Herndon, Virginia 20171

Commonalities Working Group

Andrew Sen
University of Washington
Dept. of Civil & Environmental Engineering
201 More Hall, Box 352700
Seattle, Washington 98195

Masonry Working Group

Jianyu Cheng
University of California, San Diego
Department of Structural Engineering
9500 Gilman Drive
La Jolla, California 92093

Andreas A. Koutras
University of California, San Diego
Department of Structural Engineering
9500 Gilman Drive
La Jolla, California 92093

Jeff Corson
KL&A, Inc.
1717 Washington Avenue, Suite 100
Golden, Colorado 80401

Linda Peters
KL&A, Inc.
1717 Washington Avenue, Suite 100
Golden, Colorado 80401

Soil-Structure Interaction Working Group

Lisa Star
California State University, Long Beach
Department of Civil Engineering and Construction
Engineering Management
1250 Bellflower Boulevard
Long Beach, California 90840

Jonathan P. Stewart
University of California, Los Angeles
Department of Civil and Environmental
Engineering
5731 Boelter Hall
Los Angeles, California 90095

Steel Working Group

Alex Stone
KL&A, Inc.
1717 Washington Avenue, Suite 100
Golden, Colorado 80401

Sarah Wichman
University of Washington
Dept. of Civil & Environmental Engineering
201 More Hall, Box 352700
Seattle, Washington 98195

Wood Working Group

D. Jared DeBock
California State University, Chico
Department of Civil Engineering
Chico, California 95929

Ershad Ziaei
Youssef Hachem Consulting Engineering
99 NW 27th Avenue
Miami, Florida 33125

Maria Koliou
Texas A&M University
Department of Civil and Environmental
Engineering
201 Dwight Look Engineering Building
College Station, Texas 77843

Commonalities Workshop Participants

Finley Charney
Virginia Tech
Virginia Tech Department of Civil and
Environmental Engineering, Patton Hall
Blacksburg, Virginia 24061

John Hooper
Magnusson Klemencic Associates
1301 Fifth Avenue, Suite 3200
Seattle, Washington 98101

Matt Eatherton
Virginia Tech
Virginia Tech Department of Civil and
Environmental Engineering, Patton Hall
Blacksburg, Virginia 24061

S.K. Ghosh
S.K. Ghosh Associates
334 Colfax Street, Unit E
Palatine, Illinois 60067

Steve Harris
Simpson Gumpertz & Heger
100 Pine Street, Suite 1600
San Francisco, California 94111

Emily Guglielmo
Martin/Martin Consulting Engineers
700 Larkspur Landing Circle, Suite 155
Larkspur, California 94939



FEMA

FEMA P-2139-1